

Confocal Raman Microscopy; Applications in Tissue Engineering

DISSERTATION

to obtain the doctor's degree at the University of Twente, on the authority of the
rector magnificus,
prof. dr. W.H.M. Zijm,
on the account of the decision of the graduation committee,
to be publicly defended on Friday November 4th 2005 at 13:15

by
Aart Alexander van Apeldoorn

born on February 27th, 1968
in Utrecht, the Netherlands

Promotor: Prof.Dr. Clemens Antoni van Blitterswijk
Faculty of Technological Sciences
Department of Polymer Chemistry and Biomaterials
University of Twente
The Netherlands

Copromotor: Dr. C. Otto
Faculty of Technological Sciences
Department of Biophysical Engineering
University of Twente
The Netherlands

Committee members:

Prof. Dr. Ir. A. Blik, University of Twente, the Netherlands
Prof. Dr. V. Subramaniam, University of Twente, the Netherlands
Prof. Dr. J. Greve, University of Twente, the Netherlands
Prof. Dr. J.D. de Bruijn, Queen Mary University of London, United Kingdom
Prof. Dr. G.F.J.M. Vrensen, University of Leiden, the Netherlands
Dr. H.K. Koerten, University of Leiden, the Netherlands

This dissertation describes the results of the second part of a research project funded by the Dutch Technology foundation (STW) project nr; 4554. The project was a collaboration between the department of polymer chemistry and biomaterials and the department of biophysical techniques of the faculty of technological sciences at the University of Twente, Bilthoven and Enschede, The Netherlands.

The author wishes to thank the following sponsors for the funding of this thesis:

Roper scientific BV, the Netherlands
IsoTis Orthobiologics, USA
Harlan Nederland BV, the Netherlands
Sanyo biomedical Europe BV, the Netherlands
Stichting Anna fonds
Email: info@annafonds.nl



a.a.vanapeldoorn@tnw.utwente.nl

Contents

Introduction	8
Characterization of PEOT PBT block polymers by confocal Raman spectroscopy	41
In vivo degradation of PEOT PBT block copolymers evaluated by confocal Raman microscopy	62
A preliminary study on the application of confocal Micro Raman Spectroscopy for the analysis of in vivo PEOT PBT Degradation.	87
Raman Imaging of PLGA Microsphere Degradation inside Macrophages	95
Combined confocal Raman spectroscopic and SEM study of protein incorporation into biomimetic coatings	106
Parallel high resolution Confocal Raman SEM analysis of inorganic and organic bone matrix constituents	125
The physicochemical composition of osteoporotic bone in the TTD premature aging mouse determined by confocal Raman microscopy	141

Color figures belonging to the different chapters can be found at the end of this dissertation after page 180.

Almost all objects in the universe emit, reflect and/or transmit some form of light. The distribution of this light along the electromagnetic spectrum (called the spectrum of the object) is determined by the object's composition. Several types of spectra can be distinguished depending upon the nature of the radiation coming from an object:

If the spectrum is composed primarily of thermal radiation emitted by the object itself, an emission spectrum occurs.

Some bodies emit light more or less according to the blackbody spectrum.

If the spectrum is composed of background light, parts of which the object transmits and parts of which it absorbs, an absorption spectrum occurs.

Spectroscopy is the branch of physics that deals with the characterization of matter by its spectra.

There are three main categories of spectroscopy

Absorption spectroscopy uses the range of electromagnetic spectra in which a substance absorbs. for example in atomic absorption spectroscopy, the sample is atomized and then light of a particular frequency is passed through the vapour. After calibration, the amount of absorption can be related to the concentrations of various metal ions through the Beer-Lambert law. The method can be automated and can be used to measure concentrations of ions such as sodium and calcium in blood for example. Other types of spectroscopy may not require sample atomization. For example, ultraviolet/visible (UV/ Vis) absorption spectroscopy is most often performed on liquid samples to detect molecular content and infrared (IR) spectroscopy is most often performed on liquid, semi-liquid (paste or grease), dried, or solid samples to determine molecular information, including structural information.

Emission spectroscopy uses the range of electromagnetic spectra in which a substance radiates. The substance first absorbs energy and then radiates this energy as light. This energy can be from a variety of sources, including collision (either due to high temperatures or otherwise), chemical reactions, and light.

Scattering spectroscopy measures certain physical properties by measuring the amount of light that a substance scatters at certain wavelengths, incident angles, and polarization angles. Scattering spectroscopy differs from emission spectroscopy due to the fact that the scattering process is much faster than the absorption/emission process. One of the most useful applications of light scattering spectroscopy is Raman spectroscopy.

In biophysics one makes use of techniques derived from physics to study biology.

Introduction



The logical next step in electron microscopy is the combination of Confocal Raman Microscopy with Scanning Electron Microscopy. The above figure shows the integrated system described in this dissertation used for the analysis of biomaterial and tissue engineered samples. The confocal Raman microscope setup (the black apparatus on the right hand side) is in situation connected to a FEI XL30 FEG environmental scanning electron microscope.

Introduction

A brief history of Microscopy

In the year 2004 AD a Dutch television broadcasting station organized an election on who would be the greatest Dutchman in history. The Dutch could vote for politicians, scientists, painters, writers, sportsmen, etc., basically anybody who meant anything in the history of the Netherlands. In the final round of these elections a group of ten people was selected from which the greatest Dutchman was selected, amongst these were; Willem van Oranje, Desiderius Erasmus, Rembrandt van Rijn, Johan Cruijff but also a man called Antoni van Leeuwenhoek¹. Why Antoni van Leeuwenhoek? Van Leeuwenhoek lived around 1700 AD in Delft where he owned a fancy-textile shop and used magnifying glasses to investigate the quality of textile. He received only an elementary education and spoke only Dutch. Van Leeuwenhoek designed and built several hundred small microscopes of similar design and function. The dimensions of his microscopes were fairly constant at around 5 centimetres long and 2.5 centimetres wide. The core of these microscopes consists of two flat and thin brass plates. In between the plates a small bi-convex lens capable of magnifications ranging from 70x to over 250x, depending upon the lens quality, was placed (see figure 1).

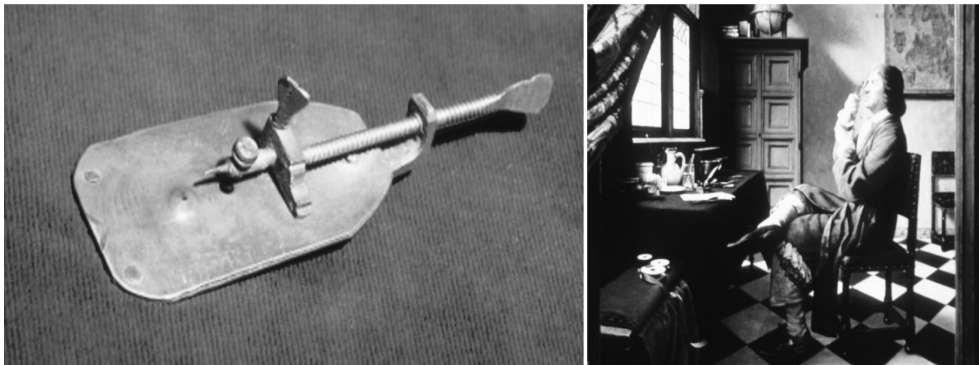


Figure 1: Original Antonie van Leeuwenhoek Microscope property of the Utrecht University museum, the Netherlands. The instrument consists of two brass plates (2.4x4.6 cm) riveted together at 3 locations. The hole contains a lens. On the tip of the sharp pin an object can be placed for observation. By using the screw on the pin one is able to focus the image. Van Leeuwenhoek made about 500 microscopes of which 9 have survived. This Utrecht example has a magnification of 266 X,

while the other remaining magnify between 70 until 170 X. The Utrecht microscope allows for the observation of samples with a size of 0,00135 mm. Only after 1840 AD it was possible to build microscopes which could be used to study smaller objects. Antonie van Leeuwenhoek was not the original inventor of the microscope. Around 1600 a spectacles maker from Middelburg in the Netherlands found out that smaller objects could be more easily observed when placing two lenses at certain distance from each other. The microscope shown here was discovered around 1850 in the physics laboratory at the Minrebroederstraat in Utrecht the Netherlands by Prof. P. Harting. It was kept in a leather lined box with the inscriptions BB. Focal point 0,94 mm, Magnification 266x, Lens aperture 0,7 mm, Resolving power 1,35 mm. The painting showing van Leeuwenhoek using his microscope is by Robert A. Thom and appeared in "Great Moments in Medicine" published by Parke Davis & Company, in 1966.

He used these microscopes to study many different biological specimens and published his findings in letters, many of which he sent to the Royal Society in London. His findings earned him the title of "Fellow" and laid the foundation of microscopy as it is used today.

In 1662 Robert Hooke was named Curator of Experiments of the Royal Society of London he became responsible for the demonstration of new experiments at the Society's weekly meetings². Hooke's reputation in the history of biology mainly rests on the book *Micrographia*, which he published in 1665 (see figure 2).

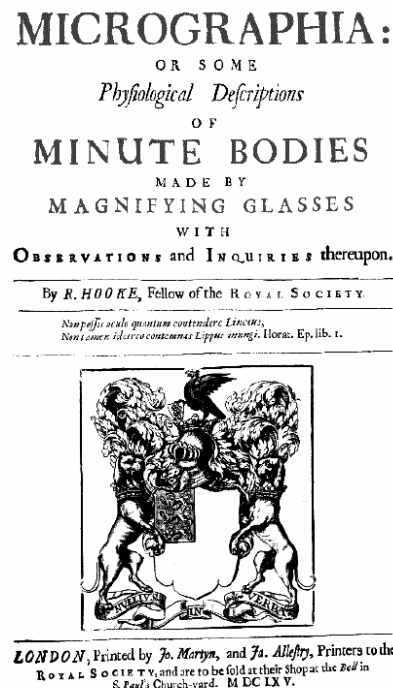


Figure 2: Cover of "Micrographia" by R. Hooke in which he described his microscopical observations

Hooke designed a compound microscope including an illumination system based upon van Leeuwenhoek's microscope. He observed insects, sponges, bryozoans (aquatic moss like organisms), foraminifera (tiny single-celled organisms that construct shells), and bird feathers. Based on his findings Hooke described fleas for example as "adorn'd with a curiously polish'd suite of sable Armour, neatly jointed" (see figure 3).

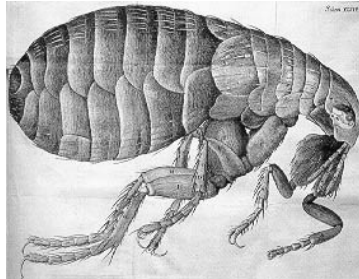


Figure 3: Drawing of a flea made by R. Hooke as it was published in "Micrographia" 1665.

Some readers criticized Hooke for investigating such unimportant subjects, a satirist of the time poked fun at him as "a Sot, that has spent 2000 £ in Microscopes, to find out the nature of Eels in Vinegar, Mites in Cheese, and the Blue of Plums which he has cunningly found out to be living creatures." One of his most renowned microscopical observations was from the study of thin slices of cork. He wrote: "I could exceedingly plainly perceive it to be all perforated and porous, much like a Honey-comb, but that the pores of it were not regular, these pores, or cells, were indeed the first microscopical pores I ever saw, and perhaps, that were ever seen, for I had not met with any Writer or Person, that had made any mention of them before this". The cells Hooke described were plant cells. Hooke invented the term "cells" because the boxlike cells of cork reminded him of the cells of a monastery. Hooke also described comparable structures in wood and in other plants. After van Leeuwenhoek had written to the Royal Society on September 7th 1674 with a report of the discovery of "animalcula" (bacteria and protozoa) in a

sample of water from the Berckelse meer (an inland lake close to Delft)³. In 1678, Hooke was asked by the Society to verify Leeuwenhoek's findings in which he succeeded after two attempts which had initially failed. Although van Leeuwenhoek's simple microscopes gave clearer images than his own compound microscope, Hooke found simple microscopes difficult to use and called them "offensive to the eye" and that they "much strained and weakened the sight".

The smallest distance between two points which can be resolved with an oil immersion objective of high quality and white light was studied by Abbe in Jena in the 19th century. The resolving power of a microscope can be described according to the following formula;

$$\text{Resolving power: } s = \frac{\lambda}{2n \times \sin i} \quad (1)$$

n is the refractive index of the oil, λ is the wavelength of the light and i is half the angle subtended by the objective front lens at the object plane. $n \times \sin i$ is called the numerical aperture (NA) of the objective (see also figure 5)

Practical problems of optics

The optimization of light microscopes dealt with 3 basic problems; chromatic aberration, spherical aberration and reaching the theoretical limit of resolution. Chester Hall found a solution to the problem of chromatic aberration around 1730. The problem of the usage of a single lens system was the unequal bending of different colors (wavelength) of light that occurs in a lens. Hall discovered that combining highly refractive lead glass, which was used for chandeliers and goblets in those days, with regular glass in a proper combination could correct for chromatic aberration. Since the refractive indices of the materials used for the two lenses were different, light passing the two lenses is bended at different angles. By using a second lens, of different shape and light bending properties, alignment of the wavelengths without losing all of the magnification of the first lens became possible (see figure 4). Around 1830 Joseph Jackson Lister solved the problem of spherical aberration, which is the unequal bending of light that hits different parts

of a lens. He discovered that by placing lenses at exact distances from each other the aberration from all except the first lens could be eliminated.

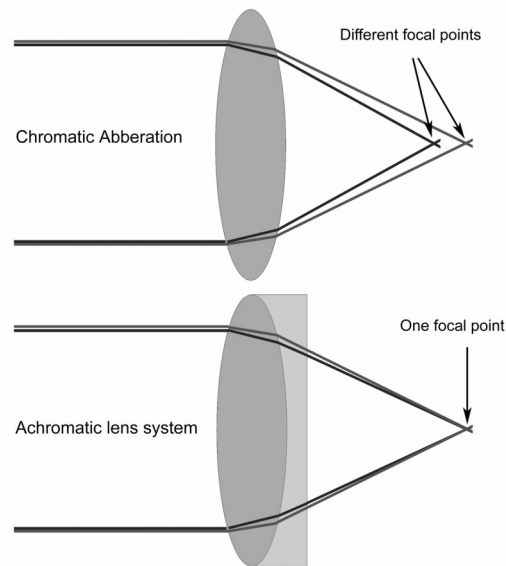


Figure 4: The problem of chromatic aberration could be solved by placing an extra the achromatic lens behind the initial single lens.

By then it was already possible to produce low power low curvature lenses having minimal aberration, so by using a lens of this type as the first in a series, spherical aberration could be nearly eliminated. In order to obtain the most optimal microscope it has to collect a cone of light that is as broad as possible. Ernst Abbe worked out the solution to this problem around 1870. Just a year after Carl Zeiss began the manufacture of the compound microscope; Abbe released a scientific paper in 1873 in which he described the mathematics leading to further improvement of the microscope. He described the physical laws about the collection of light by an objective and was able to maximize this collection by using water and oil immersion lenses. Abbe managed to accomplish about 10 times better resolution than van Leeuwenhoek had achieved about 100 years earlier.

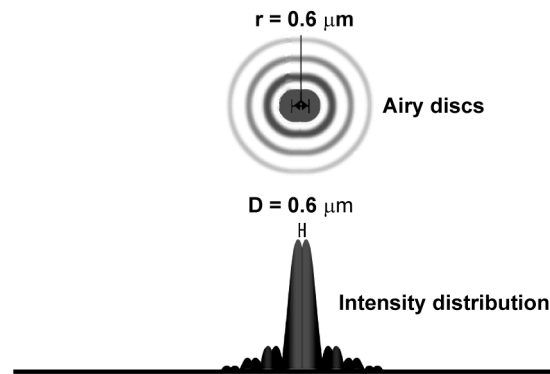


Figure 5: Resolution is the minimal distance at which two point objects still can be recognized from each other. Airy diffraction pattern sizes and their corresponding radial intensity distribution functions are depended on the combination of numerical apertures from the objective and condenser, as well as the wavelength of light used. For a well-corrected objective with a uniform circular aperture, two adjacent points are just resolved when the centres of their airy patterns are separated by a minimum distance which is equal to the radius of the central disk in the airy pattern. In this example $\lambda=685\text{nm}$ and the $\text{NA}=0.6$ and resolution $r = 1.22 \lambda / 2\text{NA}_{\text{obj}}$.

Confocal microscopy

Conventional wide field light microscopes are based upon the fact that an entire sample of interest is illuminated and can subsequently be observed by the naked eye or imaging device. The image is focused by one, or more lenses which can be moved opposite each other in order to obtain a sharp image of the object. The source for illumination in these microscopes consist of a bulky light source like the sun or candlelight in the early days, and electric light bulbs or more recently halogen light bulbs nowadays. In 1964, C.H. Townes, N.G. Basov and A.M. Prochorov received the Nobel Prize for physics for the invention of the laser, which allowed for the production of coherent radiation from electrons and atoms⁴. In other words they discovered a means to generate light (radiation) composed of photons pulsating with a well defined frequency. In this same period Minsky applied for a patent describing a stage scanning confocal microscope⁵ (see figure 6). In his own words “An ideal microscope would examine each point of the specimen and measure the amount of light scattered or absorbed by that point. But, if we try to make many such measurements at the same time then every focal image point will be clouded by aberrant rays of scattered light deflected points of the specimen

that are not the point you're looking at. Most of those extra rays would be gone if we could illuminate only one specimen point at a time"⁶.

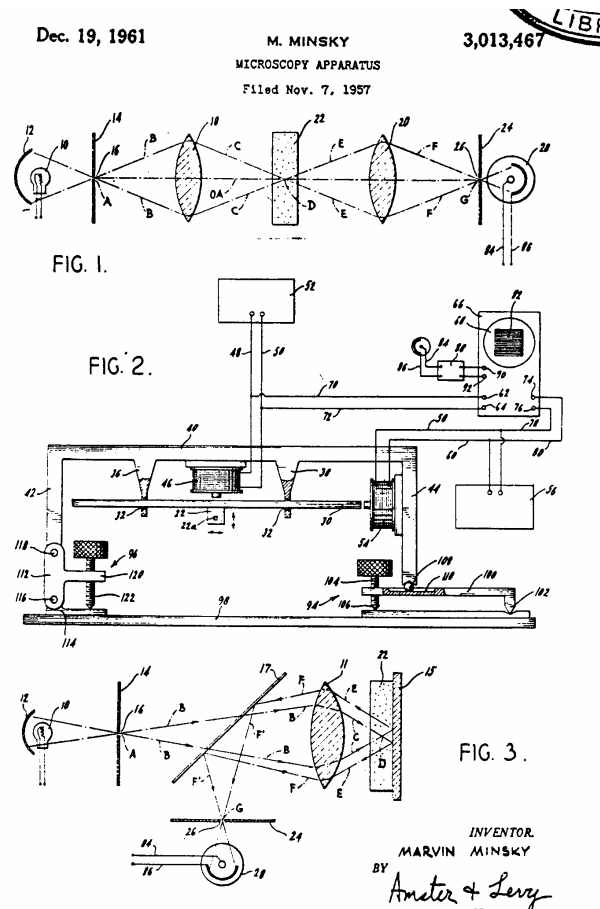


Figure 6: Original drawing of the confocal microscope design by Minsky in figure 3 a scheme of the working principle can be seen.

The fundamental difference between the confocal microscope and the conventional microscope is the use of a small focussed beam of light which scans across a sample in the confocal microscope, whereas in conventional microscopes whole samples are illuminated. The scattered light from the specimen is directed through a pinhole or slit, which blocks all "out of focus light", and is then reconstructed into an image (see figure 7). These microscopes have a number of advantages over the conventional microscopes; control of depth of field, reduction

or elimination of background information away from the focal plane, which causes image blurring, and the ability to collect serial optical sections from thick specimens.

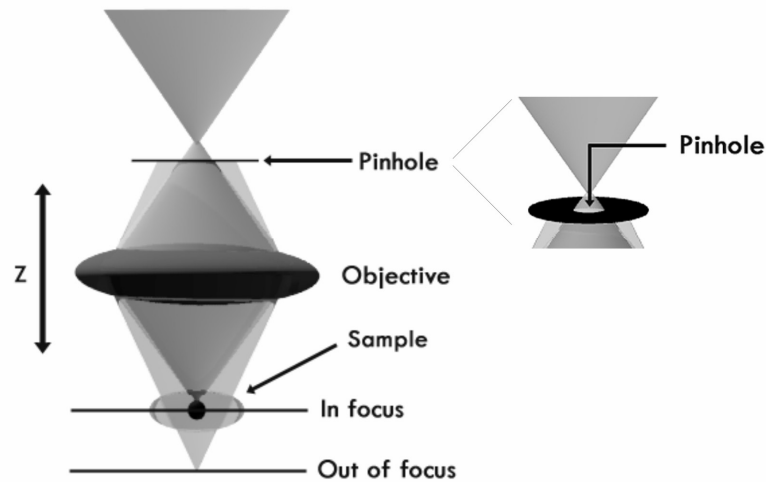


Figure 7: Principle of Confocality: by placing a pinhole in the pathway of light coming from the objective lens the out of focus light can be blocked, leading to an improved image because only the in focus light is observed.

Confocality basically makes use of spatial filtering techniques in order to eliminate out-of-focus light or so called glare in specimens whose thickness exceeds the immediate plane of focus. This concept of confocal microscopy was improved upon by Egger who used a laser to develop a working confocal scanning optical microscope⁷. The demonstration of its applicability in biology however took 10 years more when Brakenhoff et al. showed its real potential in studies on 3-dimensional chromatin distribution inside the nucleus of mammalian and insect cells⁸⁻¹⁴.

Electron microscopy

Although conventional microscopes had improved the quality of imaging tremendously the wavelength of light puts a limit on the amount of magnification at which objects still can be resolved. Using light, it is impossible to distinguish details smaller than the wavelength of the light. For a conventional microscope using

visible light, the distance between two points of an image that still can be resolved is about $0.2\text{ }\mu\text{m}$. This made it impossible to study for example the organelles within cells, so another method had to be developed which could allow for these studies. A big step forward in microscopy came when it was found possible to produce an image of an object using an electron beam. Ernst Ruska, together with his supervisor Max Knoll, began studying simple magnetic coils^{4, 15-19}. They discovered that the use of suitably-designed iron encapsulation improved the electron-optical properties. Moreover, they found that magnetic coils could be used like an optical lens. By using a lens of this type, enlarged images could be generated of a sample irradiated with electrons. Ruska subsequently worked on improvement of the details, and in 1933 the first electron microscope in the modern sense was constructed. Since then electron microscopes have been improved tremendously. Electrons are point like particles, and therefore the resolving power of Electron microscopes is theoretically unlimited. However, quantum mechanics dictate that every particle has wave properties which cause an uncertainty into the determination of its position. This sets a theoretical limit to resolution for the acceleration potentials normally used in the order of $0.5 - 1\text{ }\text{\AA}$. An interesting side effect of using a beam of electrons to observe the morphology of samples is the generation of X-rays. The electrons from the electron beam can interact with the electrons present in the atoms from which a sample is composed of. The interaction causes electrons to be ejected from an inner shell of an atom (excitation), in order to restore the charge; the ejected electron is then replaced with an electron from a higher shell, during which energy in the form of X-rays is released. Since the X-rays have a specific energy depending on the atoms by which the X-rays are released from, the detection of these can be used to build an atom specific spectrum.

Raman spectroscopy

Another analysis technique dealing with the excitation of electrons is Raman spectroscopy. The source of Raman spectroscopy is an inelastic scattering effect, where the excited molecule, induced by photons from a monochromatic light source, relaxes to a different vibration level than its original ground state. The energy difference between the incident and scattered radiations appears as a frequency shift from the incident light. These frequency shifts are specific for a given chemical bond and allow therefore molecular analysis.

The phenomenon called Raman Effect

The Raman effect was first discovered by C.V Raman, the story goes that he was fascinated by the spectacular blue color of the Mediterranean Sea, who studied the scattering of light by liquids. Raman together with Krishnan published a paper in 1928 on what they called "A New Type of Secondary Radiation"²⁰. They described this radiation as follows: "in the case of ordinary light two types of scattering, one determined by the normal optical properties of the atoms or molecules, and another representing the effect of their fluctuations from their normal state are to be expected". They did several experiments in which they converged bright sunlight by a series of lenses into several liquids and used complementary colored light-filters in order to filter out the scattered light. They discovered that although they had filtered out the light with the color (wavelength) scattered by a specific sample another color could still be observed. Soon after, these observations were confirmed by several others and the Raman effect was born.

The Raman effect

A qualitative description of Raman scattering can be found in figure 8. In literature several descriptions of Raman scattering can be found²¹⁻²³. Based on these a brief explanation of Raman scattering is given here. When a photon with certain energy interacts with a molecule, the energy state of the molecule increases.

The increase in energy of the molecule is equal to the energy of the interacting photon.

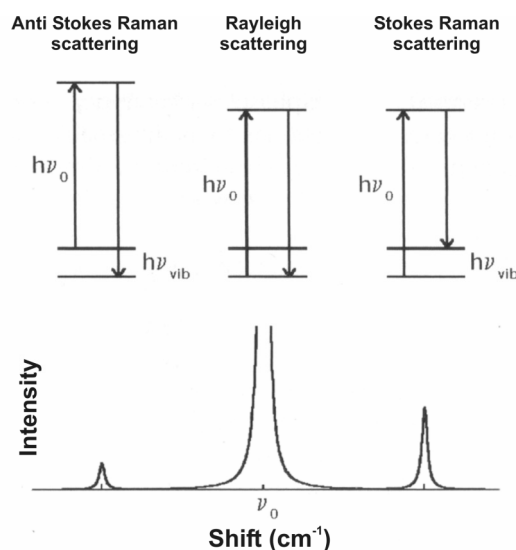


Figure 8: Schematic presentation of the energy level diagram in Raman scattering, $h\nu_0$ the initial energy of the incident photon, $h\nu_{\text{vib}}$ the energy of the scattered photon influenced by molecular vibrations.

The alterations in energy state are not fixed, meaning any of an infinite number of energy levels, or virtual states, can be assumed. The thus excited molecules do not remain stationary at these virtual states. The change in energy is in fact a distortion of a covalent bond and therefore the molecule immediately relaxes back to the original electronic (ground) state by emitting a photon. If no energy is transferred to the molecule the emitted photon will have the same energy as the initial photon. The light scattering observed will therefore consist of the same wavelength as was initially applied; this is what is referred to as Rayleigh scattering. If the molecule returns to a different electronic state (higher or lower) than the original ground state, photons will be emitted having either less energy, in case of Stokes Raman scattering, or more energy, in case of anti-Stokes Raman scattering. Molecules are basically composed of point masses (atoms) connected by springs (chemical bonds). Moreover, the vibrational frequency of a small group of atoms bound together is almost independent from the rest of the molecule. The vibrational spectrum of a

molecule can be depicted as the total sum of vibrational frequencies of each chemical bond present.

There are a number of factors which can influence Raman band intensities;

Raman data is usually displayed as a plot of Raman scattering intensity as a function of wavelength. At the x-axis the Raman shift is displayed in wavenumbers. Wavenumber is the reciprocal of wavelength in centimeters. One wavenumber is equal to a unit of energy E (see formula 2). The x-axis in Raman spectra displays the difference between the excitation wavelength and the Raman wavelength (see formula 3).

$$E = h \nu = \frac{h c}{\lambda} = h c \omega \quad (2)$$

h = Planck's constant, ν = frequency of light, c = speed of light, λ = wavelength of light, ω = wavenumber of light

$$\text{Raman shift} = \frac{1}{\lambda_0} - \frac{1}{\lambda_{\text{Raman}}} \quad (\text{cm}^{-1}) \quad (3)$$

λ_0 is excitation wavelength, λ_{Raman} is Raman wavelength

- A) Vibrations of polar chemical bonds produce weak Raman bands. Strong dipole moments localize the electron cloud which composes a chemical bond making the cloud harder to be moved by light.
- B) Crystalline materials have stronger and more intense Raman bands than non crystalline materials.
- C) Stretching vibrations are in general stronger scatterers than bending vibrations.
- D) Raman intensity of stretching vibrations increases with bond order.
- E) Symmetric vibrations are in general stronger than anti symmetric vibrations.

Since Raman spectroscopy uses a monochromatic light source for the molecular analysis of samples one can apply the basic principles of light microscopy in order to construct a confocal Raman spectroscope. In confocal Raman spectroscopy one uses the capabilities of a normal confocal microscope. The confocal Raman spectroscope, (sometimes referred to as micro Raman meter) is basically a confocal light microscope converted into a Raman microscope. It uses a laser as a monochromatic light source, which is focussed on a sample by an objective. The induced Raman scatter is collected by this objective and then directed through a

pinhole into a spectograph containing a holographic grating, which diverts different wavelengths at different angles. The decomposed wavelengths are then collected by a deep cooled CCD camera, of which the data is then recorded by a computer. By using the high resolution capabilities of this system one can not only analyse samples on a sub micrometer scale, by measuring a single point, but when combining such a “microscope” with either a scanning mirror or a scanning sample stage, so called Raman images (images revealing molecular information) can be generated. I would like to define the technology which is frequently described in literature as being confocal or micro Raman spectroscopy, as Confocal Raman Microscopy, when imaging is used and as Confocal or Micro Raman Spectroscopy when only point analysis are done.

The logical next step: combining Confocal Raman Microscopy with Electron Microscopy

The most commonly used types of electron microscopes in biology are scanning and transmission electron microscopes. The first type is used for studying the 3 D morphology of samples, while the second one is used for the observation of ultra-thin sections of samples. Both microscopes can reveal morphological and chemical information as well, whenever X-ray microanalysis is used. However, a disadvantage of X-Ray microanalysis is the difficult detection of atoms with a low atomic number, especially in case of fluor and nitrogen, while atoms with a number lower than that of carbon (5), cannot be detected. A second disadvantage of X-ray microanalysis is the fact that no discrimination between atoms can be made which belong to either organic or inorganic molecules. Moreover, no information can be obtained about the type of molecule the atom belongs to. In life sciences, X-ray microanalysis is used for studies at the organelle level in the cell, but information obtained from these measurements is severely restricted because of limitations of the measurement technique, as was mentioned before. In the past 2 decades the technique of Raman spectroscopy has been refined, which eventually

led to the design of compact confocal Raman spectro- and microscopes. The main drawback of Raman spectroscopy however is the fact that the signal obtained is very weak due to the low efficiency of Raman scattering. Nevertheless, studies done at the Biophysical Techniques department at the University of Twente led to a tremendous optimization of this analytical technique. Puppels et al. wrote a thesis on the development of a confocal Raman micro spectroscope for studying cells and chromosomes. This thesis lead to a publication in Nature in 1990²⁴, describing the study of live single cells and chromosomes by this technique. Nowadays, there are numerous studies on nucleic acids, lipids and proteins being performed by using confocal Raman spectroscopy. Recently, a thesis describing the development of a compact confocal Raman spectroscope was published by Aksenov et al.²⁵. Herein, the design of a confocal Raman system is described which can be combined with a scanning electron microscope. The rationale behind this research was the fact that the use of X-ray microanalysis for studying biological samples is not sufficient, while only the presence of carbon, oxygen and other atoms can be revealed. The information on physicochemical properties of samples is crucial for a researcher in the field of tissue engineering, where he would benefit from additional information about molecular composition and distribution in samples of interest. X-Ray microanalysis is currently the most common technique used in electron microscopy which allows for the chemical analysis without any pre-treatment of microscopic samples. Therefore, the combination of electron microscopy with confocal Raman microscopy and/or X-ray microanalysis is therefore a logical next step and can greatly expand the analytical capabilities, allowing the analysis of molecular composition at a sub micrometer scale without complicated sample preparations.

Working principle of the combined system

Let us see how the Confocal Raman Module functions in more detail. A schematic drawing of the system is given in figure 9. Once the coordinates of a location of

interest for Raman analysis is found by electron microscopy, the sample is shifted towards the exact position of the laser spot. This position is determined beforehand by calibrating the system by using small beads and using the capabilities of the module which allows for observing samples by transmission light microscopy as well.

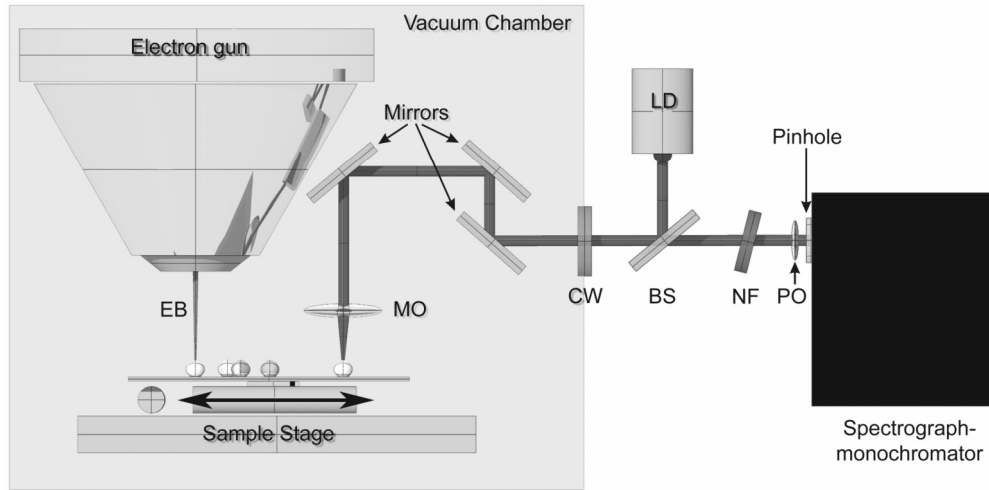


Figure 9: schematic representation of the combined confocal Raman microscope with a scanning electron microscope. Samples are analyzed by selecting a location by EM using the electron beam (EB) subsequently moving the sample into the confocal laser spot at exact coordinates. The laser source consists of a laser diode (LD) with a wavelength of 685nm and is diverted through a side port into the vacuum chamber by a beamsplitter (BS). The laser is then emitted onto the sample by a set of gold coated mirrors through a 60 x objective (MO). The induced Raman scatter is then collected by the same objective and diverted in the opposite direction, passing a notch filter (NF) to eliminate the laser light obscuring the Raman signal and focussed by a pinhole objective (PO) on a pinhole allowing for confocality of the system. Inside the spectrograph monochromator, the Raman scattering is subsequently focused on a holographic diffraction grating and the decomposed wavelengths are then detected by a thermo-electrically cooled CCD. The sample stage (allowing for nanometer movements) is equipped with a small light source to use transmission light microscopic observation for easy calibration of stage movement.

The system is composed of a spectrograph and laser diode outside the vacuum chamber of the scanning electron microscope and a mirror and lens system inside the vacuum chamber. A collimated laser beam, emitted by the laser diode is directed into the vacuum chamber through a vacuum sealed window. The beam is then diverted by a series of gold coated mirrors, through the objective lens. By focussing, an optimal focal spot is then obtained on the sample of interest. The induced Raman scattering, is collected in the opposite direction by the objective lens and guided by the mirror system through the vacuum window. The signal

subsequently passes the beam splitter and a notch filter, which blocks most photons with the initial wavelength from the diode laser. The remaining photons are focused by a small lens on a pinhole, which allows for confocality of the system. Inside the spectrograph the photons with different wavelengths are diverted by a holographic grating onto a thermo electrically cooled CCD chip connected to a computer, by which the signal can be analyzed.

Raman imaging in the Scanning Electron Microscope

Imaging of a sample can be performed as follows. A scanning stage is placed on the original sample stage of the electron microscope. This scanning stage should allow for stepwise controlled movement of the sample with high enough resolution, at least the laser spot size resolution. The scanning stage can be a piezo element or a step motor driven system depending on the dimensions of the vacuum chamber. The stage is then linked to measurement software, through laboratory processing software, allowing for stepwise movement and collection of spectra during each step. This leads to the generation of spectroscopic images which can be depicted as image files, which in turn can be related to the electron micrograph collected beforehand of the same area, a few examples of these images can be found in figure 10.

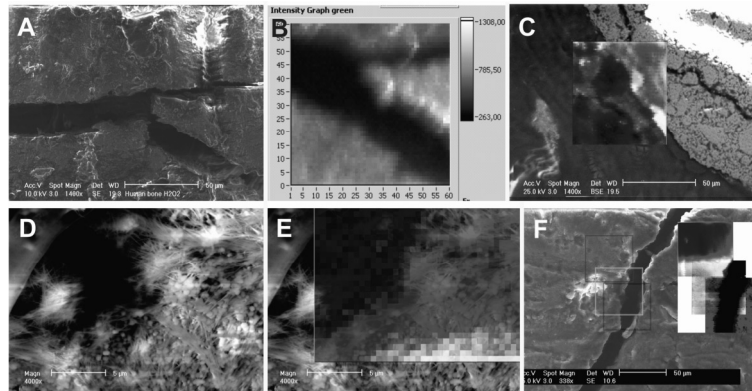


Figure 10: Examples of Raman imaging on different SEM samples. Micrographs A and B; surface of human cancellous bone and corresponding Raman image on phosphate C: typical backscatter sample of bone filler and overlaying PO43- distribution.

D: electron micrograph of bone ECM produced by osteoprogenitor cells and (E) corresponding Raman image of mineralized matrix. F: Surface of rat femoral bone and corresponding Raman images on protein (red), carbonate (green) and phosphate (blue).

Now, not only point analyses of interesting structures can be done, but also chemical maps can be made. The chemical maps can show the distribution of specific molecules in the sample, which then can be related to the morphology observed by scanning electron microscopy. This can for example give valuable information about tissue interaction with implants, phagocytosis, extra cellular matrix production, the dynamics of intra-cellular processes, etc. in the case of tissue engineering studies.

Tissue engineering and materials

In tissue engineering, one strives to combine several scientific disciplines like material science, biology, physics etc., in order to create new technologies for the repair of damaged tissues, which in most cases can not heal themselves because of the defect size. In the past 2 decades many different definitions of tissue engineering have been put forward and changes in the description have been influenced by personal opinions, background and scientific and technological developments. The central dogma here is that materials or cells alone, or in combination with (other) cells and/or bioactive factors are processed into an end product which can support new tissue formation in order to heal a defect or provide replacement for lost tissue. In case of degradable materials being applied in tissue engineering the ultimate material would be one which degrades while new tissue replaces the implanted material in the same time. Depending on their molecular composition materials can degrade in different ways a scheme of possible processes participating in degradation is depicted in figure 11. The mechanisms by which polymer (bio) materials can degrade can be described by either surface erosion or bulk erosion. Surface erosion can be defined as the

gradual degradation of a material from the surface towards the inside, layer by layer the surface is eroded away, while in bulk erosion, degradation takes place throughout the whole polymer structure²⁶.

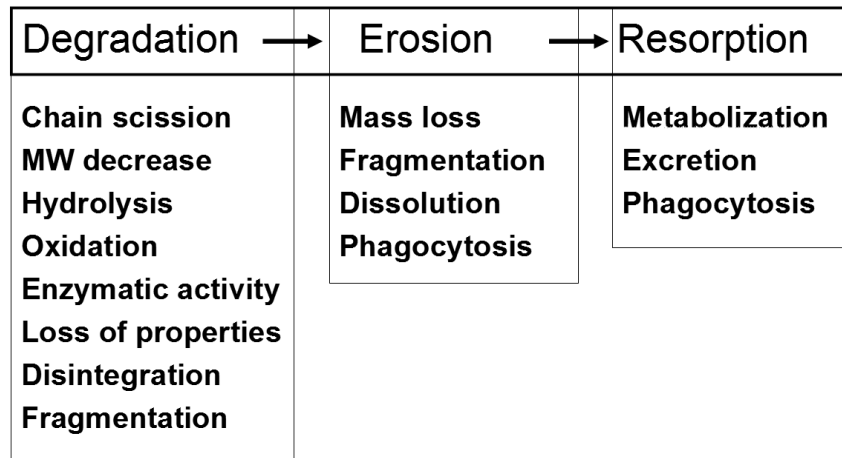


Figure 11: Schematic presentation of the processes involved in degradation of materials after implantation. Source: Dr. D. Grijpma, Dept. of Polymer Chemistry and Biomaterials, University of Twente, the Netherlands.

During surface erosion a significant mass loss can be detected while the molecular weight and mechanical properties remain largely unchanged, whereas during bulk erosion a decrease in molecular weight and mechanical properties mostly precedes mass loss²⁷. An excellent example of surface erosion was shown by Wang et al.²⁸, who studied the enzymatic degradation of poly(L-lactide)-poly(2-ethyl-2-oxazoline)-poly(L-lactide) triblock copolymers (PLLA-PEOZ-PLLA). The polymer used in this study consisted of a so called ABA triblock copolymer containing biodegradable PLLA A-blocks and water-soluble polyelectrolyte poly(2-ethyl-2-oxazoline) (PEOz) B-blocks. At least 60% weight was lost after 34 hours of incubation in a buffered solution containing a hydrolytic enzyme in order to facilitate fast degradation. After electron microscopic observations they found that degradation had taken place mainly at the surface of these polymers and that the overall pore sizes had increased after incubation. In contrast is the observation of

the change in composition of Poly(ether ester) block copolymers, which are based on polyethylene glycol and polybutylene terephthalate after implantation²⁹ (see figure 12).

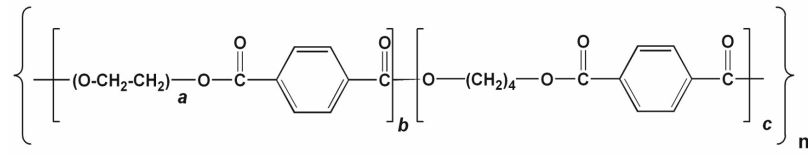


Figure 12: Polyethylene oxide terephthalate (PEOT) and poly butylene terephthalate (PBT) block copolymer. The initial length of the polyethylene oxide (PEG) segment can be varied, as can be the molar ratio of the PEOT to PBT segments. The composition is denoted as $a/b/c$, where a represents the poly(ethylene glycol) (PEG) molecular weight (MW g/mol), and b and c represent the weight percentage (wt%) of PEGT and PBT blocks respectively.

These blockcopolymers are being used as degradable materials for tissue engineering (brandname: Polyactive™) by several companies in relation to either tissue repair or drug release applications. These so called PEOT/PBT (or sometimes referred to as PEGT/PBT) multi block copolymers are thermoplastic elastomers. By varying the polyethyleneglycol terephthalate block (PEOT) and polybutylene terephthalate (PBT) block ratio and the molecular weight of the polyethyleglycol (PEG) used for synthesis a vast range of different block copolymers can be produced with different mechanical, swelling and degradation properties an extensive description of these characteristics can be found elsewhere³⁰. Depending on their composition, PEOT/PBT block copolymers have been applied as alloplastic tympanic membranes as middle ear prosthesis³¹ in skin³²⁻⁴⁰, cartilage⁴¹⁻⁴⁴ and bone⁴⁵⁻⁵⁴ tissue engineering studies. An interesting observation was made when PEOT/PBT copolymers were used with high PEO content. In several studies it was found that after implantation these polymers showed signs of calcification^{31, 51, 55}. Several authors have described a continuity in apatite crystals across the interface of PEOT/PBT implants and bone^{51, 52, 56} indicating the bone bonding capabilities of these polymers. More recently a number of studies have been done on adding either biomimetic calcium phosphate coatings^{57, 58} or mesenchymal stem cells^{54, 59}.

⁶⁰ to tissue engineering scaffolds made from PEOT/PBT block copolymers indicating the possibility to use these materials for bone tissue engineering.

Bone and Raman spectroscopy

Bone is a highly dynamic tissue undergoing constant self renewal under the influence of outside pressure. Moreover, it is essentially a composite elastic material with high stiffness composed of carbonated apatite and mainly collagen type I fibers, packed into a dense material. Depending on the location in the body it can either have a porous appearance, trabecular bone found in the marrow cavities of long bones, ileum and clavulae for example, or a dense appearance, like the compact bone layering present in the long bones and calvaria. Raman spectroscopy is a well suited technique to investigate the physico chemical properties of bone tissue. The most prominent band which can be found in bone spectra belongs to the asymmetric stretch mode (ν_1) of phosphate (960 cm^{-1}), while a carbonate specific band can be found around 1070 cm^{-1} , these bands can be used as markers for the mineral content of bone (see figure 13).

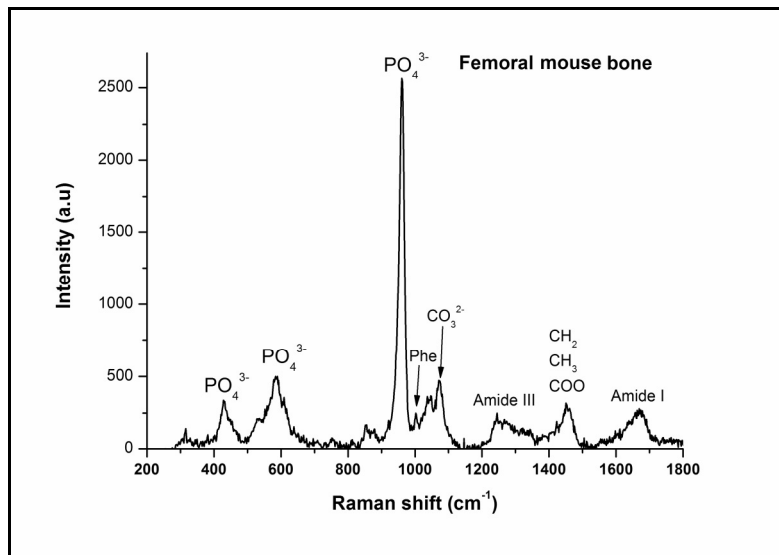


Figure 13: Typical example of a Raman spectrum of Bone showing the band positions specific for the different bone matrix constituents.

Other important Raman bands which can be found are the so called amide I (around 1650 cm^{-1}) and amide III bands (around 1250 cm^{-1}), specific for the organic matrix of bone. Morris et al.⁶¹⁻⁶³ have described the chemical composition of bone studied by Raman spectroscopy extensively. In a study done on cortical bone using Raman transects⁶³, a number of lines composed of fifty to hundred Raman spectra, they found that around osteons, the structures that form the Haversian channels in cortical bone, three distinct phosphate signatures could be found. The transects indicated a range varying from a disordered more amorphous mineral phase close to the center of the osteon towards a ordered and more crystalline phase away from the center of the osteon. A similar method was used by Schulze et al.⁶⁴, who studied the qualitative mineral content across different dental layers. Interestingly they found no change in phosphate mineral phase between dentin, enamel and cementum in teeth. However, the intensity of the C-H stretching mode (belonging to the organic matrix) was higher in enamel than in dentin and a steep increase in the interface between these two layers, the so called dental calcified junction, could be measured. These results show that Raman spectroscopy not only can be used to analyse the molecular composition of bone tissues, but can reveal information about the organisation of these hard tissues as well. Another interesting feature of Raman spectroscopy is that it can be used to study the structural changes of materials and tissues induced by mechanical pressure by monitoring the position of specific Raman bands. When bovine femora were subjected to mechanical loading, through indentation of the cortical region, it was found that Raman bands belonging to the organic matrix, related to crosslink ruptures in the Collagen network, had shifted, predominantly when shear forces were present⁶⁵. Compression of the cortex on the other hand, resulted mainly in the alteration of the mineral phase content. Although the authors could not fully explain this last mentioned result, they hypothesized that structural changes and or movements in the crystal lattice of hydroxyl and carbonate groups could have been

induced by increased pressure during the indentation process. More recently, in a study performed on Rat femoral bone, Raman microprobe measurements revealed that with increased age the mineral crystal lattice of bone becomes more organised and more carbonate ions are present⁶⁶. Furthermore, it was found that increasing mineral matrix ratio, crystallinity and type-B carbonate substitution were correlated to a deterioration of structural and tissue-level mechanical properties of aging compact bone.

Cells, tissues, materials and confocal Raman spectroscopy

One of the approaches towards tissue repair, while using tissue engineering techniques is the isolation of the patients own cells, which can then be culture expanded, eventually differentiated into the proper phenotype and seeded onto scaffold material of any shape which subsequently can be implanted into the defect area. The idea is that the cells present on these scaffolds can speed up the healing process, by either providing growth factors which can attract other cells to the implant site, or support tissue-repair itself. Without describing all the details of the different approaches taken for different types of tissues, it is evident that a selection of the proper cell source and the subsequent analysis of its performance must be crucial to the outcome of a tissue engineering study involving cells. Confocal Raman spectro- or microscopy can provide the researcher with a non destructive technique by which cells can be investigated. In the early 90's Puppels et al.^{24, 67-69}, have shown the feasibility of such a system to study single cells and chromosomes. Since these first studies, others have used comparable systems to study different cell types and their organelles. Confocal Raman spectroscopy was used to distinguish different types of bone cell lines commonly used in tissue engineering of bone, in order to develop a phenotypic identification method⁷⁰. The authors showed the feasibility of using confocal Raman microscopy to identify phenotype differences between human primary osteoblasts (HOB), SV40 transfected human alveolar bone

cells (SV40 AB) and osteoblast like human osteosarcoma MG63 cells *in vitro*. By using complex statistical analysis techniques they were able to classify 70% of all the cells observed correctly, based upon spectral differences determined by principal component analysis techniques. Although this number seems not to be extremely high, the interpretation of minute differences in the obtained spectra and the fact that single cell Raman measurements are still very technical strenuous enterprises makes it a very promising study for future research into topics as cell differentiation. Spectroscopy has been used in some studies to monitor cell proliferation and differentiation based upon the biochemical differences detected. For instance, Fourier transform infrared (FTIR) and Raman spectroscopy have been used to study proliferation of mammalian cells. FTIR measurements on different Rat fibroblast cell lines revealed that the ratio of RNA versus lipid and protein versus lipid of all cell lines increased when they were in the exponential phase of growth. These findings were confirmed by using Raman spectroscopy on the nuclei and cells derived from the same cell lines⁷¹. Moreover, the Raman data provided also detailed information about the distribution of lipid, protein, RNA and DNA in cells and nuclei. Confocal Raman measurements of murine embryonic stem cells revealed that undifferentiated and differentiated cells could be easily distinguished from each other by simply comparing their respective Raman spectra. It was found that differentiated cells had a higher RNA content than non differentiated cells, which reflected results found in previous studies on embryonic stem cells. An alternative system to study bone mineralization is the osteoblast culture. Osteoblasts are highly specialized cells involved in bone formation by producing a collagen type I containing extra cellular matrix which in turn calcifies. Primary mouse calvarial osteoblasts exhibited signs of mineralization comparable to poorly carbonated apatite after 8 days of culture in osteogenic medium, which was represented by the presence of Raman bands belonging to phosphate (960 and 1030 cm^{-1}) and B-type carbonate (1070 cm^{-1})⁷². In addition it was found that in

time the amount of carbonate increased slightly as the intensity of the carbonate specific Raman band increased which mimics more or less the development found in young mouse bone.

As was mentioned before, materials used for orthopaedic implants in bone replacement must be gradually resorbable so that they can be replaced by new bone. In bone, osteoclasts play a major role in the resorption of bone during bone remodelling. Redey and coworkers showed that crystals of type B carbonated apatite could be found in the resorption pits formed by osteoclasts on the surface of calcium carbonate by confocal Raman spectroscopy, while this could not be found in control bone slices, or pure HA⁷³. This indicated that not only calcium carbonate could be readily absorbed by these cells but that the surface changes induced by these cells could also be easily detected by using non destructive Confocal Raman microscopy. Another application of Confocal Raman spectroscopy for the analysis of biomaterials was published by de Grauw et al.⁷⁴, who showed that the physical state (being crystalline or amorphous) of a plasma sprayed calcium phosphate coating can be examined by using this technique. They established that the local degree of crystallinity in various heat treated plasma spray coatings could be determined with a precision of 0.7%. The examples of studies dedicated to bone and bone tissue engineering where Raman spectroscopy and confocal Raman microscopy is used as an important investigative tool, in order to gain in depth information on either the behaviour of cells or materials, given in this chapter prove that Raman spectro- and microscopy can be a valuable analysis method in the field of tissue engineering. The usage of different materials and biological components in this field of research provides an excellent opportunity for the usage of Raman microscopy, while this technique can provide physicochemical information on both topics in a relatively easy manner.

References

1. Katholieke Radio Omroep, De grootste Nederlander. <http://www.degrootstenederlander.nl> 2004.
2. Chapman, A., England's Leonardo: Robert Hooke (1635-1703) and the art of experiment in Restoration England. *Proceedings of the Royal Institution of Great Britain* 1996, 67, 239 - 275.
3. van Leeuwenhoek, A., Letter no. 11. *Philosophical Transactions* 1674, IX, (108), 178-182.
4. The Nobel Foundation, Nobelprize.org. www.nobelprize.org 2005.
5. Minsky, M. Microscopy Apparatus. US patent no. 3013467, 19 Dec. 1961, 1961.
6. Minsky, M., Memoir on Inventing the Confocal Scanning Microscope. *Scanning* 1988, 10, 128-138.
7. Davidovits, P.; Egger, M. D., Scanning laser microscope. *Nature* 1969, 223, (208), 831.
8. Brakenhoff, G. J.; van Spronsen, E. A.; van der Voort, H. T.; Nanninga, N., Three-dimensional confocal fluorescence microscopy. *Methods Cell Biol* 1989, 30, 379-98.
9. Brakenhoff, G. J.; van der Voort, H. T.; van Spronsen, E. A.; Nanninga, N., 3-dimensional imaging of biological structures by high resolution confocal scanning laser microscopy. *Scanning Microsc* 1988, 2, (1), 33-40.
10. Brakenhoff, G. J.; van der Voort, H. T.; Baarslag, M. W.; Mans, B.; Oud, J. L.; Zwart, R.; van Driel, R., Visualization and analysis techniques for three dimensional information acquired by confocal microscopy. *Scanning Microsc* 1988, 2, (4), 1831-8.
11. Brakenhoff, G. J.; van der Voort, H. T.; van Spronsen, E. A.; Nanninga, N., Three-dimensional imaging by confocal scanning fluorescence microscopy. *Ann N Y Acad Sci* 1986, 483, 405-15.
12. Valkenburg, J. A.; Woldringh, C. L.; Brakenhoff, G. J.; van der Voort, H. T.; Nanninga, N., Confocal scanning light microscopy of the Escherichia coli nucleoid: comparison with phase-contrast and electron microscope images. *J Bacteriol* 1985, 161, (2), 478-83.
13. Brakenhoff, G. J.; van der Voort, H. T.; van Spronsen, E. A.; Linnemans, W. A.; Nanninga, N., Three-dimensional chromatin distribution in neuroblastoma nuclei shown by confocal scanning laser microscopy. *Nature* 1985, 317, (6039), 748-9.
14. Grond, C. J.; Derksen, J.; Brakenhoff, G. J., The banding pattern of the segment 46A-48C in Drosophila hydei polytene chromosomes as studied by confocal scanning light microscopy (CSLM). *Exp Cell Res* 1982, 138, (2), 458-62.
15. Ruska, E., [A modern electron microscope.]. *Minerva Med* 1955, 46, (18), 597-9.
16. Ruska, E., [Memories of the beginnings of electron microscopy]. *Arb Paul Ehrlich Inst Georg Speyer Haus Ferdinand Blum Inst Frankf A M* 1970, 66, 19-34.
17. Ruska, E., The early development of electron lenses and electron microscopy. *Microsc Acta Suppl* 1980, (Suppl 5), 1-140.
18. Ruska, E., Nobel lecture. The development of the electron microscope and of electron microscopy. *Biosci Rep* 1987, 7, (8), 607-29.
19. Ruska, E., www.ernst.ruska.de 1998.

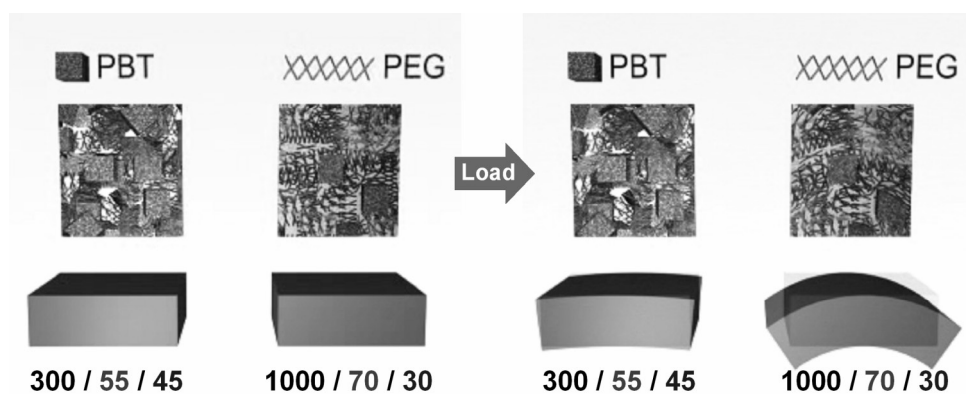
20. C. V. Raman; Krishnan, K. S., A New Type of Secondary Radiation. *Nature* 1928, 121(3048), 501.
21. Pelletier, M. J., *Analytical applications of Raman spectroscopy*. first ed.; Blackwell Science Ltd.: Oxford, 1999; p 1-478.
22. Long, D. A., *The Raman effect: A unified treatment of the theory of Raman scattering by molecules*. ed.; John Wiley and Sons Ltd.: Chichester, UK, 2002; p 1-624.
23. Lin-Vien, D.; Colthup, N. B.; Fateley, W. G.; Grasselli, J. G., *The handbook of infrared and Raman characteristic frequencies of organic molecules*. ed.; Academic Press: San Diego, USA, 1991; p 1-499.
24. Puppels, G. J.; de Mul, F. F.; Otto, C.; Greve, J.; Robert-Nicoud, M.; Arndt-Jovin, D. J.; Jovin, T. M., Studying single living cells and chromosomes by confocal Raman microspectroscopy. *Nature* 1990, 347, (6290), 301-3.
25. Aksenov, Y. Raman microscopy in an electron microscope: combining chemical and morphological analyses. Doctoral thesis, University of Twente, Enschede, The Netherlands, 2003.
26. Tamada, J. A.; Langer, R., Erosion Kinetics of Hydrolytically Degradable Polymers. *PNAS* 1993, 90, (2), 552-556.
27. D.W. Grijpma, P. B. M., Fac. Technological Sciences, University of Twente, The Netherlands, Personal communication. 2005.
28. Wang, C.-H.; Fan, K.-R.; Hsiue, G.-H., Enzymatic degradation of PLLA-PEOZ-PLLA triblock copolymers. 2005, 26, (16), 2803.
29. Deschamps, A.; van Apeldoorn, A.; Hayen, H.; de Bruijn, J.; Karst, U.; Grijpma, D.; Feijen, J., In vivo and in vitro degradation of poly(ether ester) block copolymers based on poly(ethylene glycol) and poly(butylene terephthalate). *Biomaterials* 2004, 25, (2), 247-258.
30. Deschamps, A. A. Segmented Poly (ether ester)s and poly (ether ester amide)s for use in tissue engineering. Doctoral, University of Twente, The Netherlands, Enschede, The Netherlands, 2002.
31. Grote, J. J.; Bakker, D.; Hesseling, S. C.; van Blitterswijk, C. A., New alloplastic tympanic membrane material. *Am J Otol* 1991, 12, (5), 329-35.
32. van Dorp, A. G.; Verhoeven, M. C.; Koerten, H. K.; van Blitterswijk, C. A.; Ponec, M., Bilayered biodegradable poly(ethylene glycol)/poly(butylene terephthalate) copolymer (Polyactive) as substrate for human fibroblasts and keratinocytes. *J Biomed Mater Res* 1999, 47, (3), 292-300.
33. Beumer, G.; van, B. C.; Bakker, D.; Ponec, M., A new biodegradable matrix as part of a cell seeded skin substitute for the treatment of deep skin defects: a physico-chemical characterisation. *Clin Mater* 1993, 14, (1), 21-7.
34. Beumer, G.; van, B. C.; Ponec, M., Biocompatibility of a biodegradable matrix used as a skin substitute: an in vivo evaluation. *J Biomed Mater Res* 1994, 28, (5), 545-52.
35. Beumer, G. J.; van Blitterswijk, C. A.; Bakker, D.; Ponec, M., A new biodegradable matrix as part of a cell seeded skin substitute for the treatment of deep skin defects: a physico-chemical characterisation. *Clin Mater* 1993, 14, (1), 21-7.

36. Beumer, G. J.; van Blitterswijk, C. A.; Ponec, M., Biocompatibility of a biodegradable matrix used as a skin substitute: an in vivo evaluation. *J Biomed Mater Res* 1994, 28, (5), 545-52.
37. van Dorp, A. G.; Verhoeven, M. C.; Koerten, H.; van der Nat-van der Meij, T. H.; van Blitterswijk, C. A.; Ponec, M., Dermal regeneration in full-thickness wounds in Yucatan miniature pigs using a biodegradable copolymer. *Wound Repair Regen* 1998, 6, (6), 556-68.
38. van Dorp, A. G.; Verhoeven, M. C.; Koerten, H. K.; van Blitterswijk, C. A.; Ponec, M., Bilayered biodegradable poly(ethylene glycol)/poly(butylene terephthalate) copolymer (Polyactive) as substrate for human fibroblasts and keratinocytes. *J Biomed Mater Res* 1999, 47, (3), 292-300.
39. van Dorp, A. G.; Verhoeven, M. C.; Koerten, H. K.; Van Der Nat-Van Der Meij, T. H.; Van Blitterswijk, C. A.; Ponec, M., Dermal regeneration in full-thickness wounds in Yucatan miniature pigs using a biodegradable copolymer. *Wound Repair Regen* 1998, 6, (6), 556-68.
40. Xiao, Y. L.; Riesle, J.; Van Blitterswijk, C. A., Static and dynamic fibroblast seeding and cultivation in porous PEO/PBT scaffolds. *J Mater Sci Mater Med* 1999, 10, (12), 773-7.
41. Malda, J.; Woodfield, T. B.; van der Vloodt, F.; Kooy, F. K.; Martens, D. E.; Tramper, J.; van Blitterswijk, C. A.; Riesle, J., The effect of PEGT/PBT scaffold architecture on oxygen gradients in tissue engineered cartilaginous constructs. *Biomaterials* 2004, 25, (26), 5773-80.
42. Malda, J.; Woodfield, T. B.; van der Vloodt, F.; Wilson, C.; Martens, D. E.; Tramper, J.; van Blitterswijk, C. A.; Riesle, J., The effect of PEGT/PBT scaffold architecture on the composition of tissue engineered cartilage. *Biomaterials* 2005, 26, (1), 63-72.
43. Woodfield, T. B.; Bezemer, J. M.; Pieper, J. S.; van Blitterswijk, C. A.; Riesle, J., Scaffolds for tissue engineering of cartilage. *Crit Rev Eukaryot Gene Expr* 2002, 12, (3), 209-36.
44. Woodfield, T. B.; Malda, J.; de Wijn, J. R.; Peters, F.; Riesle, J.; van Blitterswijk, C. A., Design of porous scaffolds for cartilage tissue engineering using a three-dimensional fiber-deposition technique. *Biomaterials* 2004, 25, (18), 4149-61.
45. Bouwmeester, S. J.; Kuijer, R.; Sollie-Drees, M. M.; van der Linden, A. J.; Bulstra, S. K., Quantitative histological analysis of bony ingrowth within the biomaterial Polyactive implanted in different bone locations: an experimental study in rabbits. *J Mater Sci Mater Med* 1998, 9, (4), 181-5.
46. Bulstra, S. K.; Geesink, R. G.; Bakker, D.; Bulstra, T. H.; Bouwmeester, S. J.; van der Linden, A. J., Femoral canal occlusion in total hip replacement using a resorbable and flexible cement restrictor. *J Bone Joint Surg Br* 1996, 78, (6), 892-8.
47. Kellomaki, M.; Niiranen, H.; Puumanen, K.; Ashammakhi, N.; Waris, T.; Tormala, P., Bioabsorbable scaffolds for guided bone regeneration and generation. *Biomaterials* 2000, 21, (24), 2495-505.
48. Kuijer, R.; Bouwmeester, S. J.; Drees, M. M.; Surtel, D. A.; Terwindt-Rouwenhorst, E. A.; Van Der Linden, A. J.; Van Blitterswijk, C. A.; Bulstra, S. K., The polymer

- Polyactive as a bone-filling substance: an experimental study in rabbits. *J Mater Sci Mater Med* 1998, 9, (8), 449-55.
49. Li, P.; Bakker, D.; van Blitterswijk, C., The bone-bonding polymer Polyactive 80/20 induces hydroxycarbonate apatite formation in vitro. *J Biomed Mater Res* 1997, 34, (1), 79-86.
50. Meijer, G. J.; van Dooren, A.; Gaillard, M. L.; Dalmeijer, R.; de Putter, C.; Koole, R.; van Blitterswijk, C. A., Polyactive as a bone-filler in a beagle dog model. *Int J Oral Maxillofac Surg* 1996, 25, (3), 210-16.
51. Radder, A.; Leenders, H.; van Blitterswijk, C., Interface reactions to PEO/PBT copolymers (Polyactive) after implantation in cortical bone. *J Biomed Mater Res* 1994, 28, (2), 141-51.
52. Sackers, R.; Dalmeyer, R.; de Wijn, J.; van Blitterswijk, C., Use of bone-bonding hydrogel copolymers in bone: an in vitro and in vivo study of expanding PEO-PBT copolymers in goat femora. *J Biomed Mater Res* 2000, 49, (3), 312-8.
53. van Blitterswijk, C. A.; Bakker, D.; Hesselink, S. C.; Koerten, H. K., Reactions of cells at implant surfaces. *Biomaterials* 1991, 12, (2), 187-93.
54. Claase, M. B.; Grijpma, D. W.; Mendes, S. C.; De Bruijn, J. D.; Feijen, J., Porous PEOT/PBT scaffolds for bone tissue engineering: preparation, characterization, and in vitro bone marrow cell culturing. *J Biomed Mater Res A* 2003, 64, (2), 291-300.
55. Li, P.; Bakker, D.; van Blitterswijk, C. A., The bone-bonding polymer Polyactive 80/20 induces hydroxycarbonate apatite formation in vitro. *J Biomed Mater Res* 1997, 34, (1), 79-86.
56. Meijer, G. J.; Dalmeijer, R. A.; de Putter, C.; van Blitterswijk, C. A., A comparative study of flexible (Polyactive) versus rigid (hydroxylapatite) permucosal dental implants. II. Histological aspects. *J Oral Rehabil* 1997, 24, (2), 93-101.
57. Du, C.; Klasens, P.; Haan, R.; Bezemer, J.; Cui, F.; de Groot, K.; Layrolle, P., Biomimetic calcium phosphate coatings on Polyactive 1000/70/30. *J Biomed Mater Res* 2002, 59, (3), 535-46.
58. Du, C.; Meijer, G. J.; van de Valk, C.; Haan, R. E.; Bezemer, J. M.; Hesselink, S. C.; Cui, F. Z.; de Groot, K.; Layrolle, P., Bone growth in biomimetic apatite coated porous Polyactive 1000PEGT70PBT30 implants. *Biomaterials* 2002, 23, (23), 4649-56.
59. Claase, M. B.; Olde Riekerink, M. B.; de Bruijn, J. D.; Grijpma, D. W.; Engbers, G. H.; Feijen, J., Enhanced bone marrow stromal cell adhesion and growth on segmented poly(ether ester)s based on poly(ethylene oxide) and poly(butylene terephthalate). *Biomacromolecules* 2003, 4, (1), 57-63.
60. Mendes, S. C.; Bezemer, J.; Claase, M. B.; Grijpma, D. W.; Bellia, G.; Degli-Innocenti, F.; Reis, R. L.; de Groot, K.; van Blitterswijk, C. A.; de Bruijn, J. D., Evaluation of Two Biodegradable Polymeric Systems as Substrates for Bone Tissue Engineering. *Tissue Engineering* 2003, 9, (supplement 1), 91.
61. Morris, M.; Tarnowski, C.; Timlin, J., Multivariate Raman microscopy: application to biological materials and synthetic materials. *Microbeam Analysis 2000, Proceedings* 2000, (165), 55-56.
62. Timlin, J.; Carden, A.; Morris, M., Chemical microstructure of cortical bone probed by Raman transects. *Applied Spectroscopy* 1999, 53, (11), 1429-1435.

63. Timlin, J.; Carden, A.; Morris, M.; Bonadio, J.; Hoffler, C.; Kozloff, K.; Goldstein, S., Spatial distribution of phosphate species in mature and newly generated mammalian bone by hyperspectral Raman imaging. *Journal of Biomedical Optics* **1999**, 4, (1), 28-34.
64. Schulze, K. A.; Balooch, M.; Balooch, G.; Marshall, G. W.; Marshall, S. J., Micro-Raman spectroscopic investigation of dental calcified tissues. *J Biomed Mater Res A* **2004**, 69, (2), 286-93.
65. Carden, A.; Rajachar, R.; Morris, M.; Kohn, D., Ultrastructural changes accompanying the mechanical deformation of bone tissue: a Raman imaging study. *Calcif Tissue Int* **2003**, 72, (2), 166-75.
66. Akkus, O.; Adar, F.; Schaffler, M. B., Age-related changes in physicochemical properties of mineral crystals are related to impaired mechanical function of cortical bone. *Bone* **2004**, 34, (3), 443-53.
67. Puppels, G. J.; Garritsen, H. S.; Kummer, J. A.; Greve, J., Carotenoids located in human lymphocyte subpopulations and natural killer cells by Raman microspectroscopy. *Cytometry* **1993**, 14, (3), 251-6.
68. Puppels, G. J.; Garritsen, H. S.; Segers-Nolten, G. M.; de Mul, F. F.; Greve, J., Raman microspectroscopic approach to the study of human granulocytes. *Biophys J* **1991**, 60, (5), 1046-56.
69. Puppels, G. J.; Olminkhof, J. H.; Segers-Nolten, G. M.; Otto, C.; de Mul, F. F.; Greve, J., Laser irradiation and Raman spectroscopy of single living cells and chromosomes: sample degradation occurs with 514.5 nm but not with 660 nm laser light. *Exp Cell Res* **1991**, 195, (2), 361-7.
70. Notingher, I.; Jell, G.; Lohbauer, U.; Salih, V.; Hench, L. L., In situ non-invasive spectral discrimination between bone cell phenotypes used in tissue engineering. *J Cell Biochem* **2004**, 92, (6), 1180-92.
71. Short, K. W.; Carpenter, S.; Freyer, J. P.; Mourant, J. R., Raman Spectroscopy Detects Biochemical Changes Due to Proliferation in Mammalian Cell Cultures. *Biophysical Journal* **2005**, 4274-4288.
72. Stewart, S.; Shea, D.A.; Tarnowski, C.P.; Morris, M.D.; Wang, D.; Francheschi, R.; Lin, D.L.; Keller, E., Trends in early mineralization of murine calvarial osteoblastic cultures: a raman microscopic study. *Journal of raman spectroscopy* **2002**, 33, 536-543.
73. Redey, S.; Razzouk, S.; Rey, C.; Bernache-Assollant, D.; Leroy, G.; Nardin, M.; Cournot, G., Osteoclast adhesion and activity on synthetic hydroxyapatite, carbonated hydroxyapatite, and natural calcium carbonate: relationship to surface energies. *J Biomed Mater Res* **1999**, 45, (2), 140-7.
74. de Grauw, C. J.; Otto, C.; Greve, J.; de Bruijn, J.D., Investigation of Bone and Calcium Phosphate Coatings, and crystallinity Determination using Raman Microspectroscopy. *Cells and materials* **1996**, 6, (1-3), 57-62.

Characterization of PEOT PBT block copolymers by confocal Raman spectroscopy



Schematic representation of the distribution of amorphous polyethyleneglycol terephthalate (PEOT), soft block, and crystalline polybutylene terephthalate (PBT), hard block, within PEOT PBT materials. By varying the PEG molecular weight (300 or 1000 in the example), and the wt% ratio of PEOT to PBT (55/45 or 70/30 in the example), a range of polymers can be obtained with different mechanical and degradation properties. Higher PEG MW and wt% PEOT content (i.e. 1000/70/30) results not only in a decrease in material stiffness, but also in a higher degradability.

Abstract

In this study the feasibility of using confocal Raman spectroscopy for the analysis of PEOT PBT block copolymer degradation was investigated. PEOT PBT block copolymers are thermoplastic elastomers, composed of soft hydrophilic segment called poly ethylene glycol terephthalate (PEOT) and a hard hydrophobic segment called poly butylene terephthalate (PBT). The material properties, i.e. stiffness, thermal behaviour and degradability, can be tailored by either varying the molecular weight of PEG, used for the production of these polymers and/or the PEOT to PBT mass ratio in the polymer. PEOT PBT copolymers are currently being used as degradable materials for the use in medicine and are sold under the brand name Polyactive™. A number of studies have shown the good biocompatibility of PEOT PBT made materials *in vitro* as well as *in vivo* in several different animals varying from rats to goats. Since the unique composition of these materials allows for the preparation of devices with a broad range of physical and biological properties, these materials are intensively being studied for tissue engineering applications. Several destructive chemical analysis techniques, i.e. nucleio magnetic resonance spectroscopy, gel permeation chromatography and differential scanning calorimetry, have been used in the past to study the degradation of these polymers. However, when valuable morphological information is needed to examine the effect of degradation on tissue engineering a non destructive analysis technique is preferred. Raman spectroscopy is a non destructive molecular analysis technique which uses a monochromatic light source for the detection of wavelength shifts caused by chemical bond vibrations. Until now, no studies have been done on PEOT PBT polymers by using Raman spectroscopy. Therefore it is necessary to characterize Raman spectra obtained from these polymers, not only to gain knowledge about their spectral properties for future analysis, but also to check the feasibility of using this analysis technique for studying these materials. We used a custom made confocal Raman microscope to analyze a series of different

copolymer compositions and basic building blocks from which PEOT PBT copolymers are composed in order to characterize spectra of PEOT PBT copolymers. Furthermore, we studied the degradation of 1000 PEOT70PBT30 copolymers in a fast *in vitro* degradation model by using the Raman band assignments found in this study.

Characterization of PEOT PBT block copolymers by confocal Raman spectroscopy

A.A. van Apeldoorn¹, J. de Wijn¹, Y. Aksenov², F.L.A.M.A. Peters³, C. Otto², C.A. van Blitterswijk¹

¹Department of Polymer Chemistry and Biomaterials, Faculty of Technology and Sciences, University of Twente, PO Box 98, 3720AB Bilthoven, the Netherlands,

²Department of Biophysical Techniques, Faculty of Technology and Sciences, University of Twente, PO Box 217, 7500AE Enschede, The Netherlands, Isotis NV, PO Box 98, 3720AB Bilthoven, The Netherlands

Introduction

Degradation of (bio)materials is especially important in tissue engineering, the general accepted idea is that the ideal tissue engineering scaffold is composed of a degradable material which can support cells and/or tissue in such a way that suitable time is left to heal a defect effectively, while the (bio)material is replaced by newly formed tissue. Techniques by which degradation can be studied non-destructively are preferred because valuable histological information remains, which can provide valuable information about morphologic changes. Raman spectroscopy uses a monochromatic light source to study molecular vibrations, thus providing specific information about chemical bonds in a non invasive manner. Raman spectroscopy is based on the Raman effect, which is the inelastic scattering of photons by molecules. The energy of the scattered radiation is less or more than the incident radiation. Moreover, the energy increase or decrease from the excitation is related to the vibrational energy spacing in the ground electronic state of a molecule. Therefore, the wavenumbers in Raman spectra are a direct measure of the vibrational energies of the chemical bonds in a molecule thus allowing for molecular analysis. A major part of the (bio)materials used in tissue engineering are

composed of synthetic polymers. Polymers enable the design of scaffolds for tissue-engineering with different mechanical and biological properties and degradation rates depending on the requirements of their application. The physical and chemical properties have to be tailored in such a way that these meet the demands of the implant site. Thermoplastic elastomers composed of polyethylene oxide terephthalate (PEOT) and polybutylene-terephthalate (PBT) have been studied extensively to be used as a biomaterial¹⁻⁶ for tissue engineering applications. The polymer is a block copolymer composed of a hard PBT block and a soft hydrophilic PEOT block. The soft to hard block ratio and the molecular weight of polyethyleneglycol (PEG) can be varied to change elasticity, swelling and degradation of the material. The use of several different compositions of PEOT PBT polymers has been studied in relation to bone healing⁷⁻¹⁰, cartilage repair¹¹⁻¹⁵, design of material composites^{16, 17}, skin wound repair¹⁸⁻²² and even as a tissue engineering scaffold for artificial fish skin²³. As no studies have been performed on PEOT PBT polymers by Raman spectroscopy in the past, it is necessary to characterize Raman spectra obtained from these polymers, in order to gain knowledge about their spectral properties for future analysis, and to check the feasibility of using this analysis technique for studying these materials as well. We have used a custom made confocal Raman microscope to analyze a series of different copolymer compositions and basic building blocks from which PEOT PBT copolymers are composed in order to characterize spectra of PEOT PBT copolymers. Furthermore we studied the degradation of 1000 PEOT70PBT30 copolymers in a fast *in vitro* degradation model by using the Raman band assignments found in this study.

Materials and methods

The materials used in this study were either compression molded blocks (in case of block copolymers) or pure chemicals. The copolymers are composed of Polyethylene oxide terephthalate (PEOT) and poly butylene terephthalate (PBT) (see

figure 1). The initial length of the polyethylene oxide (PEG) segment can be varied, as can be the molar ratio of the PEOT to PBT segments. The composition is denoted as $a / b / c$, where a represents the poly(ethylene glycol) (PEG) molecular weight (MW g/mol), and b and c represent the weight percentage (wt%) of PEGT and PBT blocks respectively.

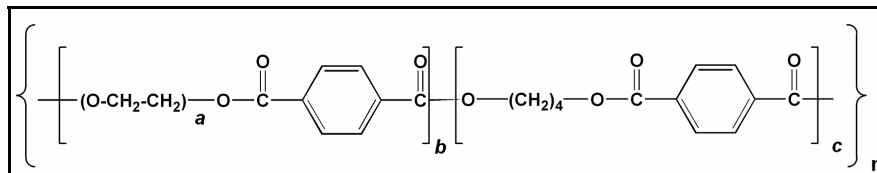


Figure 1: Molecular formula of PEOT/PBT block copolymers.

Reference Raman spectra from different polymer compositions and their building blocks were generated by using confocal Raman spectroscopy on dense blocks or gels (in case of Polyethylene glycol). The following pure chemicals were measured: Dimethyl terephthalate (DMT), Polybutylene terephthalate, Polyethyleneglycol (m.w. 1000) (PEG). In addition, a range of different copolymer compositions, as depicted in table 1, were measured in order to gain insight into band positions.

Polymer type (x /PEOT a /PBT b)	Specifications (mw and mass-ratio)
300/80/20	PEG mw 300, PEOT:PBT=8:2
600/80/20	PEG mw 600, PEOT:PBT=8:2
1000/80/20	PEG mw 1000, PEOT:PBT=8:2
4000/30/70	PEG mw 4000, PEOT:PBT=3:7
4000/55/45	PEG mw 4000, PEOT:PBT=5,5:2,5
4000/80/20	PEG mw 4000, PEOT:PBT=8:2
10000/80/20	PEG mw 10000, PEOT:PBT=8:2

Table 1: PEOT/PBT block copolymer compositions used for analysis

Degradation

In vitro fast degradation was carried out with 1000/70/30 material in Borax buffer, pH 10 at 50 °C. The samples were incubated for 0, 1, 2, 3, 10, 14, 21, 28 and 42

days, after which they were analyzed by Raman spectroscopy and gel permeation chromatography (GPC).

Confocal Raman spectroscopy

We used a in house build confocal Raman spectroscopy, which was integrated with a scanning electron microscope (Philips XL-30 FEG). The system operates as follows; a collimated and circularly symmetrical beam from a diode laser (LD) with a frequency of 685nm is reflected by a dichroic beam splitter (BS) into the vacuum chamber of the SEM through a coupling window (CW). The beam is then focused by a 60X objective(MO), $na=0.65$, on a sample of interest. The excited Raman scattering is collected by the same objective and the Stokes components of Raman frequencies pass through the BS and a notch filter (NF), which blocks photons with the initial laser wavelength. Subsequently, the scattering is focussed by a small lens on a pinhole (\varnothing 25 μ m) allowing for confocality of the system. The scattering is then collected in a spectrograph-monochromator where the incoming light is decomposed by a concave holographic diffraction grating and focused on a thermo-electrically cooled CCD (1056x256 pixels, Princeton Instruments Spec10). The theoretical spatial resolution of the system is ~ 700 nm with an effective laser power of around 6mW on the sample. The CCD is connected with a computer for data collection and analysis using WinSpec (Roper Scientific Inc., USA) and Microcal Origin (Microcal software inc., USA) data analysis software.

Results

Raman spectra were collected of the building blocks of the block copolymer to have a reference for the active Raman bands present in these molecules. The collected spectra of PBT, poly(ethylene glycol) (PEG) and dimethylterephthalate (DMT) show several prominent bands which are summarized in table 2. The average spectrum of the 3 components was also calculated and is very similar to the spectra of the actual block copolymer (see figure 2).

<i>Raman shift (cm⁻¹)</i>	<i>Group assignment</i>	<i>Ref.</i>
630	aromatic	35
705	u aromatic ring	35
800	u aromatic C-H out of plane, rCH ₂	36, 37
845	rCH ₂ , gauche-trans-gauche glycol, C-C aromatic	24, 36
888-890	rCH ₂ , u CO _(vw)	36-38
964		
1045	u CO, rCH ₂ , u C-C in PEG	36
1107		
1180		
1285	tCH ₂ , u C-H	24, 36
1310		
1400-1480	srCH ₂ , u C-H	24, 36
1620	u C=C aromatic ring	39
1725	u C=O	40

Table 2: Molecular group assignments of Raman bands present in PEOT PBT spectra.

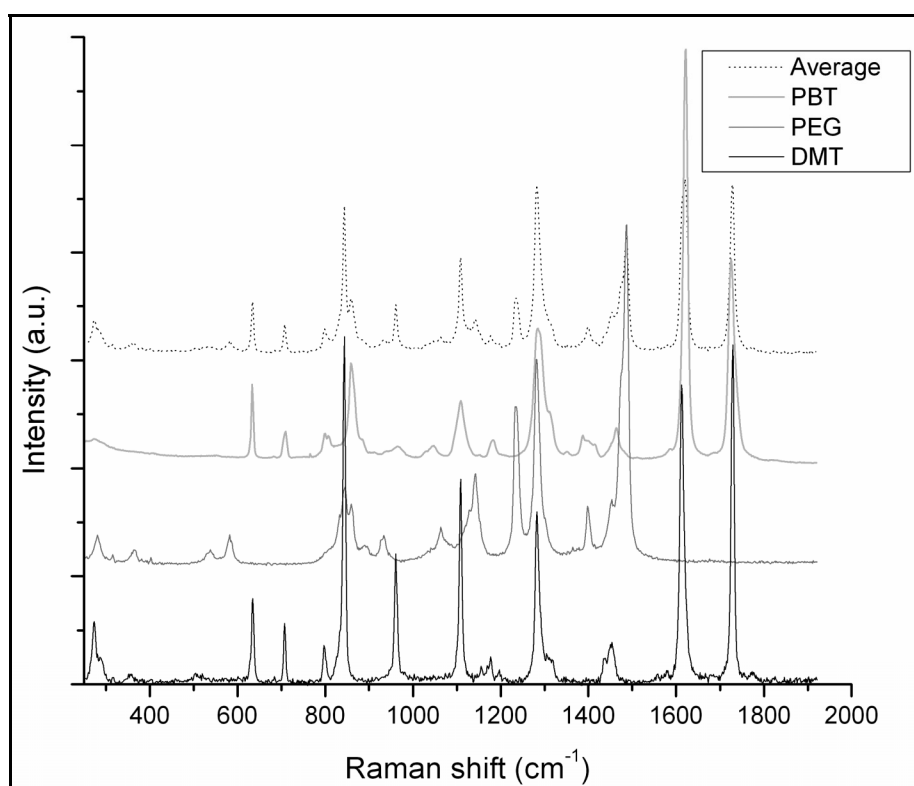


Figure 2: Raman spectra of PBT, PEG and DMT and the resultant average spectrum of the three spectra.

In figure 3 one can observe that the spectra obtained from block copolymers with similar mass ratio (PEOT:PBT=80:20) composition, but with different mw of the PEG component, show an increase in intensity of Raman bands specific for PEO at 840-850 cm^{-1} (skeleton vibrations²⁴), 1050-1120 cm^{-1} (mainly CH_2 vibrations), 1230-1280 cm^{-1} (C-H and CH_2 vibrations) and 1430-1480 cm^{-1} (CH_2 and C-H vibrations).

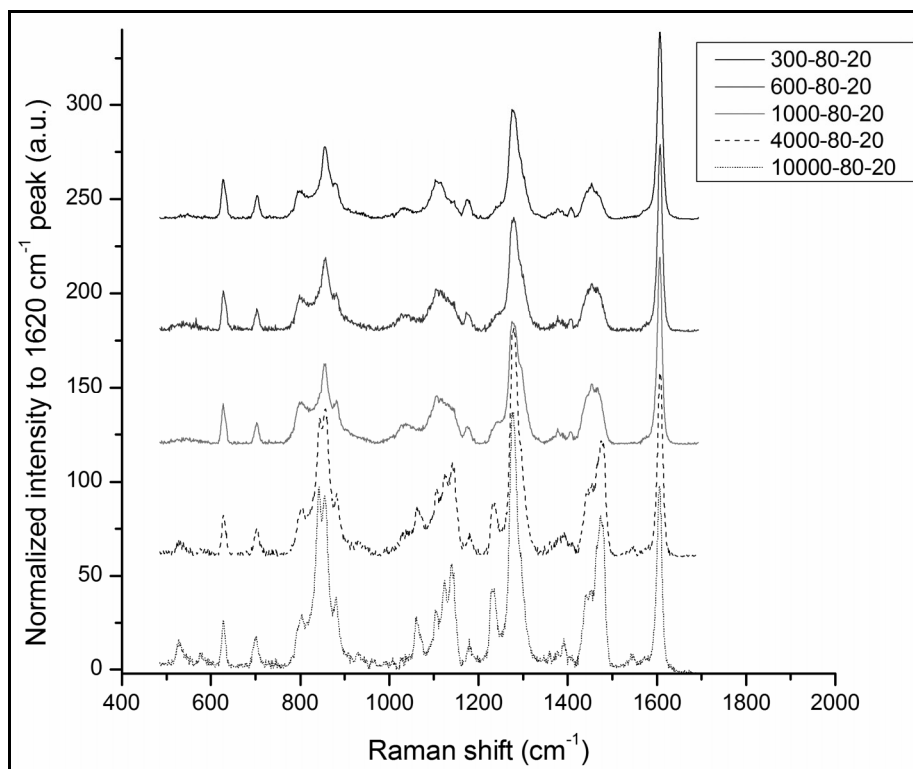


Figure 3: Raman spectra of PEOT PBT block copolymers with similar mass ratio but different molecular weight of PEG.

One has to keep in mind that the intensity of the Raman band at 1620 cm^{-1} belonging to the aromatic ring group, a fairly constant moiety in the polymer, was set at 100% to have a fair comparison between the different polymer compositions. Interestingly, the polymers with a PEG molecular weight of 300 to 1000, do not appear to show big spectral differences in their respective spectra, only around 1050-1120 cm^{-1} and the shoulder around 1230 cm^{-1} , which belong mainly to C-H

and CH_2 groups, show slight elevated intensities. The spectra of polymers with a PEG molecular weight of 4000 and 10000 however, show a major increase in intensity of PEG specific bands not only in comparison to the other polymers measured but also amongst themselves.

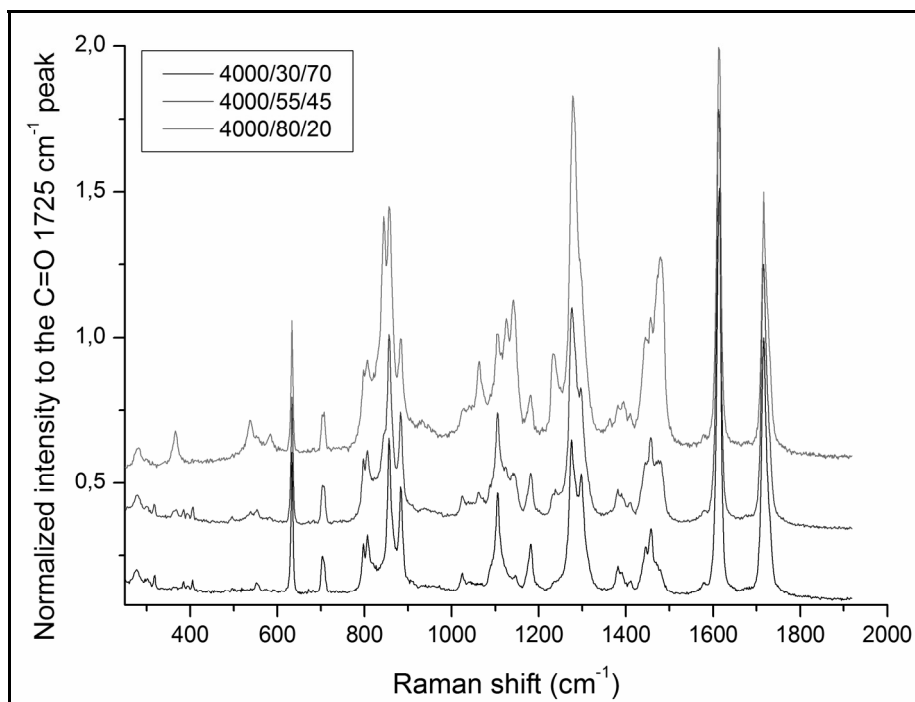


Figure 4: Raman spectra of PEOT/PBT block copolymer series with molecular weight of PEG of 4000, but with different mass ratios of PEOT and PBT.

In a similar manner a comparison was made of block copolymers with a molecular weight of PEG of 4000, but with different weight ratios of the PEOT and PBT blocks (see figure 4). Here we observed that with a relative low weight percentage of PEOT, the Raman bands specific for PBT contribute more to the total spectrum than when dealing with polymers containing a high percentage of PEOT blocks. The combination of these measurements leads to an assignment of PEOT and PBT specific Raman bands, summarized in table 3, meaning that the bands in the total spectra can be divided into two separate groups (of course with terephthalate as a constant factor in both groups). Since PBT and PEOT contain similar molecular

groups, contributions of both blocks to the total spectrum can be found at the same band position.

<i>Raman position (cm⁻¹)</i>	<i>band Copolymer assignment</i>	<i>moiety</i>
635	PBT, PEOT	
708	PBT, PEOT	
800	PBT, DMT	
843	PEOT	
859	PBT	
888	PBT	
1008	PBT	
1106	PBT	
1126	PEOT	
1062	PEOT	
1142	PEOT	
1179	PBT	
1232	PEOT	
1279	PEOT	
1300	PBT	
1448	PBT, PEO	
1465	PBT	
1478	PEOT	
1620	PBT, PEOT	
1724	PBT, PEOT	

Table 3: Raman band assignments of the PEOT and PBT block in PEOT PBT block copolymers.

Degradation study

As a model for fast *in vitro* degradation, samples of composed of 1000/70/30 polymers were incubated in Borax, pH 10 at 50°C, in order to simulate fast degradation in a short time span. The samples were observed at 0, 1, 2, 3, 10, 14, 21, 28 and 42 days after incubation (figure 5). Raman spectroscopy revealed that the intensity of the Raman band around 1280 cm⁻¹ decreases in time while the band at 1300 cm⁻¹ remains approximately the same. Another interesting trend occurring is that the shape of the Raman band around 1450 cm⁻¹ seems to become more sharper in time, indicative of a decrease in intensity of bands around this frequency since this a band composed of several active Raman frequencies.

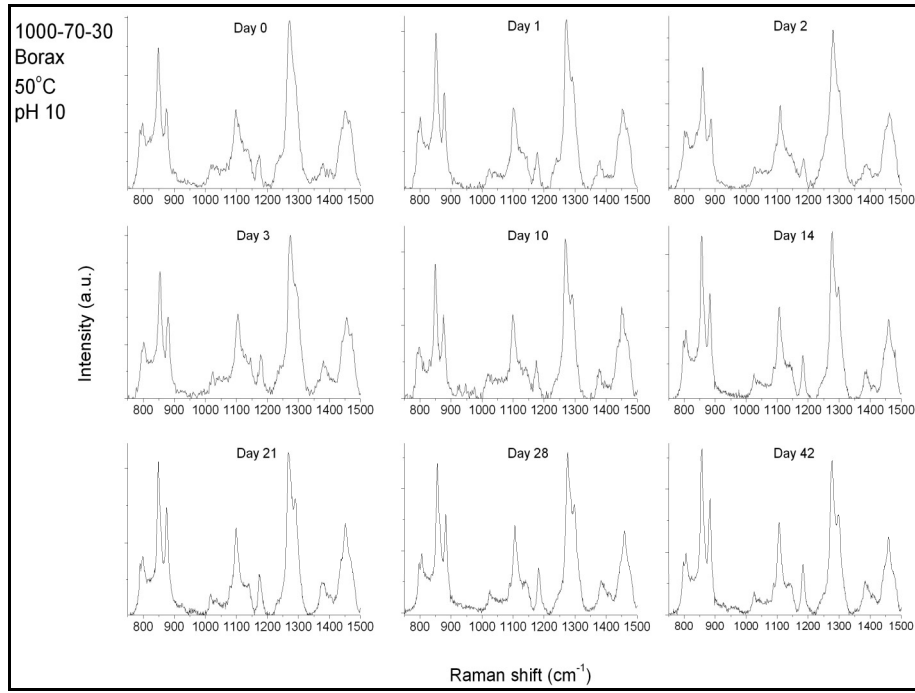


Figure 5: Raman spectra of *in vivo* implanted 1000/70/30 samples explanted at different time points.

Furthermore, the shape of the peak around 1100 cm^{-1} seems to slightly become more narrow, especially on the left hand side, indicating a decrease in intensity of a shoulder band around this position. In order to gain more knowledge of the differences observed, the spectra of non-degraded material (day 0) and degraded material (day 42) were subtracted from each other (after scaling to 1620 cm^{-1}). After subtraction, the resultant was smoothed using 10 point adjacent averaging to show only the major differences. Comparison of this data with spectra of PEG and PBT showed that after degradation bands specific for PEG have decreased, indicated by the negative intensities, implying a decrease in PEG content in these polymers (figure 6).

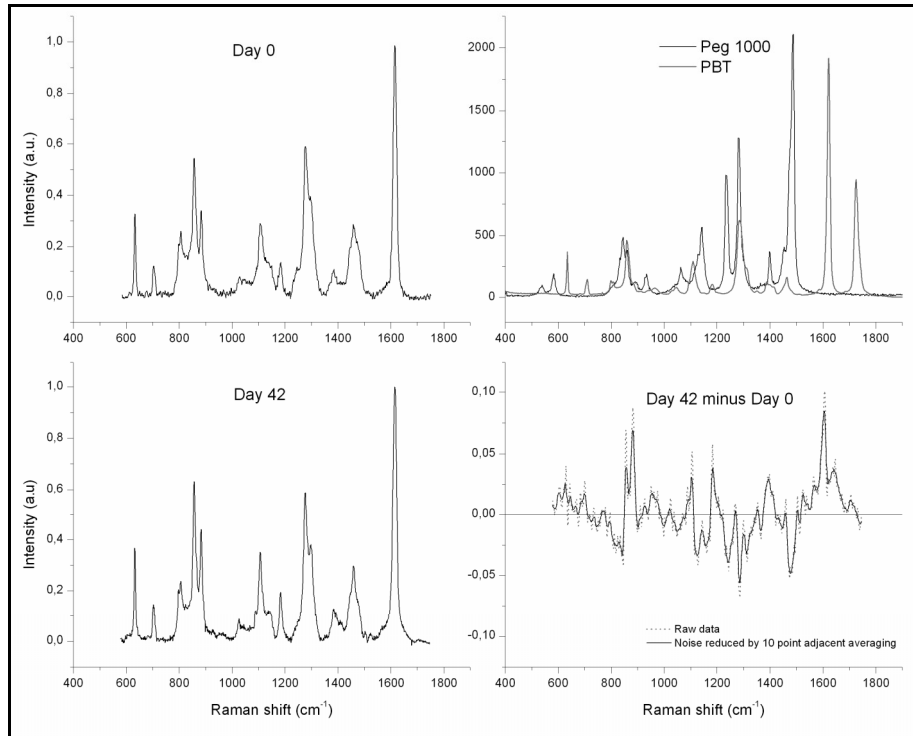


Figure 6: Comparison of Raman spectra of 1000/70/30 material before and after implantation (left panel). Raman spectra of PBT and PEG (top right panel). Difference spectrum of 1000/70/30 polymer (lower right panel) showing the intensity decrease of bands mainly belonging to PEO (under the x-axis) and bands belonging to mainly PBT (above the x-axis) after 42 days of implantation.

GPC

The relative molecular weight of the degraded polymer series was determined by GPC at each time point. The relative molecular weight, as can be observed in figure 5, has decreased to a plateau already after one week of degradation, according to an exponential decay model. Indicating that loss of PEO mainly occurs during the first week of fast *in vitro* degradation in our experimental model.

Discussion

Evaluation of Raman data

The use of polymers for tissue engineering has a direct influence on the properties of these materials. Depending on their use their physical and chemical properties have to be modified in such a manner that these meet the demands of the implant

location. Polyactive™ a poly(ether ester) copolymer composed of PEOT and PBT, has been studied in the past for its use in medicine. PEOT/PBT block copolymers have been investigated for their biocompatibility *in vivo* and no adverse tissue reactions have been observed after subcutaneous implantation studies in Goats^{19, 25}, rabbits¹⁰ and rats³. Cell adhesion, proliferation as well as differentiation of different cell types on these materials were found to be good especially after plasma treatment^{1, 2, 26, 27}. These poly(ether ester) copolymers can therefore be good candidates for scaffolds used in soft²⁸ and hard tissue engineering^{29, 30}.

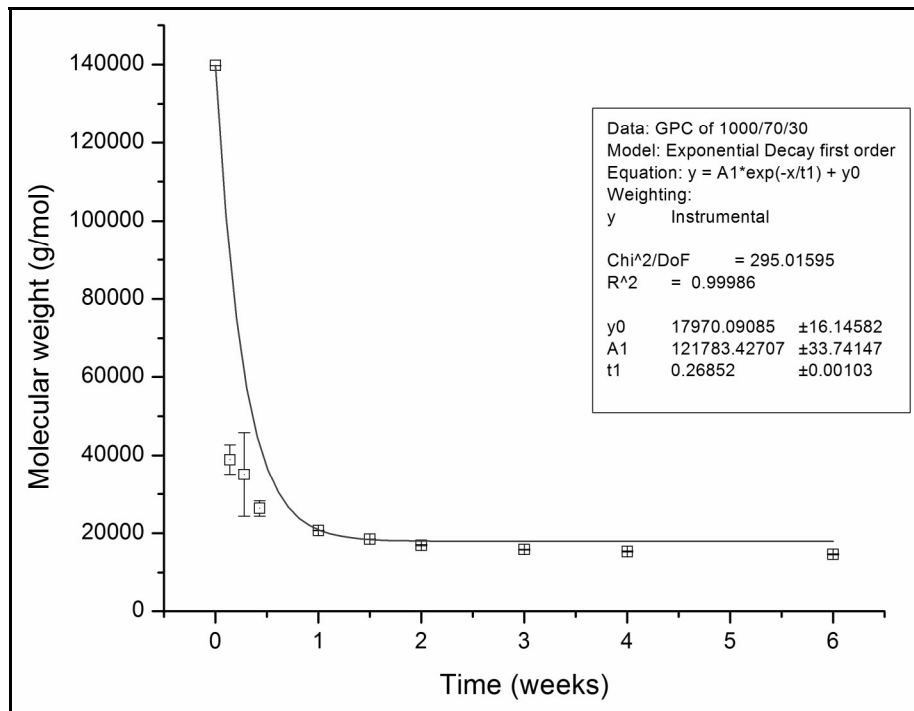


Figure 7: Change in the molecular weight of 1000/70/30 blockcopolymers in time after fast *in vitro* degradation in Borax at pH 10 and 50 °C

A prerequisite for biomaterials in tissue engineering is that they should be degradable so that the implanted material is gradually replaced in time by native tissue after implantation. In this study confocal Raman spectroscopy was used to

study PEOT/PBT block polymers in general and the degradation of 1000/70/30 block copolymers in a fast *in vitro* degradation model in more detail. In order to determine which Raman bands are specific for which molecular groups in the polymer spectra, measurements of the basic building block were taken and compared to the actual polymers. In figure 1 the average spectrum of PEG, PBT and DMT shows great similarity with the spectra from the different polymer compositions depicted in figure 3. We conclude that one can consider these polymers as being build up of separate molecular groups belonging to either PBT and/or PEO. The data obtained from the polymer series where the weight ratio of PEOT and PBT is kept equal (8:2), but the molecular weight of PEG is varied from 300-10000 g/mole (figure 3) clearly show an increase in intensity of PEO specific Raman bands at higher MW, which further supports our conclusion. Based on these results and what has been published by others on similar polymers, assignments of the different Raman bands could be made (a summary can be found in table 2). Moreover, we observed that Raman bands specific for PEG at 840-850 cm^{-1} (skeleton vibrations²⁴), 1050-1120 cm^{-1} (mainly CH_2 vibrations), 1230-1280 cm^{-1} (C-H and CH_2 vibrations) and 1430-1480 cm^{-1} (CH_2 and C-H vibrations) increase in intensity with increase of the molecular weight of PEG. Likewise, the intensity of these bands increases dramatically in polymers where the molecular weight of PEG is 4000 and higher. This is probably indicative of the increasing importance of the contribution of the PEO group vibrations to the total spectrum, caused by the fact that the chain length of PEO in these materials becomes very long (increase in the number of CH_2 groups) and therefore the skeletal vibrations become more important in these spectra, of these polymers. The clear increase in intensity of the band around 840-850 cm^{-1} specific for skeleton vibrations supports this finding.

Results obtained from polymers with molecular weight of PEG of 4000, but with different weight ratios of PEOT/PBT (figure 4) showed that the bands in the spectra can be divided into two separate groups, summarized in table 3, one belonging to the soft block and one to the hard block. The assignments made here are similar to what van Loon et al.³¹ found when studying PEOT PBT copolymers after intramuscular implantation in goats for 1 year by confocal Raman spectroscopy. Difficulty in the interpretation of these bands is that overlap of certain Raman band assigned to PBT or PEOT is caused by the fact that both groups contain similar molecular groups. These bands are mainly caused by similar C-H and CH₂ vibrations present in both blocks and which can therefore be found at similar wave number positions.

Degradation

PEOT/PBT polymers can undergo degradation through hydrolysis and oxidation, which was established after using *in vitro* experiments³². The main process for degradation of these polymers *in vivo*, seems to be hydrolysis, although many macrophage like cells, known for their ability to produce oxidative reagents, can be seen surrounding these materials after implantation³³. The fact that hydrolysis seems to be the main driving factor during degradation of these polymers, a decrease in intensity of bands belonging to the PEO group can be expected and our findings seem to concur this. The GPC results show a rapid decrease of the molecular weight, from approximately 1.4 E 5 to 2E4 g/mole, already after the first week of our *in vitro* degradation experiment. This steep decline levels off after one week to a plateau decreasing at much lower rate. In a comparable study these polymers were found to degrade in a similar way, but much slower, when they were immersed in PBS at 37 °C for 37 days reaching the plateau after 20 days at 2.8E4 g/mole³⁴. After degradation the samples became more and more brittle depending on the time point of observation, until the polymer samples had fallen

apart completely after 42 days. This is similar to results published elsewhere³³ where we submersed the same material for 14 days, at 100 °C in phosphate buffered saline. These results suggest that mainly the soft segment and PEO content is reduced during degradation. The Raman data shown in figures 5 and 6 confirm these findings. These spectra show decrease of intensity of certain PEO Raman bands, indicating a possible loss of PEO specific molecular groups. The resultant after subtraction of the spectra of untreated material from the 42 days degraded material, clearly shows that PEO specific bands, around 850 cm⁻¹, 1100-1150 cm⁻¹, 1250 and 1300 cm⁻¹, and at 1440-1480 cm⁻¹, have decreased to some extent as they appear as negative bands beneath the x-axis. When comparing the Raman spectra of the different time points the intensity of the PEOT specific band around 1280cm⁻¹ appear to decrease during prolonged degradation. The negative trend becomes apparent after 14 days of degradation, which might indicate that only after a longer period of incubation a loss of PEO content can be found. The abovementioned observation is in contrast with the GPC data, which show a rapid decrease of molecular weight already in the first week of degradation (figure 7). A possible explanation for this could be that Raman spectra are a representation of all the molecular groups present in the material. The PBT and PEOT segments in these materials contain similar chemical bonds and a decrease of soft segment content does apparently not show up immediately in this data. A possible reason for this could be that PEO chains, which are scissioned from the block copolymer, stay confined in the bulk material and only after longer time have had the ability to diffuse out of the bulk material. The Raman spectra shown in figure 2 more or less confirms this hypothesis as the average spectrum of PEG, PBT and DMT shows a Raman spectrum very much similar to the actual spectrum of the block copolymer. This indicates that although these polymers can be seen as composed of two separate blocks, a mixture of the building blocks without any chemical bond between them also shows a spectrum equal to the Raman spectrum of the actual

block copolymer. As a result differences between the spectra of polymers when PEG has a molecular weight of 300-1000 are not only very small, a chain scission caused by degradation, either through hydrolysis or oxidation, can not very well be detected as well. In addition the heat of fusion and melting temperature of the PBT segment from PEOT PBT block copolymers were found to have increased after *in vitro* and *in vivo* degradation studies³³ indicating that crystallinity of these had increased because of degradation. The positive bands specific for PBT observed in figure 6 are likely to be a result of this increase in crystallinity of these polymers. Raman bands will become sharper and increase in intensity with increasing crystallinity of materials. The reason for this is that chemical bonds in crystalline materials are more constricted in their movements, meaning the molecular vibrations will be more restrained than when dealing with more amorphous materials. As a result a narrowing and increase in intensity of Raman bands can be observed.

Conclusions

The differences between degraded and non degraded samples in the Raman spectra found in this study are caused by a combination of changes in crystallinity and a loss of PEO from these polymers. Raman spectroscopy can be used to evaluate PEOT/PBT block copolymers mainly in a qualitative manner because of the similarity in molecular composition of the soft and hard block. The loss of PEO content observed in this study confirms the results found by others on the degradation of these polymers. The use of Raman spectroscopy for future *in vivo* degradation studies could provide information whether these polymers degrade in a similar manner or that the presence of macrophages, actively involved in the uptake and removal of implanted materials, leads to different degradation behaviour.

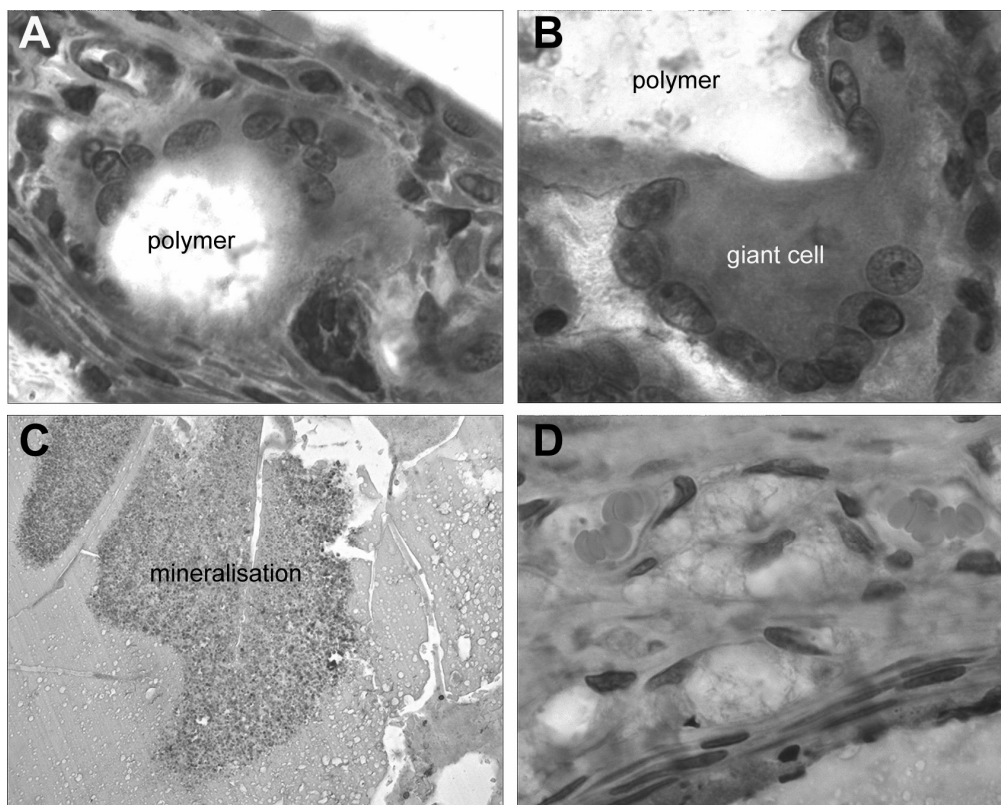
References

1. Claase, M. B.; Grijpma, D. W.; Mendes, S. C.; De Bruijn, J. D.; Feijen, J., Porous PEOT/PBT scaffolds for bone tissue engineering: preparation, characterization, and in vitro bone marrow cell culturing. *J Biomed Mater Res A* 2003, 64, (2), 291-300.
2. Claase, M. B.; Olde Riekerink, M. B.; de Bruijn, J. D.; Grijpma, D. W.; Engbers, G. H.; Feijen, J., Enhanced bone marrow stromal cell adhesion and growth on segmented poly(ether ester)s based on poly(ethylene oxide) and poly(butylene terephthalate). *Biomacromolecules* 2003, 4, (1), 57-63.
3. Beumer, G. J.; van Blitterswijk, C. A.; Poncet, M., Biocompatibility of a biodegradable matrix used as a skin substitute: an in vivo evaluation. *J Biomed Mater Res* 1994, 28, (5), 545-52.
4. Grote, J. J.; Bakker, D.; Hesselink, S. C.; van Blitterswijk, C. A., New alloplastic tympanic membrane material. *Am J Otol* 1991, 12, (5), 329-35.
5. Meijer, G. J.; Heethaar, J.; Cune, M. S.; De Putter, C.; Van Blitterswijk, C. A., Flexible (Polyactive) versus rigid (hydroxyapatite) dental implants. *Int J Oral Maxillofac Surg* 1997, 26, (2), 135-40.
6. van Blitterswijk, C. A.; Bakker, D.; Hesselink, S. C.; Koerten, H. K., Reactions of cells at implant surfaces. *Biomaterials* 1991, 12, (2), 187-93.
7. Bulstra, S. K.; Geesink, R. G.; Bakker, D.; Bulstra, T. H.; Bouwmeester, S. J.; van der Linden, A. J., Femoral canal occlusion in total hip replacement using a resorbable and flexible cement restrictor. *J Bone Joint Surg Br* 1996, 78, (6), 892-8.
8. Du, C.; Meijer, G. J.; van de Valk, C.; Haan, R. E.; Bezemer, J. M.; Hesselink, S. C.; Cui, F. Z.; de Groot, K.; Layrolle, P., Bone growth in biomimetic apatite coated porous Polyactive 1000PEG70PBT30 implants. *Biomaterials* 2002, 23, (23), 4649-56.
9. Sakkers, R.; Dalmeyer, R.; de Wijn, J.; van Blitterswijk, C., Use of bone-bonding hydrogel copolymers in bone: an in vitro and in vivo study of expanding PEO-PBT copolymers in goat femora. *J Biomed Mater Res* 2000, 49, (3), 312-8.
10. Kuijter, R.; Bouwmeester, S. J. M.; Drees, M. M. W. E.; Surtel, D. A. M.; Terwindt-Rouwenhorst, E. A. W.; van der Linden, A. J.; van Blitterswijk, C. A.; Bulstra, S. K., The polymer Polyactive as a bone-filling substance: an experimental study in rabbits. *Journal of Materials Science: Materials in Medicine* 1998, 9, (8), 449-55.
11. Malda, J.; Woodfield, T. B.; van der Vloodt, F.; Kooy, F. K.; Martens, D. E.; Tramper, J.; van Blitterswijk, C. A.; Riesle, J., The effect of PEGT/PBT scaffold architecture on oxygen gradients in tissue engineered cartilaginous constructs. *Biomaterials* 2004, 25, (26), 5773-80.
12. Malda, J.; Woodfield, T. B.; van der Vloodt, F.; Wilson, C.; Martens, D. E.; Tramper, J.; van Blitterswijk, C. A.; Riesle, J., The effect of PEGT/PBT scaffold architecture on the composition of tissue engineered cartilage. *Biomaterials* 2005, 26, (1), 63-72.
13. Miot, S.; Woodfield, T.; Daniels, A. U.; Suetterlin, R.; Peterschmitt, I.; Heberer, M.; van Blitterswijk, C. A.; Riesle, J.; Martin, I., Effects of scaffold composition and architecture on human nasal chondrocyte redifferentiation and cartilaginous matrix deposition. *Biomaterials* 2005, 26, (15), 2479-89.
14. Woodfield, T. B.; Bezemer, J. M.; Pieper, J. S.; van Blitterswijk, C. A.; Riesle, J., Scaffolds for tissue engineering of cartilage. *Crit Rev Eukaryot Gene Expr* 2002, 12, (3), 209-36.
15. Woodfield, T. B.; Malda, J.; de Wijn, J. R.; Peters, F.; Riesle, J.; van Blitterswijk, C. A., Design of porous scaffolds for cartilage tissue engineering using a three-dimensional fiber-deposition technique. *Biomaterials* 2004, 25, (18), 4149-61.
16. Du, C.; Klasens, P.; Haan, R.; Bezemer, J.; Cui, F.; de Groot, K.; Layrolle, P., Biomimetic calcium phosphate coatings on Polyactive 1000/70/30. *J Biomed Mater Res* 2002, 59, (3), 535-46.

17. Liu, Q.; de Wijn, J.; van Blitterswijk, C., Composite biomaterials with chemical bonding between hydroxyapatite filler particles and PEG/PBT copolymer matrix. *J Biomed Mater Res* 1998, 40, (3), 490-7.
18. AG, v. D.; Verhoeven, M.; Koerten, H.; van, B. C.; Ponec, M., Bilayered biodegradable poly(ethylene glycol)/poly(butylene terephthalate) copolymer (Polyactive) as substrate for human fibroblasts and keratinocytes. *J Biomed Mater Res* 1999, 47, (3), 292-300.
19. Beumer, G.; van, B. C.; Ponec, M., Biocompatibility of a biodegradable matrix used as a skin substitute: an in vivo evaluation. *J Biomed Mater Res* 1994, 28, (5), 545-52.
20. Beumer, G. J.; van Blitterswijk, C. A.; Bakker, D.; Ponec, M., A new biodegradable matrix as part of a cell seeded skin substitute for the treatment of deep skin defects: a physico-chemical characterisation. *Clin Mater* 1993, 14, (1), 21-7.
21. van Dorp, A. G.; Verhoeven, M. C.; Koerten, H. K.; van Blitterswijk, C. A.; Ponec, M., Bilayered biodegradable poly(ethylene glycol)/poly(butylene terephthalate) copolymer (Polyactive) as substrate for human fibroblasts and keratinocytes. *J Biomed Mater Res* 1999, 47, (3), 292-300.
22. van Dorp, A. G.; Verhoeven, M. C.; Koerten, H. K.; Van Der Nat-Van Der Meij, T. H.; Van Blitterswijk, C. A.; Ponec, M., Dermal regeneration in full-thickness wounds in Yucatan miniature pigs using a biodegradable copolymer. *Wound Repair Regen* 1998, 6, (6), 556-68.
23. Pouliot, R.; Azhari, R.; Qanadilo, H. F.; Mahmood, T. A.; Triantafyllou, M. S.; Langer, R., Tissue engineering of fish skin: behavior of fish cells on poly(ethylene glycol terephthalate)/poly(butylene terephthalate) copolymers in relation to the composition of the polymer substrate as an initial step in constructing a robotic/living tissue hybrid. *Tissue Eng* 2004, 10, (1-2), 7-21.
24. Kozielski, M.; Muhle, M.; Blaszcak, Z., The Raman scattering study of selected polyoxyethyleneglycols. 2004, 111, (1-3), 1.
25. Jansen, J. A.; de Ruijter, J. E.; Janssen, P. T.; Paquay, Y. G., Histological evaluation of a biodegradable Polyactive/hydroxyapatite membrane. *Biomaterials* 1995, 16, (11), 819-27.
26. Mendes, S. C.; Bezemer, J.; Claase, M. B.; Grijpma, D. W.; Bellia, G.; Degli-Innocenti, F.; Reis, R. L.; de Groot, K.; van Blitterswijk, C. A.; de Bruijn, J. D., Evaluation of two biodegradable polymeric systems as substrates for bone tissue engineering. *Tissue Eng* 2003, 9 Suppl 1, S91-101.
27. Papadaki, M.; Mahmood, T.; Gupta, P.; Claase, M.; Grijpma, D.; Riesle, J.; van Blitterswijk, C.; Langer, R., The different behaviors of skeletal muscle cells and chondrocytes on PEGT/PBT block copolymers are related to the surface properties of the substrate. *J Biomed Mater Res* 2001, 54, (1), 47-58.
28. Xiao, Y. L.; Riesle, J.; van Blitterswijk, C. A., Static and dynamic fibroblast seeding and cultivation in porous PEO/PBT scaffolds. *Journal of Materials Science: Materials in Medicine* 1999, 10, (12), 773.
29. Deschamps, A. A.; Claase, M. B.; Sleijster, W. J.; de Bruijn, J. D.; Grijpma, D. W.; Feijen, J., Design of segmented poly(ether ester) materials and structures for the tissue engineering of bone. *J Control Release* 2002, 78, (1-3), 175-86.
30. Radder, A.; Leenders, H.; van, B. C., Application of porous PEO/PBT copolymers for bone replacement. *J Biomed Mater Res* 1996, 30, (3), 341-51.
31. van Loon, J. A. Biocompatibility testing of degradable polymers. Dissertation, Leiden University, Leiden, 1995.
32. Deschamps, A.; Grijpma, D.; Feijen, J., Poly(ethylene oxide)/poly(butylene terephthalate) segmented block copolymers: the effect of copolymer composition on physical properties and degradation behavior. *Polymer* 2001, 42, (23), 9335-9345.
33. Deschamps, A.; van Apeldoorn, A.; Hayen, H.; de Bruijn, J.; Karst, U.; Grijpma, D.; Feijen, J., In vivo and in vitro degradation of poly(ether ester) block copolymers based on poly(ethylene glycol) and poly(butylene terephthalate). *Biomaterials* 2004, 25, (2), 247-258.

34. Bezemer, J.; Grijsma, D.; Dijkstra, P.; van Blitterswijk, C.; Feijen, J., A controlled release system for proteins based on poly(ether ester) block-copolymers: polymer network characterization. *Journal of controlled release* **1999**, 62, (3), 393-405.
35. Fernandez, M.; Merino, J.; Pastor, J., Injection molding of poly(ethylene terephthalate): Differential Scanning Calorimetry and Confocal Micro-Raman Spectroscopy investigations of the skin-core morphology. *Polymer engineering and science* **2000**, 40, (1), 95-107.
36. Di Noto, V.; Zago, V.; Biscazzo, S.; Vittadello, M., Hybrid inorganic-organic polymer electrolytes: synthesis, FT-Raman studies and conductivity of $\{Zr[(CH_2CH_2O)_{8.7}][rho]/(LiClO_4)_z\}_n$ network complexes. **2003**, 48, (5), 541.
37. Mak, C. L.; Wong, Y. W.; Chan, W. N., Application of Raman spectroscopy to determine the strain-level in polybutylene terephthalate (PBT). **1998**, 17, (6), 451.
38. Ellis, G.; Roman, F.; Marco, C.; Gomez, M. A.; Fatou, J. G., FT Raman study of orientation and crystallization processes in poly(ethylene terephthalate). **1995**, 51, (12), 2139.
39. Lesko, C. C. C.; Rabolt, J. F.; Ikeda, R. M.; Chase, B.; Kennedy, A., Experimental determination of the fiber orientation parameters and the Raman tensor of the 1614 cm^{-1} band of poly(ethylene terephthalate). **2000**, 521, (1-3), 127.
40. Pellow-Jarman, M. V.; Hendra, P. J.; Hetem, M. J. J., Poly(butylene terephthalate) polycarbonate transesterification: monitoring its progress with Fourier transform Raman spectroscopy. **1995**, 51, (12), 2107.

In vivo degradation of PEOT PBT block copolymers evaluated by confocal Raman microscopy



After implantation of block copolymers composed of polyethylene oxide terephthalate and polybutylene-terephthalate. Certain compositions show fast degradation, especially the materials where the molecular weight of polyethylene glycol is 1000 g/mole and higher. In many occasions so called giant cells, which are fused macrophages, can be found surrounding polymer fragments (A and B) and macrophages containing small polymer fragments (D). An interesting feature of this material is that it can mineralise *in vivo*, which is thought to enhance the bone bonding capability of this material, which appears as dark purple granulated regions in the polymer (C).

Abstract

Synthetic polymers comprise a large number of the (bio)materials used for tissue engineering applications. One of the major advantages of using polymers is that they enable the design of scaffolds for tissue-engineering with different mechanical and biological properties and degradation rates depending on the requirements for their application. Block copolymers composed of polyethylene oxide terephthalate (PEOT) and polybutylene-terephthalate (PBT) are thermoplastic elastomers which have been studied extensively for their utility as a biomaterial in tissue engineering. In order to sustain scaffold structure after implantation, which allows for the observation of structural changes and tissue reactions to the implant, techniques by which degradation can be studied in a non-destructive manner are preferred. In this manner important chemical information can be studied whilst in the same time the scaffold morphology is preserved. One of the techniques which can be used for non-destructive analysis is Raman spectroscopy. We have investigated the feasibility of using confocal Raman spectroscopy for the analysis of *in vivo* degraded PEOT PBT polymers. As a simulation model for degradation we analyzed 300PEOT55PBT45, 300PEOT70PBT30 and 1000PEOT70PBT30 copolymers after submersion for 14 days in PBS at 100 °C in order to evaluate the spectra obtained here with the spectra obtained after subcutaneous implantation. Only for 1000PEOT70PBT30 polymer discs clear signs of degradation could be detected, by a loss in PEOT content, while for 300PEOT70PBT30 and 300PEOT55PBT45 no change in composition was found after 12 weeks of implantation. Additionally, histology revealed that macrophage-like cells clearly play an active role in the removal of these materials through phagocytosis and possible further degradation of polymer fragments. Furthermore, Raman and histological data revealed that mineralized spots start to appear already after 4 weeks of subcutaneous implantation in 2 of the 3 different polymer compositions observed which is comparable to previous studies done by others on these materials.

In vivo degradation of PEOT PBT block copolymers evaluated by confocal Raman microscopy

A.A. van Apeldoorn¹, J. de Wijn¹, Y. Aksenov², A.A. Deschamps¹, F.L.A.M.A. Peters³, J.D. de Bruijn¹, C. Otto², C.A. van Blitterswijk¹

¹Department of Polymer Chemistry and Biomaterials, Faculty of Technology and Sciences, University of Twente, PO Box 98, 3720AB Bilthoven, the Netherlands,

²Department of Biophysical Techniques, Faculty of Technology and Sciences, University of Twente, PO Box 217, 7500AE Enschede, The Netherlands, Isotis NV, PO Box 98, 3720AB Bilthoven, The Netherlands

Introduction

Materials applied for tissue replacement in tissue engineering are frequently composed of materials which are degradable. The conventional idea is that the optimal tissue engineering scaffold should be composed of a degradable material which can sustain cells or tissue in such a way that sufficient time is left to repair a defect, while in the same time the material is exchanged by native tissue. The selection of material properties is to a great extent influenced by the location of the implant site. Depending on the location the physical and chemical properties of materials have to be customized in such a way that these meet the mechanical and physiological demands of the implant site. Thermoplastic materials, such as Polyactive™, a block copolymer composed of a hard hydrophobic polybutylene terephthalate (PBT) block and a soft hydrophilic poly ethylene glycol terephthalate (PEOT) block, have been extensively studied as a material for tissue engineering applications. The advantage of using such a polymer is that its properties can be tailored, by not only varying the soft to hard block ratio, but the molecular weight of poly ethylene glycol (PEO) as well, in order to change elasticity, water uptake

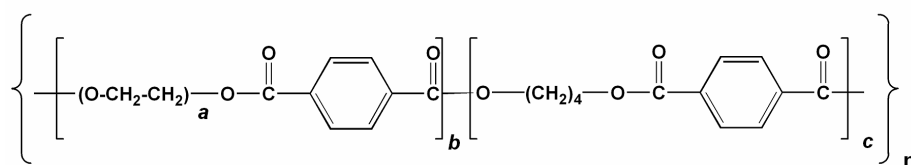
and degradability of the material. PEOT PBT block copolymers are thought to degrade through hydrolysis of the ester bond and to a smaller extent oxidation of the ether bond present in these polymers¹. PEOT PBT polymers were the molecular weight of polyethyleneglycol is 300 g/mole and the mass ratio of the soft versus the hard block is equal to 55:45 have been used in studies related to cartilage²⁻⁴ and skin repair⁵⁻⁷ because of their optimal elastic properties. In addition, copolymers were the molecular weight of PEG is 1000 g/mole and the mass ratio of PEOT and PBT is 70:30 have been extensively studied for use as bone fillers⁸⁻¹¹ and material for dental implants¹² because of their tissue interaction. Moreover, interesting properties of these copolymers are that, depending on their composition, they can not only have bone bonding capacity¹³, but have the ability to mineralize as well^{14, 15}. In the past these materials were studied by using destructive chemical analysis techniques, such as nuclear magnetic resonance spectroscopy, gel permeation chromatography and differential scanning calorimetry, which do not allow for the observation of morphological changes during degradation studies. Techniques by which degradation can be studied in a non-destructive manner are preferred because valuable chemical information can be studied while in the same time the scaffold structure is preserved. One of the techniques which can be used for non-destructive analysis is Raman spectroscopy. Raman spectroscopy is based on inelastic scattering of photons by molecules¹⁶. The energy of the scattered radiation can be less or more than the incident radiation. The energy increase, or decrease, from the excitation is related to the vibrational energy spacing in the ground electronic state of a molecule. Therefore, the wavenumbers in Raman spectra are a direct measure of the vibrational energies of the chemical bonds in a molecule. Since Raman spectroscopy uses a monochromatic light (Laser) source to study molecular vibrations, it allows for chemical analysis in a non-destructive manner. In this study we investigated the feasibility of using confocal Raman spectroscopy for the study of *in vivo* degraded PEOT PBT polymers by characterizing Raman

spectra obtained from PEOT PBT block copolymers of 3 different compositions after subcutaneous implantation. Raman and histological data revealed that the onset of mineralized spots appears already at 4 weeks of subcutaneous implantation in 2 of the 3 different polymer compositions.

Material and methods

Polymers

Several different polymers and their separate building blocks were used for characterization. The nomenclature of the polymers is as follows aPEOTbPBTc, The composition is denoted as $a / b / c$, where a represents the poly(ethylene glycol) (PEG) molecular weight (MW g/mol), and b and c represent the weight percentage (wt%) of PEOT and PBT blocks respectively. In this study the following compositions were measured by confocal Raman spectroscopy after subcutaneous implantation in Wistar rats; 300PEOT55PBT45, 300PEOT70PBT30 and 1000PEOT70PBT30.



Formula 1: Molecular composition of PEOT/PBT block copolymers

Polymer processing

Samples were provided by the Department of Chemical Technology, Twente University, The Netherlands. In short, polymer samples were created by compression molding (laboratory press THB008, Fontijne, The Netherlands). The molding temperatures were 140°C for 1000PEGT70PBT30, 150°C for 300PEGT70PBT30 and 300PEGT55PBT45. In this manner 400-600µm thick samples were produced. Subsequently, 15 mm diameter discs for degradation experiments were cored out.

In vivo implantation

The melt pressed discs (n=8) were implanted subcutaneously in the back of young male Wistar rats (Harlan BV, the Netherlands) along the dorso-medial line. Before implantation, the discs were sterilized by γ -irradiation under vacuum. The sterilization method is known not to affect the polymer properties. The samples were implanted according to a randomized square method, 4 samples per animal. After insertion of the discs, the wounds were closed with Vicryl[®] suture. The samples were explanted after 1, 2, 4, 12 weeks. Simulation of degradation was done by immersion of the samples in phosphate buffered saline (PBS), pH 7.4, for 14 days at a 100°C.

Confocal Raman spectroscopy

A collimated and circularly symmetrical beam from a diode laser (LD) (Mitsubishi electronics) with a frequency of 685nm is reflected by a dichroic beam splitter (BS) into the vacuum chamber of a FEI ESEM XL30-FEG through a coupling window. The beam is then focused by a 60X objective (n.a. 0.65) on a sample of interest. The excited Raman scattering is collected by the same objective and the Stokes components of Raman frequencies pass through the BS and a notch filter on a pinhole (\varnothing 25 μ m) allowing confocality of the system. The scattering is collected in a spectrograph-monochromator where the incoming light is decomposed by a concave holographic diffraction grating and focused on a thermo-electrically cooled CCD (1056x256 pixels, Princeton Instruments Spec10). The theoretical spatial resolution of the system is \sim 700nm with an effective laser power of 6mW on the sample. The CCD is connected with a computer for data collection and analysis using WinSpec (Roper Scientific Inc., USA) and Microcal Origin (Microcal software inc., USA) data analysis software.

Confocal Raman measurements were done on wet samples after retrieval and fixation. In general 8 random locations on the samples were measured 10 times to account for measurement errors. The difference spectra were determined by subtracting Raman spectra of 1 week implanted samples from Raman spectra of the implanted samples at later time points. In order to ensure all spectra were compared in the same way, the data were corrected by relating all intensities to the 1725 cm^{-1} band belonging to the carboxyl stretch mode from the terephthalate group in the polymer. An internal standard like this makes subtraction of the spectra possible, because major absolute intensities generated by measurement differences, due to differences in surface characteristics for example, can then be accounted for. The method of using an internal standard was applied to both the *in vitro* and *in vivo* degraded samples

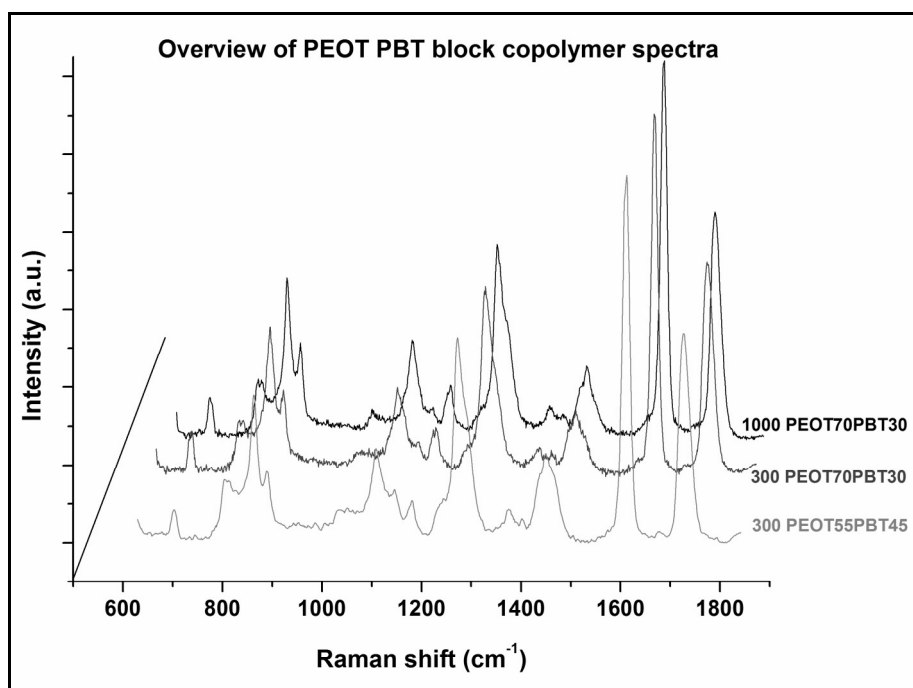


Figure 1: Raman spectra of PEOT PBT block copolymers before degradation

Histology

In order to observe morphological changes during implantation at the different time points mentioned before, the explanted samples were fixed in a 4% paraformaldehyde solution (Sigma, the Netherlands) and washed in PBS. Subsequently, the samples were dehydrated in an increasing ethanol series. After dehydration, samples were embedded in GMA (Sigma, the Netherlands). After embedding 5 μ m sections were made on a microtome (HM 355S, microtome, Germany) and stained with hematoxylin/eosin staining (Sigma, the Netherlands) to be evaluated by light microscopy.

Results

Raman spectroscopy on 300PEOT55PBT45 polymers

After *in vitro* degradation of 300PEOT55PBT45 polymers no difference in intensity of Raman bands observed in spectra obtained before and after degradation could be found. Subtracting the spectrum obtained before degradation from the one obtained after degradation resulted in a difference spectrum showing several peaks above and under the baseline (see figure 2). The absence of single negative or positive peaks in these spectra, which can be related to a decrease in the amount of either PEOT or PBT, and the fact that positive or negative peaks are preceded or followed by an opposite peak indicated that the resultant spectra were mainly showing peak shape differences (narrowing or widening) of Raman bands. After implantation of these polymers, subtraction of the spectrum obtained after 1 week of implantation from the spectra obtained at 2, 4 and 12 weeks (figure 3) did not show a clear decrease in time of Raman bands in any of the spectra observed. In addition, the spectra obtained from the implanted samples showed a result similar to what was found for the *in vitro* degraded samples.

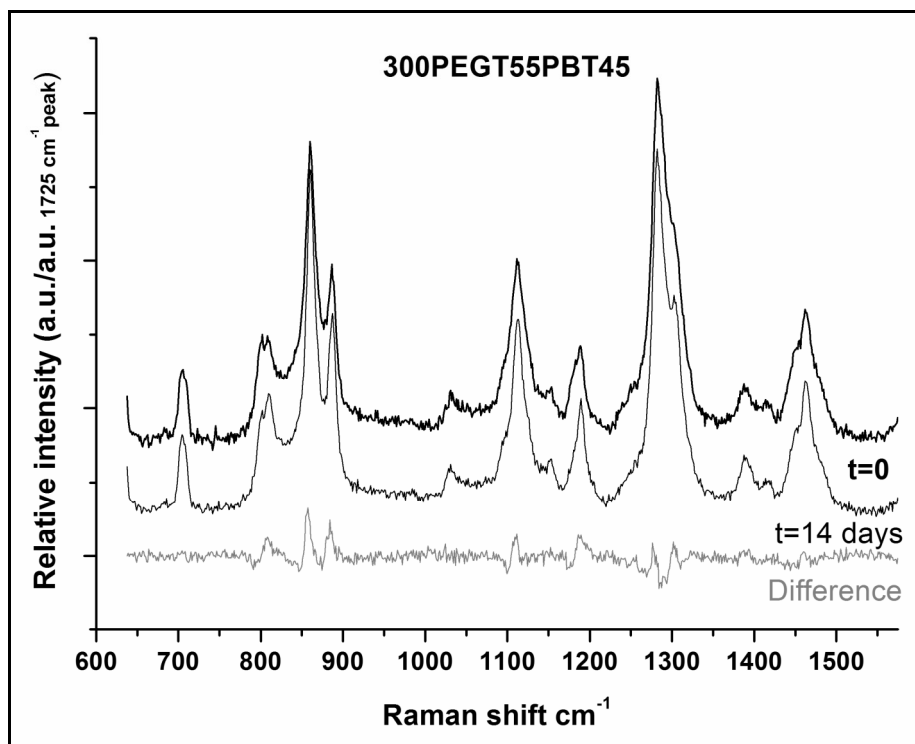


Figure 2: Raman spectra of 300/55/45 polymer before and after *in vitro* degradation as well as the difference spectrum.

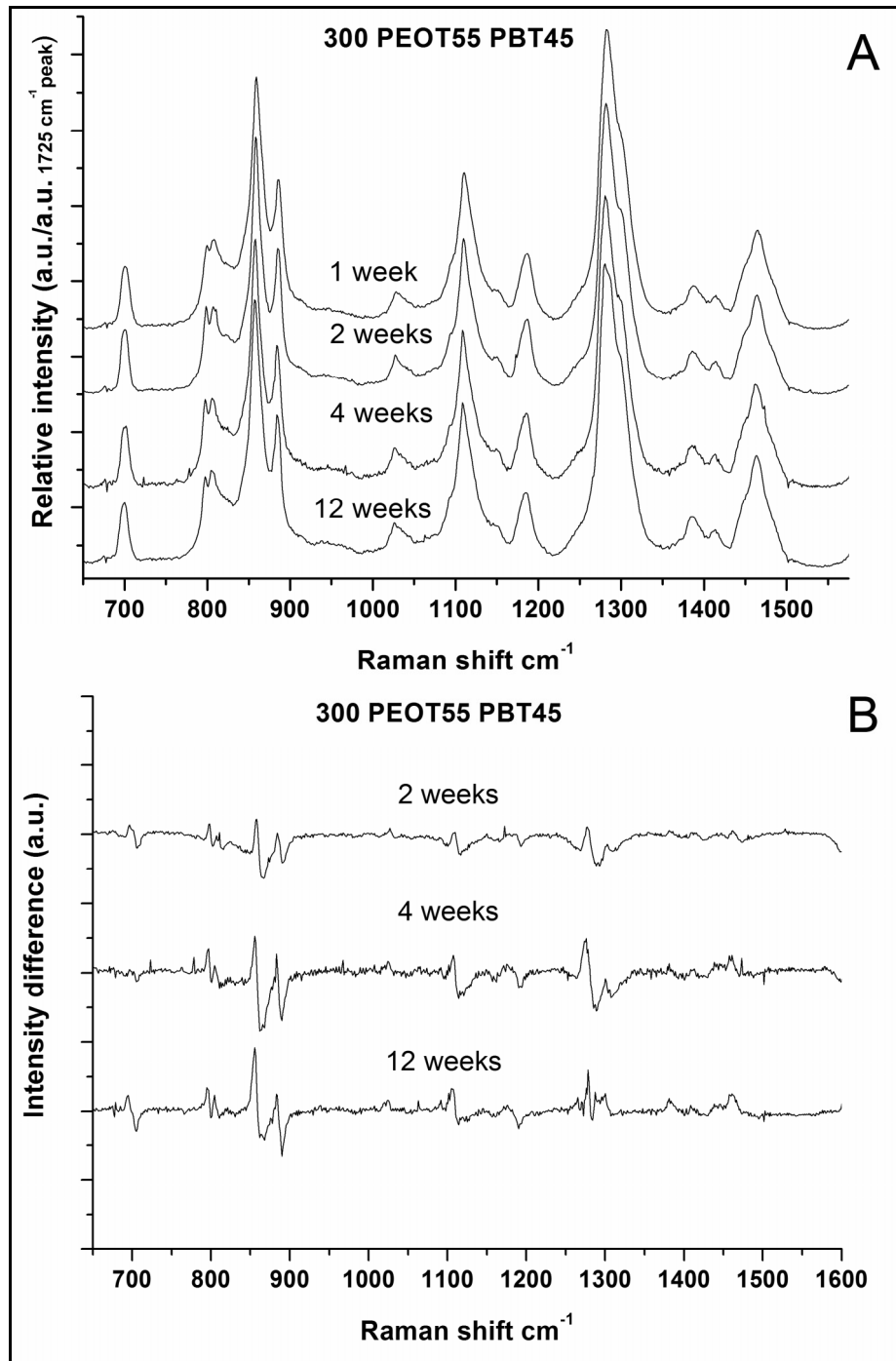


Figure 3; A) Raman spectra of 300PEOT55PBT45 polymers after implantation at different time points. B) Raman difference spectra of implanted samples.

Raman spectroscopy on 300PEOT70PBT30 polymers

After subtraction of spectra obtained before degradation from the spectra of *in vitro* degraded 300PEOT70PBT30 polymers a decrease in intensity of Raman bands at positions specific for PEO, especially around 1280 cm^{-1} , which is a band specific for νCH_2 and $\nu\text{C-H}$ vibrations within this group, was found (figure 4). In contrast, the resultant spectra of the *in vivo* degradation experiment (figure 5) did not show a clear decrease of any molecular group specific Raman band at all of the different time points observed. However, after 4 weeks of implantation a small peak around 960 cm^{-1} begins to appear, which seemed to have increased after 12 weeks.

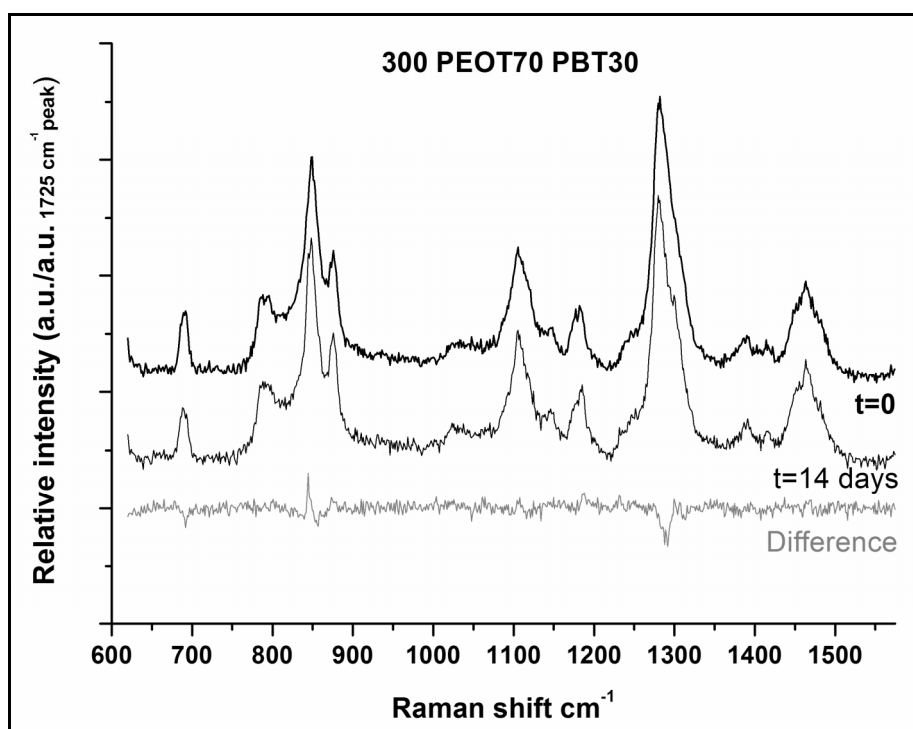


Figure 4: Raman spectra of 300PEOT70PBT30 polymer before and after *in vitro* degradation as well as the difference spectrum.

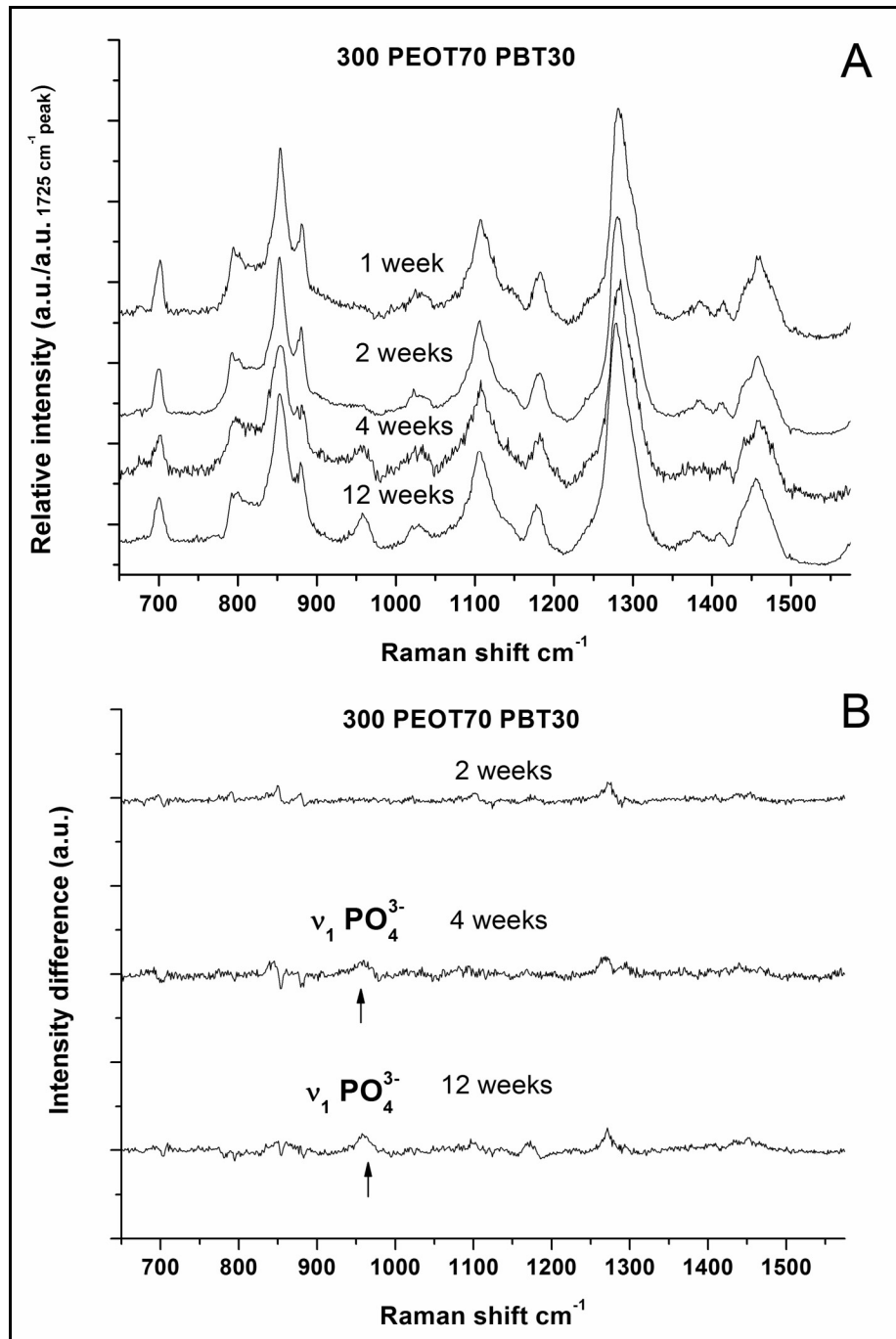


Figure 5: A) Raman spectra of 300PEOT70PBT30 polymers after implantation at different time points. B) Raman difference spectra of implanted samples, note the appearance of the phosphate specific Raman band.

Raman spectroscopy of 1000PEOT70PBT30 polymers

The Raman difference spectrum of *in vitro* degraded 1000PEOT70PBT30 polymers showed a clear appearance of a shoulder band around 1300 cm^{-1} , while in the same time the intensity of the 1285 cm^{-1} band had decreased (figure 6). A slight reduction in intensity around 1470 cm^{-1} was found. In addition, between 850 and 890 cm^{-1} the appearance of 2 positive bands could be found. Furthermore after subtraction, around 1180 cm^{-1} a positive band could be observed which indicates an increase in intensity of this Raman band. The difference spectra of subcutaneous implanted samples had a similar appearance as the *in vitro* degraded samples, be it that the intensity of the resultant bands in the Raman difference spectra of implanted samples was much lower (figure 7). After 12 weeks of implantation the difference spectrum showed considerably more noise than what could be observed for 2 and 4 weeks. Another observation we did during the analysis was that a high intensity Raman band around 960 cm^{-1} in certain regions of the implant could be found. Moreover, the presence of this Raman positive band was found to be non-homogenous, meaning some regions showed clearly higher intensity than other regions. The difference spectra in figure 7 all show a slight elevated intensity band around this position. Whereas the spectra in figure 8 show the results from a Raman measurement at a location where a very high intensity 960 cm^{-1} band could be found. Whenever this Raman band was detected when measuring 1000PEOT70PBT30 material it always had a much higher intensity than what could be observed for the 300PEOT70PBT30 polymer.

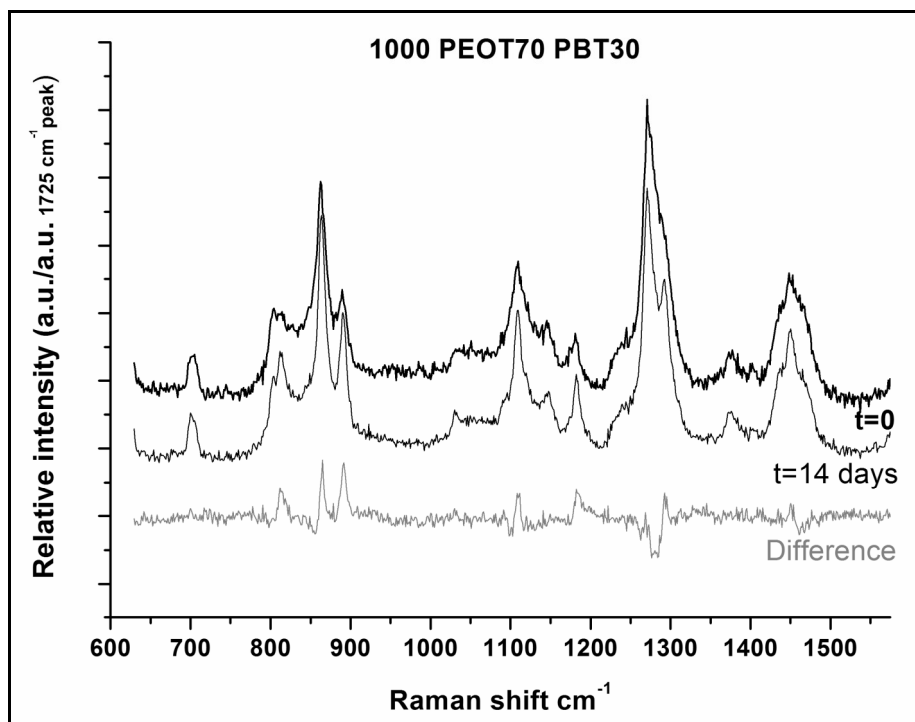


Figure 6: Raman spectra of 1000PEOT70PBT30 polymer before and after *in vitro* degradation as well as the difference spectrum.

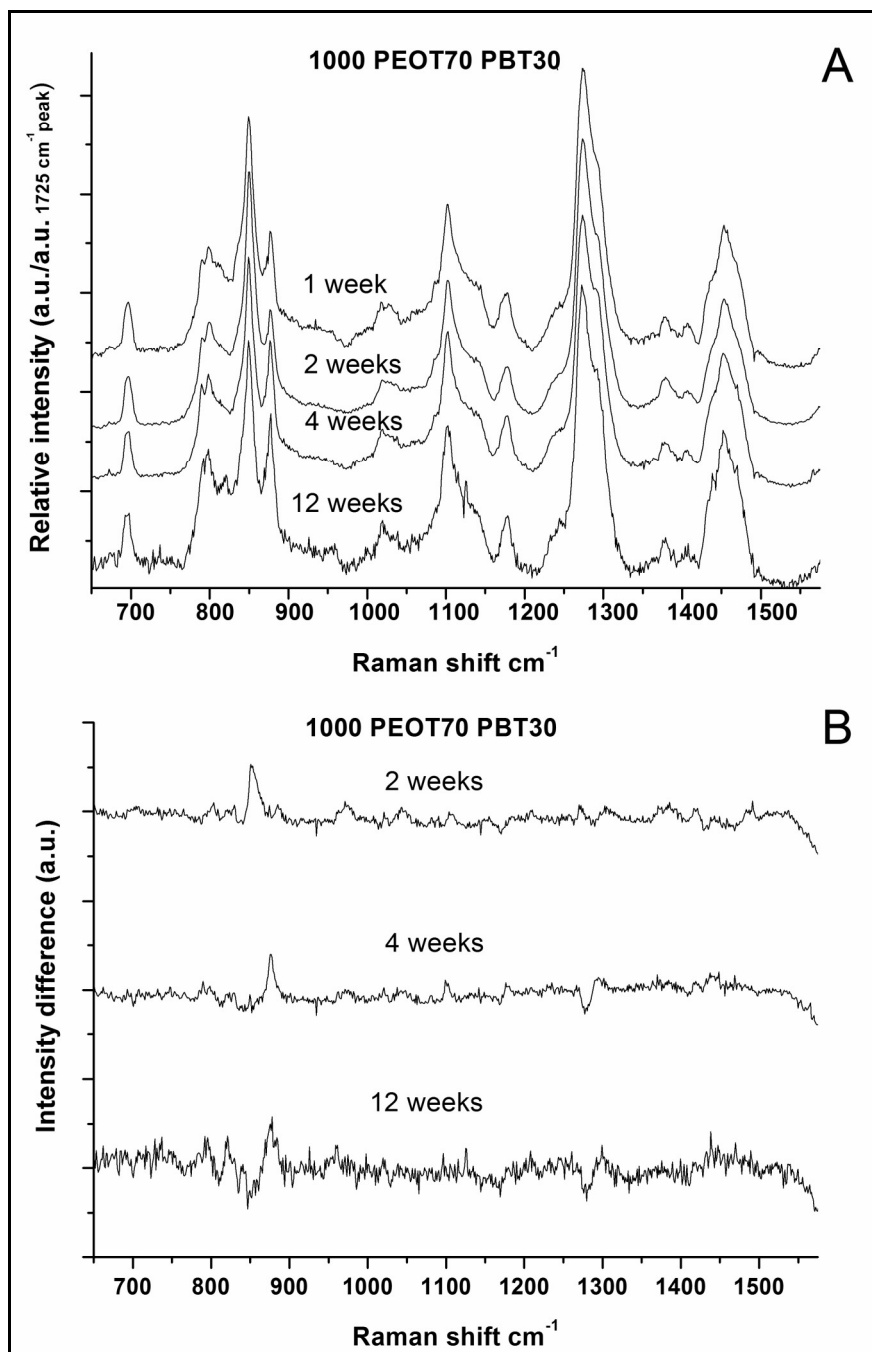


Figure 7: A) Raman spectra of 1000PEOT70PBT30 polymers after implantation at different time points. B) Raman difference spectra of implanted samples

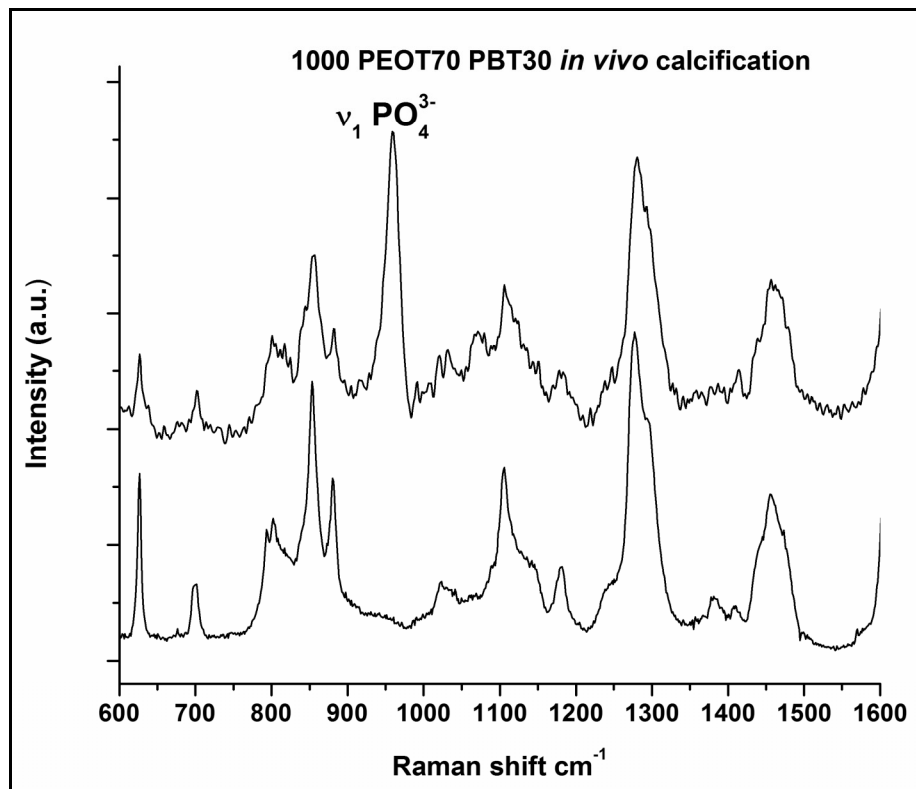


Figure 8: Raman spectra of 1000PEOT70PBT30 polymers before (bottom) and after (top) implantation (12 weeks) showing the high intensity band for phosphate indicating vast calcification of the polymer.

Histology

In general the polymers with a molecular weight of PEG of 300 showed less fragmentation than the 1000PEOT70PBT30 block copolymer. In case of 300PEOT55PBT45 no real changes in structure of the polymer discs could be observed apart from slight surface erosion after 12 weeks of implantation (figure 9). The samples had remained intact and could easily be retrieved from the implantation site. Furthermore, the samples were surrounded by a rim of connective tissue, indicative of a mild foreign body reaction. The 300PEOT70PBT30 samples showed some fragmentation of the surface at 12 weeks as can be observed in figure 10.

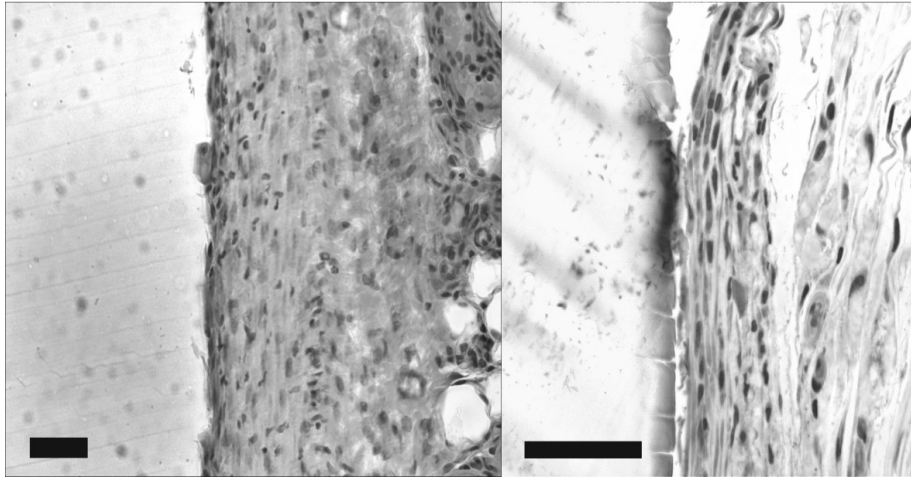


Figure 9: Light micrograph of 300PEOT55PBT45 polymer at 1 week (left) and 12 weeks of implantation (right). Apart from a slight change of surface morphology no effects on polymer morphology can be observed after 12 weeks of implantation. Scalebars are 100 μ m.

In general the samples appeared to be intact after retrieval from the implantation sites. Moreover, by using polarized light microscopy (a technique by which polymers and connective fibers can be observed as bright light scattering structures in the microscope sections), at this time point several small polymer fragments, present in the surrounding connective tissue, were found. In addition, a thin layer of what appears to be mineralization on the surface was found from 4 weeks on. This mineralization showed as a layer of dark blue and purple colored patchwork on the surface of the polymer, with a thickness of around 5 μ m. However, no regions other than the interface between tissue and polymer could be found showing signs of calcification. During retrieval of the 1000PEOT70PBT30 samples it became clear that these samples were much more defragmented, especially at the later time points, than the other polymers observed in this study (figure 11). After 1 week of implantation no major morphological changes were observed on the surface. The samples were surrounded by connective tissue like the other materials used in this study. However, after 2 weeks of implantation, clear signs of surface erosion could be detected in the form of lacunae present on the surface.

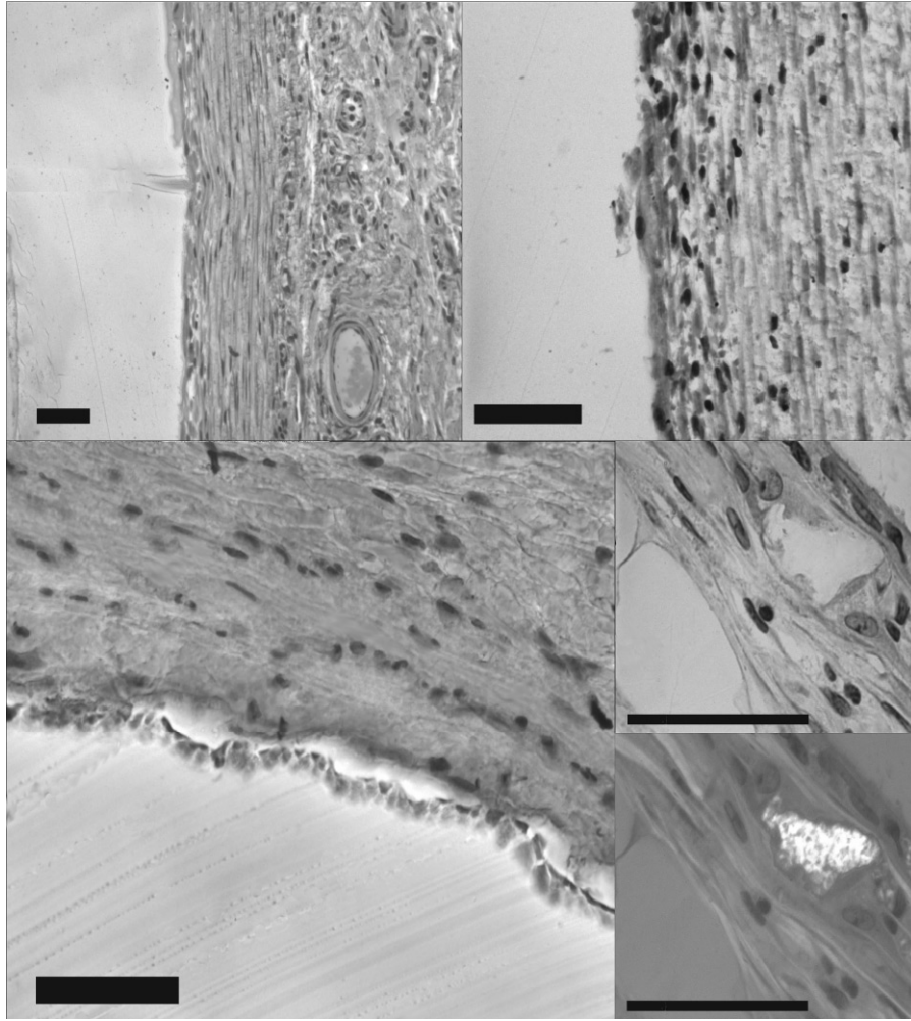


Figure 10: Light micrographs of 300PEOT70PBT30 polymer at 1 (top left) 4 (top right) and 12 (bottom left) weeks of implantation. Bottom right small polymer fragments observed by normal light microscopy (bottom right top) and polarized light microscopy (bottom right bottom) at 12 weeks. The dark blue granulation at the polymer surface at 12 weeks, indicates calcification of the polymer. Scalebars are 100 μm .

Additionally, Macrophage-like cells could be observed on the surface where the lacunae had formed. After 4 weeks of implantation, cracks had formed, which were filled with connective tissue, throughout the sample causing the discs to fragment. In some regions intensely stained dark blue and purple granular regions could be found, which indicated possible mineralization. These calcified regions were not

only found close to the surface of the polymer, but also within the polymer itself (especially after 12 weeks of implantation).

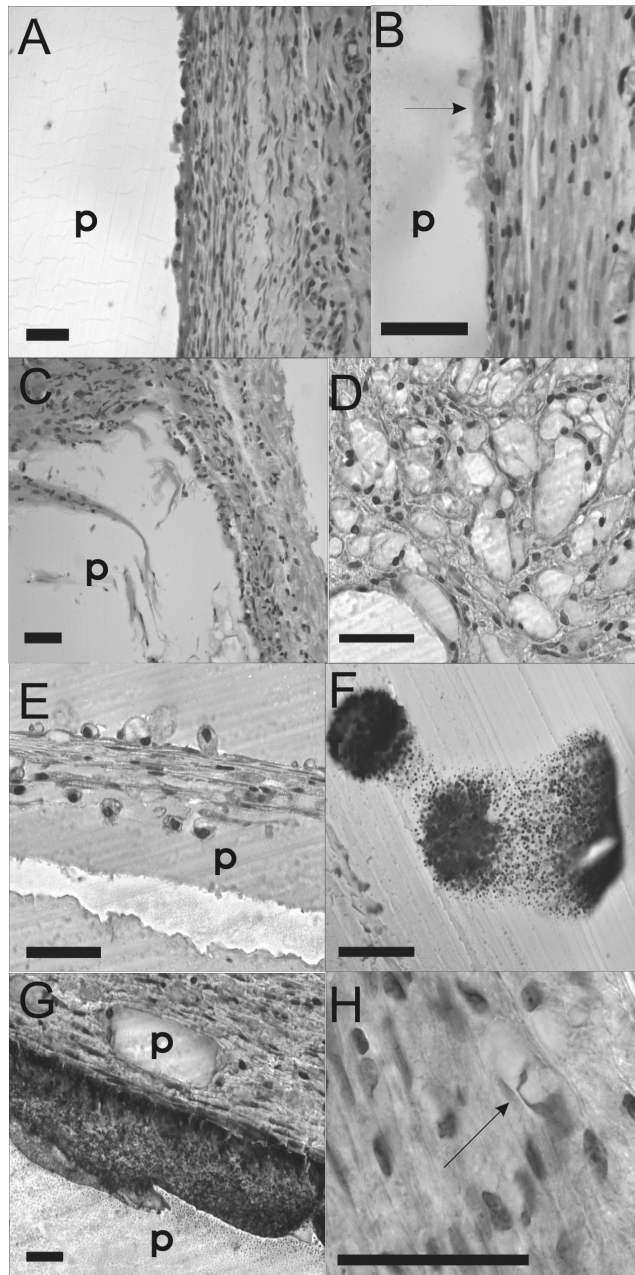


Figure 11: Light micrographs of 1000PEOT70PBT30 polymer at 1 (A), 2 (B), 4 (C) and 12 weeks (E-H) of implantation. A shows the onset of beginning lacunae formation on the polymer (p) surface, which progressed after 2 weeks (B), where macrophage-like cells (arrow) occupying the lacunae can be observed. After 4 weeks of implantation (C) large cracks have

formed throughout the polymer filled with connective tissue. After 12 weeks of implantation severe defragmentation of the polymer discs was observed (D and E), and also signs of extensive calcification (dark blue and purple granulation) not only at the surface (C) but also inside the polymer (F). Figure G and H not only show that a large number of small polymer fragments were present in the connective tissue surrounding the implant, but in the cytoplasm of macrophage-like cells as well (arrow). Scalebars are 100 μm .

Moreover, a distribution of large and smaller polymer fragments surrounded by Macrophage like cells were present in the connective tissue around the implant (see figure 11G). In some areas, using high magnification, macrophage like cells could be observed containing small polymer fragments within their cytoplasm of which a typical example can be seen in figure 11H).

Discussion

Polymers used for tissue engineering or implantations should be biocompatible and have specific mechanical, water absorption and degradation properties depending upon their application. The aim of this study was to investigate the possibility of applying confocal Raman spectroscopy for the analysis of degradation of PEOT PBT block copolymers with different composition after subcutaneous implantation. As a simulation model for degradation we analyzed 300PEOT55PBT45, 300PEOT70PBT30 and 1000PEOT70PBT30 after submersion for 14 days in PBS at 100 $^{\circ}\text{C}$ in order to compare the data obtained with the data derived from subcutaneous implanted samples. The simulated degradation of 300PEOT55PBT45 samples revealed no large changes in Raman band intensities when comparing degraded with non-degraded material. The absence of single freestanding negative or positive bands in the difference spectra between the treated and non-treated material, confirms the idea that the small bands observed in these spectra are mainly caused by slight shape changes of these bands rather than intensity differences. Interesting is the fact that these shape changes seem to occur mainly around positions where bands specific for PEOT are located (850 and 1280 cm^{-1}) belonging to rCH_2 , gauche-trans-gauche glycol and tCH_2 , $\nu\text{C-H}$ vibrations^{17, 18} respectively. The simulated degradation of 300PEOT70PBT30 polymers resulted in

a slight decrease in intensity of the 1280 cm^{-1} band similar to 300PEOT55PBT45, however, the effect on the Raman band around 850 cm^{-1} seems to be much smaller. Based on these data it seems that hardly any changes in the molecular composition took place after in vitro degradation of these polymers. The effects observed here are more likely results of a change in crystallinity and or conformational changes of these polymers. In a previous study done with the exact same batch of polymers we determined the ΔH and T_m of the hard block after fast simulated degradation by using differential scanning calorimetry (DSC). The ΔH_{hard} and T_m of these polymers were found to change from 4 to 14 J/g and 131 to 148 °C for 300PEOT70PBT30 and from 10 to 32 J/g and 169 to 178 °C for 300PEOT55PBT45, after degradation¹⁹. The increase in heat of fusion and melting temperature indicated an increase in crystallinity, which in turn is known to lead to an increase in intensity and narrowing of Raman bands. This observation is also illustrated by the fact that for all polymer compositions observed a shoulder band around 1300 cm^{-1} , known to be specific for PBT, begins to appear after degradation, which indicates a possible narrowing of the neighbouring 1280 cm^{-1} band. Moreover, the change in shape of the 850 cm^{-1} band specific for gauche-trans-gauche glycol skeletal vibrations also indicates a possible change in the physical state of the polymer. Although less clear, the data obtained from the subcutaneous implanted samples were similar to those found after simulated degradation in PBS. As difference spectra between 1 week and the other time points did not reveal a clear change of band intensities in time for both implanted 300PEOT55PBT45 and 300PEOT70PBT30 polymers, it is likely that no major changes in molecular composition of 300PEOT55PBT45 and 300PEOT70PBT30 during 12 weeks of implantation had occurred. Interestingly, the appearance of a minor positive band around 960 cm^{-1} , known to be specific for the PO_4^{3-} ν_1 stretch mode, in 300PEOT70PBT30 polymers after 4 weeks of implantation showed the on start of mineralization of these polymers. The granular lining of the polymer

surface after 4 weeks revealed by histology, indicative of mineralization, confirms this observation. Some small polymer fragments in the tissue surrounding 300PEOT70PBT30 discs were found after 12 weeks at the implantation site. Moreover, macrophage-like cells were always found in the vicinity of these fragments, likely to be involved in the uptake of these particles for further degradation. In contrast, 300PEOT55PBT45 polymers did not show clear changes in morphology and the structural integrity after implantation remained largely intact; While the abovementioned block copolymers showed only minor changes in histology, with respect to structural integrity, and Raman spectroscopy, with respect to chemical composition, 1000PEOT70PBT30 polymers showed more clear effects of degradation after implantation.

Simulated degradation of 1000PEOT70PBT30 polymers resulted in similar difference spectra as for the other two polymer compositions. However, the decrease of the Raman band around 1470 cm^{-1} , belonging to C-H and CH_2 vibrational modes of mainly the PEO group, in combination with the much clearer shape changes, caused by both narrowing and decreasing intensities, are indicative of not only changes in polymer composition but crystallinity as well. The Raman difference spectra of *in vivo* implanted samples showed a decrease in intensity of the 1280 cm^{-1} PEOT specific band in time, while another PEOT specific band around 850 cm^{-1} also seems to have decreased especially after 12 weeks of implantation. The decrease of these PEOT specific Raman bands implies a possible loss of PEOT content. The positive bands observed after *in vitro* and *in vivo* degradation are probably related to a change in crystallinity comparable to the other polymers observed in this study, as the ΔH_{hard} and T_m increased from 9.9 to 36.5 J/g and 157 to 165 °C for *in vitro*, and from 9.9 to 14.9 J/g and 157 to 160 °C *in vivo* (results published by us elsewhere¹⁹) degraded samples. The fact that the amount of noise in these spectra increases in time, caused by increasing

background fluorescence, indicates that more and more proteins and other biological factors infiltrate the material with prolonged implantation time. Light microscopy showed that the implanted samples begin to collapse already after 4 weeks of implantation. After 12 weeks of implantation further fragmentation of these materials lead to the presence of numerous small polymer fragments which are surrounded by macrophage-like cells. Moreover, similar cells can be found around the implant containing internalized polymer particles in their cytoplasm, which indicates an active role for these cells in possible further degradation of these polymers. The presence of dark purple granular patches on the surface and inside of the polymer discs and the fact that Raman measurements revealed an intense Raman band at 960 cm^{-1} belonging to the asymmetric stretch mode of PO_4^{3-} , typically present in calcium phosphate materials, indicates that this material becomes heavily calcified after in vivo implantation. Our results regarding the calcification of 1000PEOT70PBT30 are similar to what others have found after implantation of similar compositions, showing the bone bonding capabilities of these materials^{12, 15, 20, 21}.

Mineralization

The interesting finding of mineralization in the 300PEOT70PBT30 and 1000PEOT70PBT30 polymers, are in line with a study done by Sakkars et al.²⁰. They suggested that PEOT PBT polymers with a high PEO content were likely to calcify. Although the molecular weight of PEO in the 300 series is lower than for the 1000PEOT70PBT30 series, the amount of PEO chains is relatively high, in order to compensate for the mass ratio of soft versus hard blocks in the polymer, which might in turn facilitate mineralization. The COOH groups produced by hydrolysis during degradation of PEOT PBT copolymers are thought to play a role in mineralization of these polymers¹⁵. The length of PEO chains and uptake of water in the last mentioned polymer are higher, which increases the changes of these

materials to be hydrolyzed more than 300PEOT70PBT30 polymers because of the shorter PEO molecular chain length in the last mentioned material. This might explain the observation that calcification in 300PEOT70PBT30 polymers occurs after 4 weeks at a much lower level than was observed for the 1000PEOT70PBT30 polymers.

The effects of degradation, picked up by Raman spectroscopy, related to changes in chemical composition seem to be small in all material compositions observed. The reason for this could be two fold, the two major molecular groups in PEOT PBT polymers are very similar. The only real difference in the two groups is the chain length of PEO, a repetition of ethylene glycol groups, whereas PBT consists of a steady number of four C atoms linked to each other in a butyl formation coupled to a terephthalate group by an ester bond, which is similar for both PBT and PEOT. Moreover, the blocks are distributed in the polymer as phase separated soft and hard blocks in areas ranging from 5 to 20 nm size²². As the spot size of the microscope can only reach around 700 nm in the spatial direction, in the most optimal setup, confocal Raman measurements will always show a mixed signal from both PEOT and PBT molecular groups. A recent study on the degradation of PEOT PBT copolymers showed that the amount of the soft block in the total polymer decreases in time, while the amount of PBT remained relatively constant¹ during degradation. It was found that PEOT PBT polymers are degraded through 2 mechanisms; one being hydrolysis and the other oxidation, which mainly take place in the soft segment of the polymer. Because degradation through oxidation requires the presence of oxygen radicals and hydrogen peroxides, hydrolysis is a more likely event to occur during in vivo degradation of these materials. The process of hydrolysis leads to chain scissoring of the ester bond, mainly in the PEOT block, resulting in free PEO chains in the polymer. Therefore, one would expect a decrease in intensity of the Raman band which can be assigned to the ester bond.

However, Raman spectra show the resultant of a mixture of all Raman active chemical bonds present in a sample. Therefore, the decrease in intensity of the Raman band belonging to the ester bond in PEOT PBT copolymers can be obscured by the total number of Raman bands in the spectra, which are obtained from both the PBT and PEOT blocks and to lesser extent from the free PEO chains still present in the bulk of the sample, since these are located at similar positions. The most important reason for this is the fact that the molecular groups of which PEOT PBT copolymers are composed are comparable to each other, making it very hard to pick up small changes in the chemical composition of these materials by Raman spectroscopy. Another important factor contributing to the difficult interpretation of these data is the fact that changes in crystallinity or conformation can cause shape changes in certain Raman bands. An increase in crystallinity generally leads not only to a narrowing of Raman bands, but also to an increase in intensity of these bands¹⁶. Since the polymers observed in this study show increased crystallinity after degradation, based on heat of fusion and melting temperature of the hard block, it is likely that some of the positive bands found in the difference spectra are caused by this change. Only for 1000PEOT70PBT30 polymer discs clear signs of degradation could be detected, by a loss in PEOT content, while for 300PEOT70PBT30 and 300PEOT55PBT45 no change in composition was found even after 12 weeks. Interestingly, histology revealed that macrophage-like cells clearly play an active role in the uptake and possible further degradation of these materials. Since a number of authors have described the presence of macrophages or giant cells containing polymeric particles in the vicinity of PEOT PBT implants^{10, 23, 24} our observations seem to be in line with these findings. For future experiments a study regarding the intracellular degradation of these materials could shed some light on the advanced in vivo degradation by macrophages. After phagocytosis by these cells, degradation possibly will continue inside the phagosome, an organelle which plays a crucial role in the degradation of

internalized materials. Macrophages are known to produce oxidative reagents and enzymes which can contribute to further degradation of internalized polymeric particles. The creation of an in vitro system by which the uptake and subsequent degradation of small polymer particles inside single cells can be studied is therefore recommended.

References

1. Deschamps, A.; Grijpma, D.; Feijen, J., Poly(ethylene oxide)/poly(butylene terephthalate) segmented block copolymers: the effect of copolymer composition on physical properties and degradation behavior. *Polymer* **2001**, *42*, (23), 9335-9345.
2. Miot, S.; Woodfield, T.; Daniels, A. U.; Suetterlin, R.; Peterschmitt, I.; Heberer, M.; van Blitterswijk, C. A.; Riesle, J.; Martin, I., Effects of scaffold composition and architecture on human nasal chondrocyte redifferentiation and cartilaginous matrix deposition. *Biomaterials* **2005**, *26*, (15), 2479-89.
3. Woodfield, T. B.; Bezemer, J. M.; Pieper, J. S.; van Blitterswijk, C. A.; Riesle, J., Scaffolds for tissue engineering of cartilage. *Crit Rev Eukaryot Gene Expr* **2002**, *12*, (3), 209-36.
4. Woodfield, T. B.; Malda, J.; de Wijn, J. R.; Peters, F.; Riesle, J.; van Blitterswijk, C. A., Design of porous scaffolds for cartilage tissue engineering using a three-dimensional fiber-deposition technique. *Biomaterials* **2004**, *25*, (18), 4149-61.
5. Wang, H. J.; Bertrand-De Haas, M.; Riesle, J.; Lamme, E.; van Blitterswijk, C. A., Tissue engineering of dermal substitutes based on porous PEGT/PBT copolymer scaffolds: comparison of culture conditions. *J Mater Sci Mater Med* **2003**, *14*, (3), 235-40.
6. van Dorp, A. G.; Verhoeven, M. C.; Koerten, H. K.; Van Der Nat-Van Der Meij, T. H.; Van Blitterswijk, C. A.; Poncet, M., Dermal regeneration in full-thickness wounds in Yucatan miniature pigs using a biodegradable copolymer. *Wound Repair Regen* **1998**, *6*, (6), 556-68.
7. Beumer, G. J.; van Blitterswijk, C. A.; Poncet, M., Biocompatibility of a biodegradable matrix used as a skin substitute: an in vivo evaluation. *J Biomed Mater Res* **1994**, *28*, (5), 545-52.
8. Du, C.; Meijer, G. J.; van de Valk, C.; Haan, R. E.; Bezemer, J. M.; Hesseling, S. C.; Cui, F. Z.; de Groot, K.; Layrolle, P., Bone growth in biomimetic apatite coated porous Polyactive 1000PEGT70PBT30 implants. *Biomaterials* **2002**, *23*, (23), 4649-56.
9. Kuijter, R.; Bouwmeester, S. J.; Drees, M. M.; Surtel, D. A.; Terwindt-Rouwenhorst, E. A.; Van Der Linden, A. J.; Van Blitterswijk, C. A.; Bulstra, S. K., The polymer Polyactive as a bone-filling substance: an experimental study in rabbits. *J Mater Sci Mater Med* **1998**, *9*, (8), 449-55.
10. Meijer, G. J.; van Dooren, A.; Gaillard, M. L.; Dalmeijer, R.; de Putter, C.; Koole, R.; van Blitterswijk, C. A., Polyactive as a bone-filler in a beagle dog model. *Int J Oral Maxillofac Surg* **1996**, *25*, (3), 210-16.
11. Bulstra, S. K.; Geesink, R. G.; Bakker, D.; Bulstra, T. H.; Bouwmeester, S. J.; van der Linden, A. J., Femoral canal occlusion in total hip replacement using a resorbable and flexible cement restrictor. *J Bone Joint Surg Br* **1996**, *78*, (6), 892-8.
12. Meijer, G.; Radder, A.; Dalmeijer, R.; de Putter, C.; van Blitterswijk, C., Observations of the bone activity adjacent to unloaded dental implants coated with Polyactive or HA. *J Oral Rehabil* **1995**, *22*, (3), 167-74.
13. Radder, A.; Leenders, H.; van Blitterswijk, C., Interface reactions to PEO/PBT copolymers (Polyactive) after implantation in cortical bone. *J Biomed Mater Res* **1994**, *28*, (2), 141-51.

14. Radder, A.; Davies, J.; Leenders, H.; van Blitterswijk, C., Interfacial behavior of PEO/PBT copolymers (Polyactive) in a calvarial system: an in vitro study. *J Biomed Mater Res* **1994**, 28, (2), 269-77.
15. Li, P.; Bakker, D.; van Blitterswijk, C. A., The bone-bonding polymer Polyactive 80/20 induces hydroxycarbonate apatite formation in vitro. *J Biomed Mater Res* **1997**, 34, (1), 79-86.
16. Pelletier, M. J., *Analytical applications of Raman spectroscopy*. first ed.; Blackwell Science Ltd.: Oxford, 1999; p 1-478.
17. Kozielski, M.; Muhle, M.; Blaszcak, Z., The Raman scattering study of selected polyoxyethyleneglycols. **2004**, 111, (1-3), 1.
18. Di Noto, V.; Zago, V.; Biscazzo, S.; Vittadello, M., Hybrid inorganic-organic polymer electrolytes: synthesis, FT-Raman studies and conductivity of $\{Zr[(CH_2CH_2O)_{8.7}][r\ho]/(LiClO_4)_z\}_n$ network complexes. **2003**, 48, (5), 541.
19. Deschamps, A.; van Apeldoorn, A.; Hayen, H.; de Bruijn, J.; Karst, U.; Grijpma, D.; Feijen, J., In vivo and in vitro degradation of poly(ether ester) block copolymers based on poly(ethylene glycol) and poly(butylene terephthalate). *Biomaterials* **2004**, 25, (2), 247-258.
20. Radder, A. M.; Leenders, H.; van Blitterswijk, C. A., Interface reactions to PEO/PBT copolymers (Polyactive) after implantation in cortical bone. *J Biomed Mater Res* **1994**, 28, (2), 141-51.
21. Radder, A. M.; Davies, J. E.; Leenders, H.; van Blitterswijk, C. A., Interfacial behavior of PEO/PBT copolymers (Polyactive) in a calvarial system: an in vitro study. *J Biomed Mater Res* **1994**, 28, (2), 269-77.
22. Deschamps, A. A. Segmented Poly (ether ester)s and poly (ether ester amide)s for use in tissue engineering. Doctoral, University of Twente, The Netherlands, Enschede, The Netherlands, 2002.
23. Radder, A. M.; Loon, J. A.; Puppels, G. J.; Blitterswijk, C. A., Degradation and calcification of a PEO/PBT copolymer series. *Journal of Materials Science: Materials in Medicine (Historical Archive)* **1995**, 6, (9), 510.
24. van Dijkhuizen-Radersma, R.; Hesseling, S. C.; Kaim, P. E.; de Groot, K.; Bezemer, J. M., Biocompatibility and degradation of poly(ether-ester) microspheres: in vitro and in vivo evaluation. **2002**, 23, (24), 4719.

Annex

This short study was presented as a poster at the European society for biomaterials conference in september 2001 in London (UK) and indicated that our in house build confocal Raman system could actually be used to study implanted biomaterials. The outcome of this preliminary study lead to two ideas. First the degradation of PEOT PBT block copolymers had to be studied in a well defined *in vivo* model in combination with a simulated degradation model. Second, since the uptake of small polymer fragments by cells seemed to play a major role in polymer degradation a model had to be defined for the study of intra cellular biomaterial degradation.

A preliminary study on the application of confocal Micro Raman Spectroscopy for the analysis of in vivo PEOT PBT Degradation.

A. A. van Apeldoorn^{1,3}, Y. Aksenov², J.D. de Bruijn¹, C.Otto², C.A. van Blitterswijk^{1,3}

¹Isotis NV, P.O box 98, 3723AB Bilthoven, The Netherlands, ²Dept.of Biophysical Techniques, Technical Physics, University of Twente, The Netherlands, ³Dept.

Chemical Technology, University of Twente, The Netherlands.

Introduction

Polyactive™ (PA) is a degradable block copolymer composed of poly (butylene)terephthalate (PBT) and poly (ethyleneglycol) terephthalate (PEOT). The composition and therefore the mechanical and chemical properties of the copolymer can be tailored depending on the application, by varying the ratio of PEOT:PBT and changing the Mw of PEG, a basic component in the production of the polymer. As a major application of PA include its use as implant material in the form of a tissue-engineering scaffold, it is crucial to study the *in vivo* degradation of this material. Confocal Raman spectroscopy could be a valuable tool for the study of intra and extra cellular degradation processes as it can be used for non

destructive molecular analysis of biological samples at a high resolution. In this study we used an in house build confocal micro Raman spectrometer, which collects Raman scattering, through an infinity-corrected objective, in a backscatter configuration. A pinhole is chosen such that it functions as a confocal diaphragm. The system uses a thermo electrically cooled CCD, which can be used for spectrum and image formation with a high signal to noise ratio. We found signs of degradation of *in vivo* implanted PA similar to samples degraded by using a simulated degradation protocol. Furthermore, we were able to make Raman images of polymer fragments found by histology with our in house build confocal Raman system.

Materials and methods

The nomenclature of the polymers used in this study is as follows aPEOTbPBTc, The composition is denoted as $a / b / c$, where a represents the poly (ethylene glycol) (PEG) molecular weight (MW g/mol), and b and c represent the weight percentage (wt%) of PEOT and PBT blocks respectively. As a model for simulated degradation samples were submersed in phosphate buffered saline for 14 days at 100°C

Implantation

Sterile 1000PEOT70PBT30 discs of 15.5mm diameter were implanted for 3 years into the os ilium of adult Dutch milk goats. After implantation the ilia were explanted, fixated in a 4% paraformaldehyde solution, dehydrated in an increasing ethanol series and embedded in Methylmetacrylate.

Histology

Saw sections were prepared with a diamond innerlock saw (Leica microsystems, Germany) and stained either with methylene blue and basic fuchsin for histology,

or were left unstained. The stained sections were examined by light microscopy and the unstained material was used for Raman measurements.

Raman spectroscopy

Measurements were done with a custom made confocal Raman microscope using a diode laser ($\lambda=685$ nm) with 15-20 mW effective power at the sample surface and having a spatial resolution of 700nm. Non degraded and *in vitro* degraded, PA 1000/70/30 was measured as a reference.

Results

Raman spectroscopy

The retrieved fragments were characterized as being PA (see figure 1).

Several bands, 800, 1280, 1623 and 1725 cm^{-1} , typical for PA were used for imaging the observed fragments (figure 2C). A clear peak shape change around 1280 cm^{-1} was found not only after *in vitro* degradation but *in vivo* implantation as well.

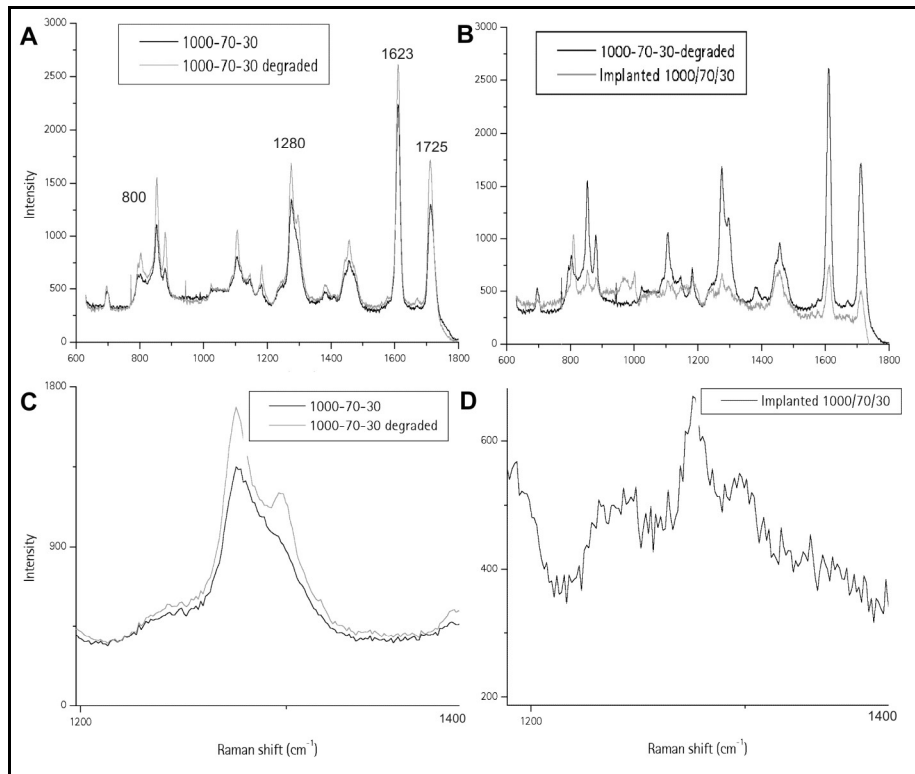


Figure 1 A: Raman spectra of non degraded vs. degraded PA. C: 1280 cm^{-1} band (magnification of 1A). B: Raman spectra of implanted PA vs. *in vitro* degraded PA, D: 1280 cm^{-1} band of implanted PA, note the similarity in shape with 1C.

Histology

Fragmentation of implant material was observed. Concentrations of macrophage like cells, containing PA fragments, in the area of fragmentation were observed (Figure 2). Bone surrounding the implant had a normal appearance and showed signs of bone remodelling.

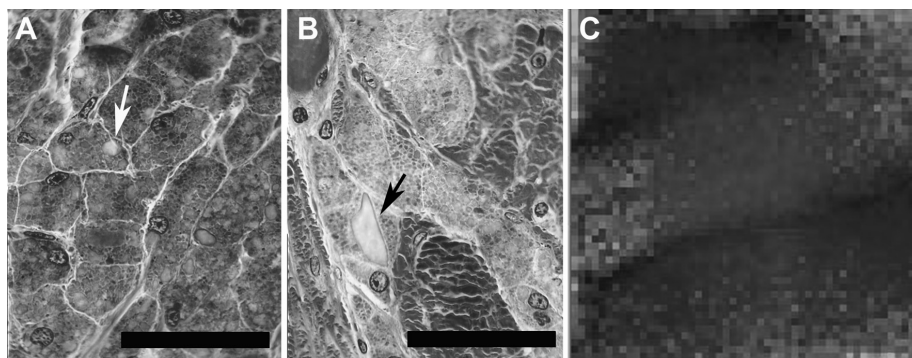


Figure 2. A: Light micrograph (100x) of cells containing polymer fragments (arrow) B: Light micrograph of macrophage like cells containing polymer fragments (arrow) C: Composite Raman image (90x90 μm) of an *in vivo* polymer fragment showing the intensity of the 800 (blue), 1280 (green), 1623 (dark Red) and 1725 cm^{-1} (red) Raman bands.

Conclusions

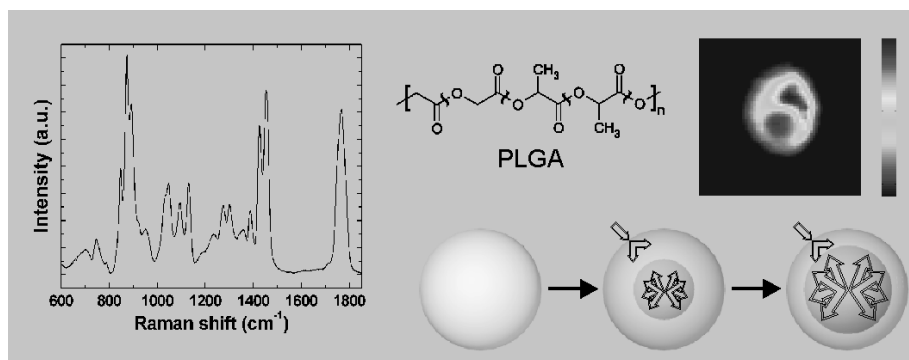
We were able to measure PA fragments found by histology.

The observed PA fragments showed possible signs of degradation similar to *in vitro* degraded specimens.

By selecting typical Raman bands we were able to image the observed PA fragments by selecting specific Raman bands.

These results show that confocal micro Raman spectroscopy can be a valuable tool to characterize and study the degradation of PA *in vitro* and *in vivo*.

Raman imaging of PLGA microsphere degradation inside macrophages



In order to study material degradation by single cells we developed an *in vitro* cell culture model. Adding microspheres composed of polylactic-co-glycolic-acid (PLGA), which were first incubated with serum, to a macrophage cell line allowed the study of material degradation in individual cells. In literature there is a debate whether, autocatalytic degradation, a rapid self sustaining degradation process caused by an accumulation of acidic end groups in the interior of implants composed of PLGA, also takes place in small devices. Observing the degradation by confocal Raman imaging, lead to the finding that both fast autocatalytic (inside out) and slow homogenous (outside in) degradation processes were present. Moreover, PLGA degradation seems to occur for the most part through scissioning of the glycolic acid bonds. By using this information we were able to design a schematic model depicting the aforementioned degradation process.

Abstract

Understanding the degradation behavior of polymeric microspheres is crucial for the successful application of such devices in controlled drug delivery. The degradation mechanism of poly(lactic-co-glycolic acid) (PLGA) microspheres inside phagocytic cells is not known, but different models for degradation in aqueous solution have been proposed. We have used confocal Raman spectroscopy and imaging to study the intracellular degradation of PLGA microspheres inside individual macrophages. Our results show that ingested microspheres degrade in a heterogeneous manner, with a more rapid degradation in the center. Comparison of Raman spectra from degrading beads with those of non-ingested beads reveals that ester hydrolysis occurs throughout the phagocytosed microspheres, with a selective loss of glycolic acid units. Furthermore, we show that PLGA degradation is a cell-mediated process, possibly caused by the low pH of the phagosome and/or the presence of hydrolytic enzymes. In conclusion, we have demonstrated that the chemical composition of degrading polymers inside cells can be probed by Raman spectral imaging. This technique will expand the capabilities of investigating biomaterial degradation in vivo.

Raman Imaging of PLGA Microsphere Degradation inside Macrophages

Aart A. van Apeldoorn¹, Henk-Jan van Manen², Jeroen M. Bezemer³, Joost D. de Bruijn¹, Clemens A. van Blitterswijk¹ and Cees Otto²

¹Polymer Chemistry and Biomaterials Group, and ²Biophysical Engineering Group, Faculty of Science & Technology, Biomedical Technology Institute, University of Twente, P.O. Box 98, 3723 AB Bilthoven, The Netherlands, and ³Octopus Technologies BV, Zernikedreef 12, 2333 CL Leiden, The Netherlands

Introduction

One of the key issues in successful application of biomaterials for tissue engineering and drug delivery is a well-characterized *in vivo* biodegradation behavior. Poly(lactic-co-glycolic acid) (PLGA) has been used for a wide variety of medical applications, from resorbable sutures to bone screws and microspheres for drug delivery. Degradation of PLGA *in vitro* as well as *in vivo* mainly takes place through either hydrolysis of the ester linkages and/or enzymatic degradation^{1, 2} (see the chemical structure in Figure 1). It has been reported that devices of PLGA degrade in a heterogeneous manner³. A model describing this process was proposed by Park⁴ based on work by Vert and coworkers, in which the degradation proceeds more rapidly in the center than at the exterior^{3, 5, 6}. This phenomenon is thought to be caused by autocatalytic action of the carboxylic acid end groups of the degrading material trapped in the internal milieu. It has been questioned whether this model is also valid when dealing with microspheres⁷. A more homogenous microsphere degradation, has been postulated on the basis of observation of homogenous degradation of small devices such as thin films⁸. In many cases, implantation of a biomaterial results in a foreign body reaction involving macrophages, which phagocytose small particles of the degrading materials. After

phagocytosis by these cells, degradation may continue inside the phagosome, which plays a crucial role in degradation of internalized materials.

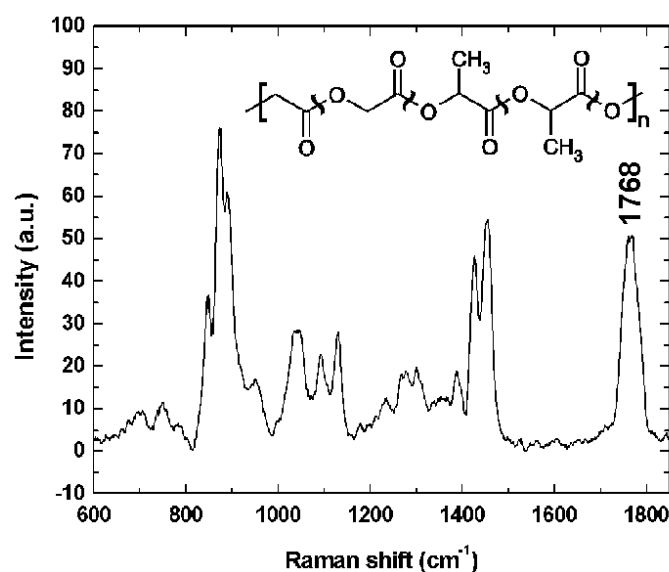


Figure 1. Raman spectrum and chemical structure of PLGA. In the structure, two glycolic acid units are shown on the left, whereas lactic acid units are displayed on the right. The ester bonds (marked “~”), which are hydrolyzed upon degradation, are characterized by a carbonyl stretching vibration at 1768 cm^{-1} .

The *in vivo* response to implanted biomaterials is in general studied by histology, which examines the tissue reaction by light microscopy. The limitation of these studies is that, although morphological changes can be studied, no information about the chemical composition of the degrading materials can be obtained from such measurements. Raman spectroscopy allows one to study the chemical bonds involved in degradation of these polymers by detecting intensity and wavelength changes in the vibrational bands of these bonds. We studied the degradation of PLGA microspheres, after macrophage phagocytosis *in vitro*, by nonresonant confocal Raman spectroscopy and imaging.

Materials and methods

The PLGA microspheres (50:50% glycolide/lactide by weight) were produced by a so-called salting-out procedure described before^{9, 10}. Scanning Electron Microscopy

(SEM) showed that their size varied between 1-10 μm in diameter and that they were of solid nature (Figure 3E). The microspheres were sterilized in 70% ethanol for 15 min and then washed in sterile PBS. After washing, the material was opsonized for 30 min using human serum. The microspheres were then added to a macrophage cell line (RAW 264.7) cultured on poly-L-lysine coated CaF_2 slides, in RPMI 1640 medium containing 10% FBS, 2 mM L-glutamine, and antibiotics. The cells were cultured for 1 and 2 weeks at which point they were fixed using 4% paraformaldehyde for 30 min. The samples were washed and placed in PBS for Raman measurements, which were performed using a home-built confocal Raman microscope as described previously¹¹. A pinhole of 15 μm diameter was employed, providing an axial resolution (FWHM) of 1.5 μm . During Raman imaging, we scanned an intracellular area of $7.5 \times 7.5 \mu\text{m}^2$, using a signal accumulation time of 1 s per pixel at 100 mW 647.1 nm excitation.

Results and discussion

The internalized microspheres showed signs of intracellular degradation already after 1 week of cell culture. Light microscopy revealed what appeared to be a cavity in the center of the microspheres at 1 and 2 weeks of cell culture (Figure 3A and C). Confocal Raman spectroscopy and imaging of degraded PLGA spheres confirmed these observations. In contrast, PLGA microspheres incubated under identical conditions, but in the absence of macrophages (insets Figure 3C and D), did not show any signs of degradation. Raman images of phagocytosed microspheres constructed in the 1768 cm^{-1} band specific for the ester groups of PLGA clearly show a low intensity of this band in the internal area of several particles already after 1 week (Figure 3B). This indicates the loss of PLGA ester bonds from the center of these microspheres. We scaled both the pure PLGA spectrum (Figure 1) and averaged spectra taken from the high- and low-intensity regions of the PLGA microsphere in Figure 3D to the 875 cm^{-1} band, which is

assigned to the C–COO stretch vibration of lactic acid¹² and is not affected by hydrolysis. Analysis of the spectroscopic data after Raman imaging revealed that 2 weeks after phagocytosis a ~30% reduction in the ester bond intensity was found in both the low- and high-intensity area of the internalized microsphere, compared to pure PLGA. This is demonstrated by the negative band in Figure 2A and B at 1768 cm⁻¹ after subtraction of the scaled spectra of pure PLGA. Moreover, the difference spectrum in Figure 2A shows bands specific for the cell cytoplasm. Based on the presence of bands at 1004 cm⁻¹ (phenylalanine) and 1662 cm⁻¹ (amide I) and the 1440 cm⁻¹ band assigned to CH₂ groups predominantly found in lipids, we conclude that both proteins and lipids are present in the degradation-induced void present in the microspheres. It is unlikely that these molecules have diffused through the intact outer shell of the microspheres, since this particular composition of PLGA is rather hydrophobic. Proteins and lipids have probably traveled through one or more pores formed by degradation which connect the cavity in the centre to the phagosomal milieu. Such a mechanism is also indicated by the collapsed microsphere in the top right corner of the Raman image in Figure 3B. Using either 3D Raman imaging or observation of the microsphere surface by SEM after isolation from the macrophages will probably resolve these issues.

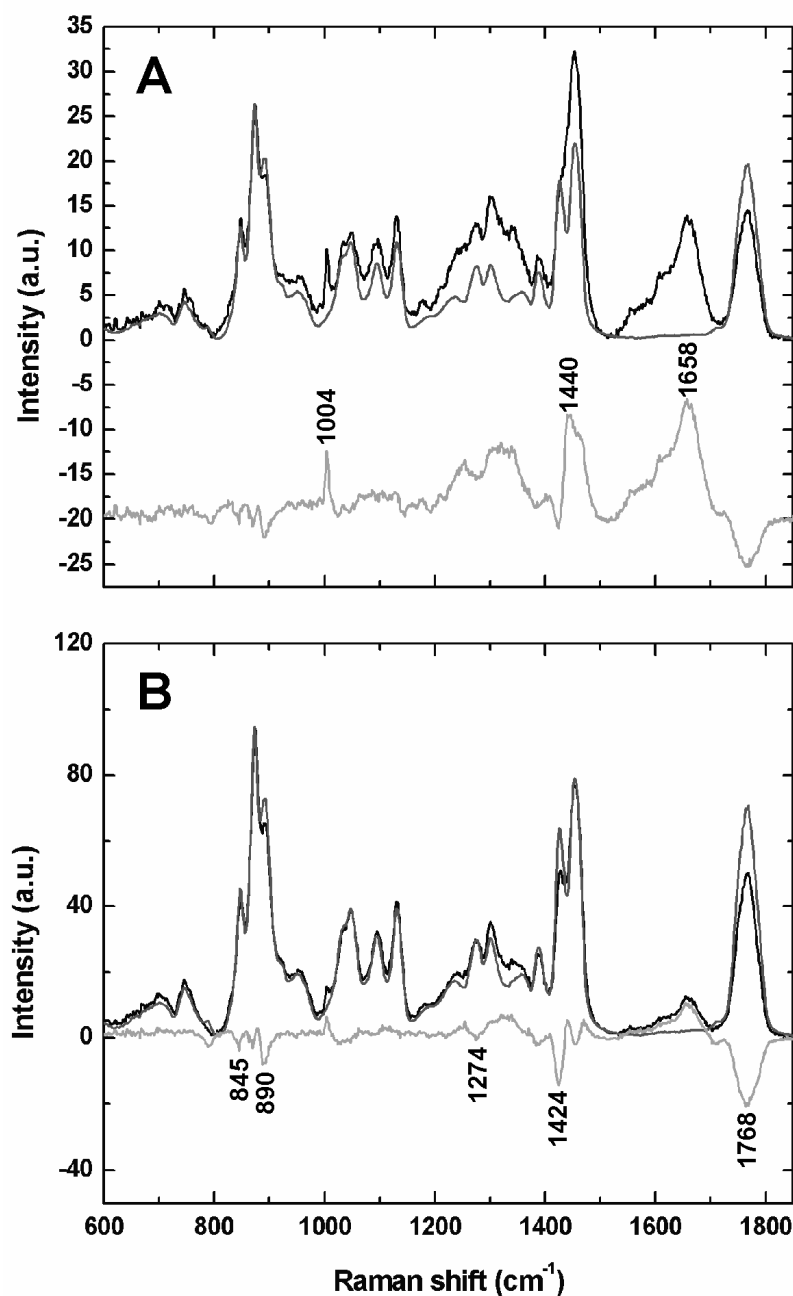


Figure 2. Raman spectra (in black) of the low- (A) and high-intensity (B) regions of the PLGA microsphere in Figure 3D. Pure PLGA is shown in red, and difference spectra (after scaling to the 875 cm⁻¹ band) in green. Note the negative band at 1768 cm⁻¹, indicating a decrease of ester bonds, and the negative bands specific for glycolic acid at 845, 890, 1274, and 1424 cm⁻¹.¹²

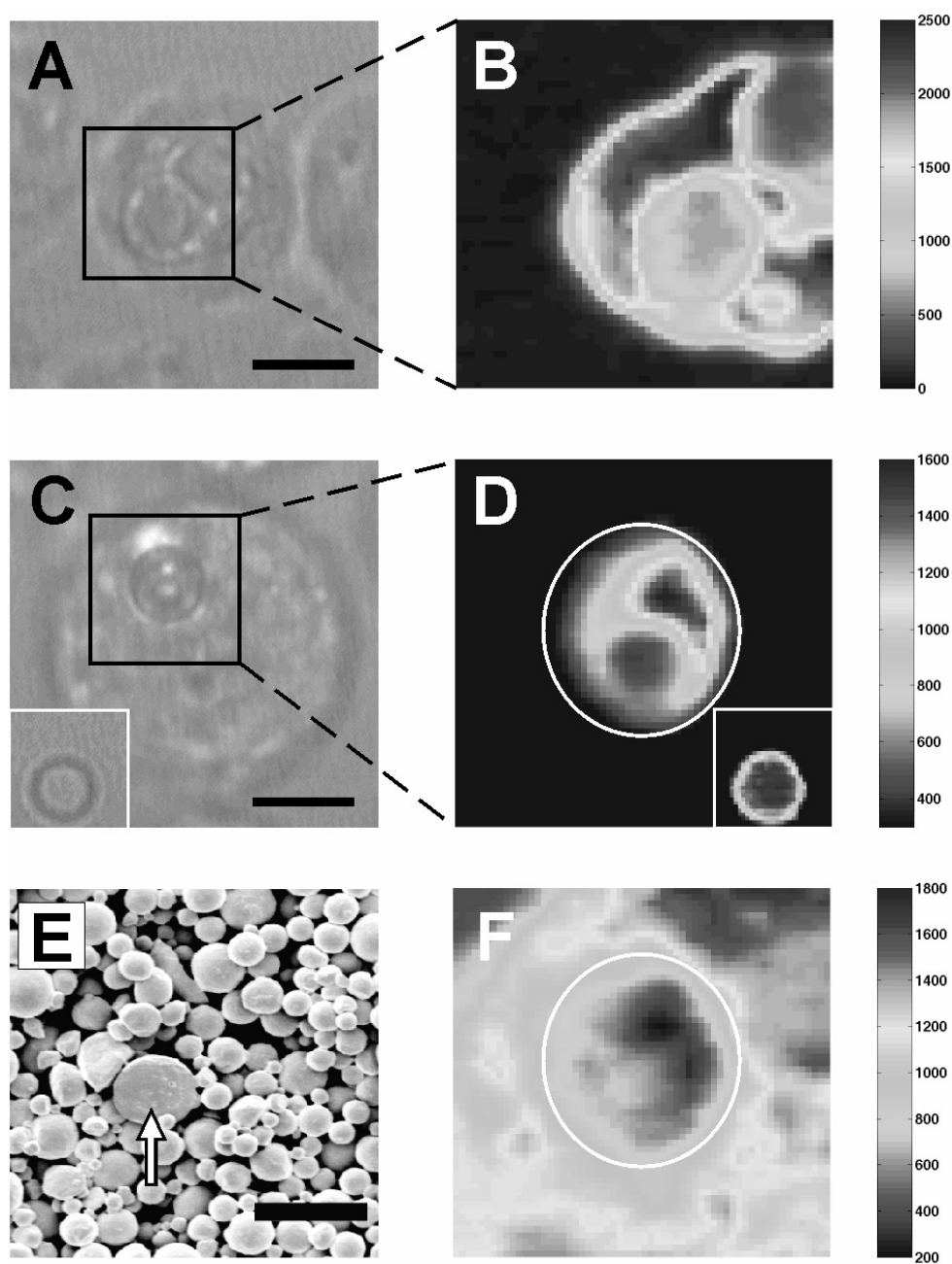


Figure 3. (A and C) Light micrographs of macrophages containing phagocytosed beads cultured for 1 and 2 weeks, respectively (scale bar 5 μm). The Raman images ($7.5 \times 7.5 \mu\text{m}^2$) of these beads are shown in B and D. The scale in B and D shows the relative intensity of the 1768 cm^{-1} band used for imaging (specific for PLGA ester bonds). Insets in C and D show controls (image size $7.5 \times 7.5 \mu\text{m}^2$). The Raman image in 3F depicts the intensity of the 1527-1714 cm^{-1} region, which contains bands from cytoplasmic species. (E) Electron micrograph of PLGA microspheres after freezing and crushing in liquid nitrogen. A cross-section of a broken sphere, showing the solid center, can be seen (arrow) (scale bar 10 μm).

The outcome of our study adds not only histological but also chemical data to the model proposed by Park⁴ and Vert,^{3, 5, 6} describing heterogeneous degradation of PLGA starting from the center and going outwards. The degradation of PLGA leading to the induction of concentric cavities in the microspheres after uptake by macrophages, as described here, is in favor of that model. However, analysis of the spectroscopic data strongly suggests that degradation takes place throughout the whole microsphere by hydrolysis of the ester bonds preferentially related to the glycolic acid block in the polymer, as indicated by the negative bands in Figure 2A and B. This finding is more related to the suggestion of homogenous degradation by Li when dealing with microspheres⁷. As existing models do not take into account the influence of the cell on the microsphere degradation process, they must be different from a phagosomal degradation mechanism. Our results indicate that the PLGA degradation behavior shown here is a cell-mediated process, caused by either the low pH (~ 5.5) and/or the presence of hydrolytic enzymes in the phagosome, since control samples lacking macrophages did not show any degradation after 1 and 2 weeks (insets Figure 3).

Conclusions

In conclusion, we have demonstrated that confocal Raman spectroscopy and microscopy are unique, label-free tools to study intracellular microsphere degradation after *in vitro* phagocytosis. These techniques allow detailed information about the chemical composition of the degrading polymer particles to be obtained. In addition, they will enable studies directed at the chemical investigation of biomaterial degradation *in vivo*.

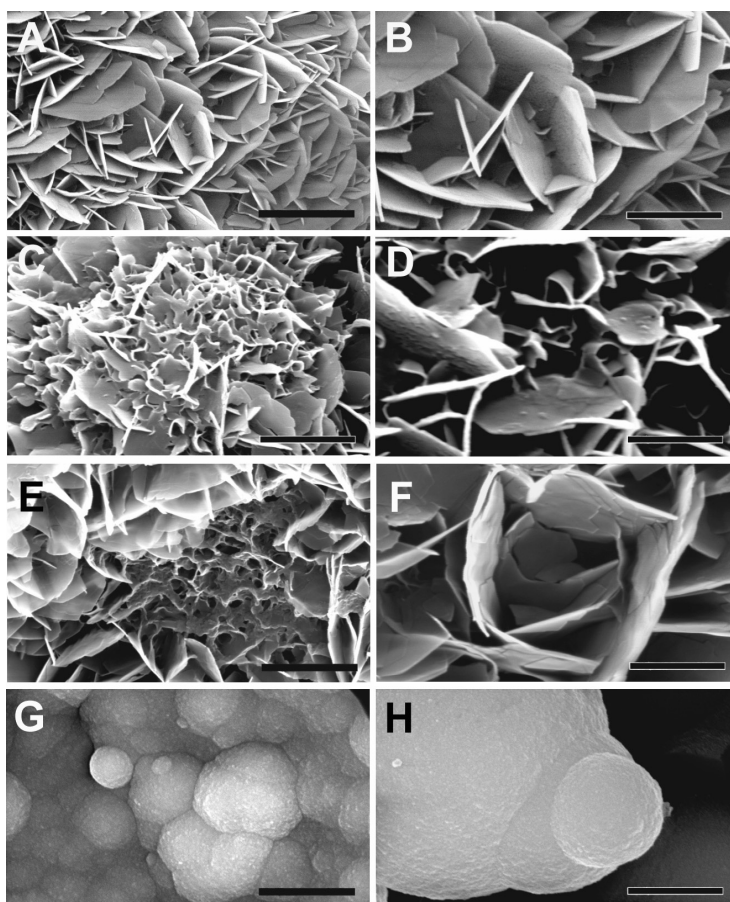
Acknowledgement

We thank Ms. S. Métairie from Octoplus Technologies BV for preparing the microspheres. Funding was provided by the Dutch Technology Foundation (STW).

References

1. Edlund, U., Albertsson, A.C., Degradable polymer microspheres for controlled drug delivery. *Advances in polymer science* **2002**, *157*, 67-112.
2. Schliecker, G.; Schmidt, C.; Fuchs, S.; Wombacher, R.; Kissel, T., Hydrolytic degradation of poly(lactide-co-glycolide) films: effect of oligomers on degradation rate and crystallinity. *Int J Pharm* **2003**, *266*, (1-2), 39-49.
3. Therin, M.; Christel, P.; Li, S.; Garreau, H.; Vert, M., In vivo degradation of massive poly(alpha-hydroxy acids): validation of in vitro findings. *Biomaterials* **1992**, *13*, (9), 594-600.
4. Park, T. G., Degradation of poly(lactic-co-glycolic acid) microspheres: effect of copolymer composition. *Biomaterials* **1995**, *16*, (15), 1123-30.
5. Li, S. M., Garreau, M., Vert, M., Structure-property relationships in the case of the degradation of massive aliphatic poly-(alfa-hydroxy acids) in aqueous media, part 1: poly(DL-lactic acid). *Journal of materials science: materials in medicine* **1990**, *1*, 123-130.
6. Li, S. M., Garreau, M., Vert, M., Structure-property relationships in the case of the degradation of massive aliphatic poly-(alfa-hydroxy acids) in aqueous media, part 2: Degradation of lactide-glycolide copolymers: PLA37.5GA25 and PLA75GA25. *Journal of materials science: materials in medicine* **1990**, *1*, 131-139.
7. Li, S., Hydrolytic degradation characteristics of aliphatic polyesters derived from lactic and glycolic acids. *J Biomed Mater Res* **1999**, *48*, (3), 342-53.
8. Grizzi, I.; Garreau, H.; Li, S.; Vert, M., Hydrolytic degradation of devices based on poly(DL-lactic acid) size-dependence. *Biomaterials* **1995**, *16*, (4), 305-11.
9. Maa, Y. F.; Hsu, C. C., Effect of primary emulsions on microsphere size and protein-loading in the double emulsion process. *J Microencapsul* **1997**, *14*, (2), 225-41.
10. Lu, W.; Park, T. G., Protein release from poly(lactic-co-glycolic acid) microspheres: protein stability problems. *PDA J Pharm Sci Technol* **1995**, *49*, (1), 13-9.
11. Uzunbajakava, N.; Lenferink, A.; Kraan, Y.; Volokhina, E.; Vrensen, G.; Greve, J.; Otto, C., Nonresonant confocal Raman imaging of DNA and protein distribution in apoptotic cells. *Biophys J* **2003**, *84*, (6), 3968-81.
12. Geze, A.; Chourpa, I.; Boury, F.; Benoit, J. P.; Dubois, P., Direct qualitative and quantitative characterization of a radiosensitizer, 5-iodo-2'-deoxyuridine within biodegradable polymeric microspheres by FT-Raman spectroscopy. *Analyst* **1999**, *124*, (1), 37-42.

Combined confocal Raman spectroscopic and SEM study of protein incorporation into biomimetic coatings



Sometimes the outcome of research can result in wonderful pieces of art. The coprecipitation of proteins with a different charge (pI-value), but equal in size, into biomimetic carbonated apatite like coatings resulted in interesting changes in surface topography of these materials. A and B; electron micrographs of a regular biomimetic carbonated apatite like coating. C and D; incorporation of bovine serum albumin, results in curved crystals and cauliflower shaped structures. E and F; haemoglobin, the oxygen carrying protein in red blood cells, incorporation resulted in areas containing small and larger crystals which seem to be stacked on each other. G and H; the incorporation of poly aspartic acid resulted in an astounding surface structure composed of globules, which seem to grow on top of each other. Scale bars on the left are all 2 μm , while the scalebars on the right are all 1 μm .

Abstract

Biomimetic calcium phosphate coatings on the contrary to plasma spray coatings are in general produced at ambient temperatures and a controlled pH and consequently allow the incorporation of proteins. Recent studies on protein incorporation in biomimetic calcium phosphate coatings showed an effect of protein on crystal shape. In these studies bovine serum albumin (BSA) was used at different concentrations in the precipitation solution in order to study its incorporation into the coating. The outcome of these studies was that not only BSA had coprecipitated with a carbonate apatite like coating, but the crystal structure had been affected as well. The use of increasing concentrations of BSA lead to alterations in crystal size and shape which could be observed by scanning electron microscopy (SEM). Nonetheless, the precise effect of the alteration in crystal size and shape on the crystallinity remained unclear. In this study the consequence of different concentrations of BSA incorporated into biomimetic carbonated apatite coatings in relation to the effect on crystal size, crystallinity and physical appearance was studied. The biomimetic coatings were examined by thin film X-ray diffraction (TF-XRD), and a combination of confocal Raman spectroscopy and SEM. Results obtained during this study showed that not only the presence of protein could be detected in a non destructive manner, but also information about the relative amount of protein present in the coating could be obtained as well by using confocal Raman microscopy. Although, the increase of the BSA concentration did not seem to influence the crystallinity towards a great extent, the increase in standard deviation of the calculated values together with SEM observations suggest that the coating structure had become more heterogeneous in its nature. The combination of SEM and confocal Raman spectroscopy proved to be a feasible analysis technique to investigate not only the morphology of these coatings but also their physiochemical composition.

Combined confocal Raman spectroscopic and SEM study of protein incorporation into biomimetic coatings

A. A. van Apeldoorn¹, Y. Aksenov², M. Stigter³, J. D. de Bruijn¹, J. Greve², C. Otto²,
C. A. van Blitterswijk¹

¹Department of Polymer Chemistry and Biomaterials, Faculty of Technology and Sciences, University of Twente, PO Box 98, 3720 AB Bilthoven, The Netherlands,

²Department of Biophysical Techniques, Faculty of Technology and Sciences, University of Twente, PO Box 217, 7500AE Enschede, The Netherlands, ³Isotis NV, PO Box 98, 3720 AB Bilthoven, The Netherlands

Introduction

Titanium and its alloys are generally used to design orthopedic implants mainly because of their excellent mechanical properties. In order to enhance bone-bonding capacities these implants can be coated with calcium phosphate coatings. Nowadays, coatings are mainly deposited on these surfaces by using the plasma spray technique. However, the plasma spray technology is a line of sight process at extremely high temperature, and does not allow for the incorporation of proteins, like growth factors and antibiotics. The use of specific growth factors in order to stimulate bone formation, like bone morphogenic proteins, could speed up the process of integration of an implant with bone¹⁻³. In contrast, biomimetic calcium phosphate coatings are generally produced at ambient temperatures at a controlled pH^{4,5} and therefore allow the incorporation of proteins. Recently protein incorporation was studied on biomimetic calcium phosphate coatings^{6,7}. In these studies bovine serum albumin (BSA) was used at different concentrations in the precipitation solution in order to study its incorporation. Results showed that not

only BSA had coprecipitated with a carbonate apatite like coating, but the crystal structure of this coating was affected as well. The use of increasing concentrations of BSA lead to an alteration in crystal size and shape as was observed by scanning electron microscopy. However, the exact effect of the change in crystal size and shape on the crystallinity remained unclear. Crystallinity and crystal structure of calcium phosphate coatings are well described factors which can influence the dissolution behavior of these materials^{8,9}. A study on the effect of calcium phosphate on bone cell mineralization revealed that release of calcium ions from calcium phosphates promotes mineralization and could be crucial for the bioactivity¹⁰ of coatings and ceramics. Coathup and coworkers found that hydroxyapatite coatings have a significantly greater interfacial contact with bone when compared to a roughened titanium surface, and significantly more bone had attached to a crystalline HA coating compared with the HA coating of lower crystallinity, though significantly more bone had formed in the vicinity of the lower crystalline HA coating¹¹. In our study the effect of different concentrations of BSA incorporated into biomimetic carbonated apatite coatings in relation to the effect on crystal size, crystallinity and physical appearance was investigated. We used thin film X-ray diffraction (TF-XRD), and a combination of confocal Raman spectroscopy and scanning electron microscopy to study these biomimetic coatings. In a previous study we showed the advantage of using a confocal Raman microscope (CRM) integrated with a scanning electron microscope (SEM) to study osteoblast mineralization on titanium alloy surfaces. In this particular study it was found that by using the CRM in combination with SEM inorganic (calcium phosphate) and organic (protein) components of mineralized bone matrix and their distribution related to the morphology could be analyzed on these samples¹². Since Raman spectroscopy allows for the non-destructive molecular analysis of samples by measurement of wavelength shifts from an incident monochromatic light source (Laser), which are caused by chemical bond vibrations, it is highly suitable for

studying the effects of protein incorporation into biomimetic calcium phosphate coatings when combined with a SEM. We were not only able to detect the presence of BSA, but also its effect on the relative crystallinity of carbonated apatite like biomimetic coatings which were deposited on a titanium alloy surface. Furthermore, it was found that by increasing concentrations of BSA in the precipitation solution the surface morphology was altered from consisting of sharp rectangular crystals in a fairly homogenous distribution to small and big rounded crystals with an irregular distribution.

Materials and methods

Preparation of carbonated apatite coatings (CO₃-AP)

All CO₃-AP coatings (5 samples per group) were prepared on sandblasted Ti6Al4V (Smitford Staal BV, The Netherlands) square plates with a surface area of 10 mm² and 1 mm thickness. The plates were ultrasonically cleaned for 15 min. in acetone, 70% ethanol and demineralized water in sequence. The CO₃-AP coatings with different crystallinity were prepared according to a precipitation method developed by Barrere et al.^{4,13}. In short, coatings were prepared from different salt solutions as shown in table 1.

<i>Biomimetic coatings:</i>		
Low crystalline	Medium crystalline	High crystalline
733.5 mmol/l NaCl	733.5 mmol/l NaCl	733.5 mmol/l NaCl
7.5 mmol/l MgCl ₂	1.5 mmol/l MgCl ₂	0.75 mmol/l MgCl ₂
12.5 mmol/l CaCl ₂	12.5 mmol/l CaCl ₂	12.5 mmol/l CaCl ₂
10 mmol/l HCO ₃	10 mmol/l HCO ₃	7.5 mmol/l HCO ₃
5 mmol/l HPO ₄	5 mmol/l HPO ₄	5 mmol/l HPO ₄

Table 1: Composition of the precipitation solutions

The precipitation process took place at 37 °C for 24 hours. Increasing the Mg²⁺ concentration inhibits the precipitation process and favors the formation of an amorphous calcium phosphate coating. In addition a series of coatings was prepared similar to the high crystalline coating mentioned before in which bovine

serum albumin (BSA) was added to a concentration of 1, 10 and 100 mg/l. The coatings were analyzed by TF-XRD and a scanning electron microscope using a FEI ESEM, model XL-30 FEG in which an in house built confocal Raman microscope was fitted. As a reference 100% crystalline stoichiometric hydroxyapatite (HA) material calcined at 1000 °C for 10 hours was used and measured both with Raman spectroscopy and TF-XRD.

Combined Confocal Raman Scanning Electron Microscope (CRESEM)

We have integrated a confocal Raman microscope with a FEI XL-30 FEG ESEM, a schematic drawing of this system can be seen in figure 1.

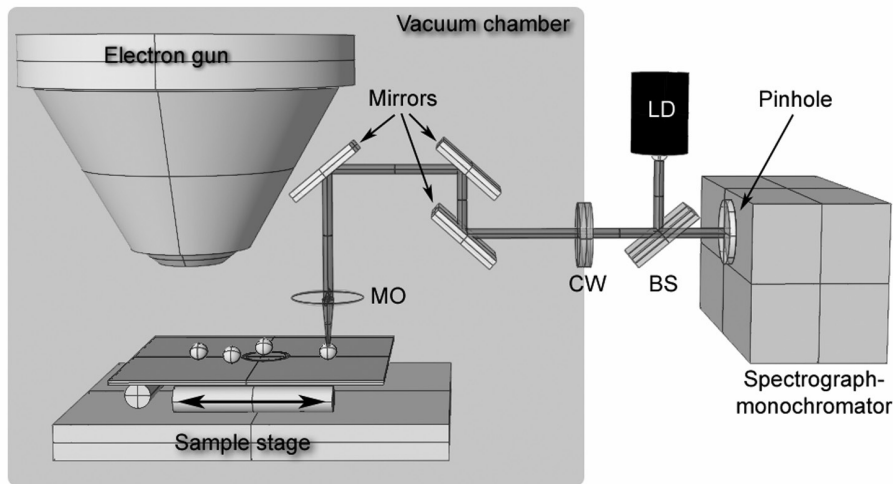


Figure 1: schematic drawing of the CRESEM setup (for an elaborate explanation see materials and methods).

A collimated and circularly symmetrical beam from a diode laser (LD) (Mitsubishi electron corp.) with a frequency of 685nm is reflected by a dichroic beam splitter (BS) into the vacuum chamber of the SEM through a coupling window (CW). The beam is then focused by a 60X microscope objective (MO) (Zeiss, West-Germany) on a sample of interest. The excited Raman scattering is collected by the same objective and the Stokes components of Raman frequencies pass through the BS, a notch filter (NF), which blocks photons with the initial laser wavelength, and a pinhole (\varnothing 25 μ m), allowing for confocality of the system. Subsequently, the

scattering is collected in a spectrograph-monochromator where the incoming light is decomposed by a concave holographic grating and focused on a thermoelectrically cooled CCD (1056x256 pixels, Princeton Instruments Spec10). The theoretical spatial resolution of the system is $\sim 700\text{nm}$ with an effective laser power of 6mW on the sample¹⁴. The CCD is connected with a computer for data collection and analysis by using WinSpec and Microcal Origin data analysis software. The setup was calibrated by using 5 and 20 μm \varnothing polystyrene beads to establish the coordinates needed for lateral movement from the electron gun to the laser spot.

CRESEM on biomimetic CO_3 -AP coatings

In order to ensure that all samples were measured in a similar manner, CRESEM measurements were collected in the centre from cross sections of the coating. The samples were positioned in such a way that the coordinates of the laser spot would fall in the middle of a cross-section of the coating thus ensuring similar measurements for each sample. Various measurements, at least 10 per sample, were done at different locations and sufficient time was taken to ensure a relatively low signal to noise ratio of each measurement. We used a method developed by others¹⁵ to calculate the relative crystallinity of the obtained coatings. The full width half maximum (FWHM) of the 960 cm^{-1} peak was determined after Gaussian curve fitting of at least 10 different measurements per sample. The relative crystallinity was then determined according to the following formula:

$$\text{Relative crystallinity} = \text{FWHM}_{\text{coat}} / \text{FWHM}_{\text{HA}} * 100\% \quad (1)$$

TF-XRD analysis

X-ray diffraction measurements were taken with a Rikagu miniflex goniometer with Cu radiation (Cu $K\alpha$, $\lambda = 1.54\text{\AA}$, 30kV, 15mA) directly at the sample surface. A single peak was chosen from the spectrum of each sample at around 25 degrees

($2\theta/\theta$) to determine relative differences in crystallite dimensions, which was calculated according to “the Debye-Scherrer equation”:

$$D_c = K\lambda / \theta_{1/2} \cos \theta_B \quad (2)$$

(D_c =crystallite dimension in angstrom, k =shape constant 0.9, λ =wavelength of X-ray, $\theta_{1/2}$ =FWHM of diffraction peak, θ_B = diffraction angle).

All XRD patterns were recorded at the same conditions, scan range $2\theta=15$ to 60° , scan speed: $2.00^\circ/\text{min}$ while the scan step was 0.02°

Results

CRESEM on biomimetic CO₃-AP coatings

All Raman spectra obtained from the coatings showed characteristic peaks for the phosphate group vibration modes (see figure 2): 960 cm^{-1} ν_1 , $430\text{--}450\text{ cm}^{-1}$ ν_2 , $1030\text{--}1040\text{ cm}^{-1}$ ν_3 , $580\text{--}590\text{ cm}^{-1}$ ν_4 and a band around 1070 cm^{-1} which can be assigned to the ν_1 stretch vibration of the carbonate group. A decrease in FWHM of the ν_1 phosphate group vibration (symmetrical stretch mode band) could be observed with increase in crystallinity (table 2 and 3).

<i>Coating type</i>	<i>Mean FWHM (cm^{-1})</i>	<i>SD (+/-) (cm^{-1})</i>	<i>Crystallinity (%) Raman</i>	<i>$\Theta_{1/2}$ of 25 degree peak (degrees Θ)</i>	<i>D_c (\AA)</i>
CO ₃ -AP 1	20.57	0.42	21.2	0.60688	146
CO ₃ -AP 2	18.01	1.53	24.6	0.44241	200
CO ₃ -AP 3	15.62	0.70	31.2	0.31652	279
Hydroxyapatite	4.57	0.35	100.0	0.15426	572

Table 2: Summary of properties from coatings without protein determined by Raman spectroscopy and TF-XRD.

<i>Coating type</i>	<i>Mean</i> <i>FWHM</i> <i>(cm⁻¹)</i>	<i>SD (+/-)</i> <i>(cm⁻¹)</i>	<i>Crystallinity</i> <i>(%)</i> <i>Raman</i>	<i>Θ_{1/2} of 25 degree</i> <i>peak (degrees Θ)</i>	<i>D_c (Å)</i>
1 mg/l BSA	16.71	0.37	27.9	0.21846	404
10 mg/l BSA	16.08	0.53	28.4	0.25749	343
100 mg/l BSA	18.12	1.16	25.2	0.29785	296
Hydroxyapatite	4.57	0.35	100.0	0.15426	572

Table 3: Summary of properties from BSA containing coatings determined by Raman spectroscopy and TF-XRD.

In addition bands (1450 cm⁻¹, 1580 cm⁻¹) known to be protein related began to appear when higher concentrations of BSA (10 and 100mg/l) were used for the preparation of the BSA containing coatings (figure 2).

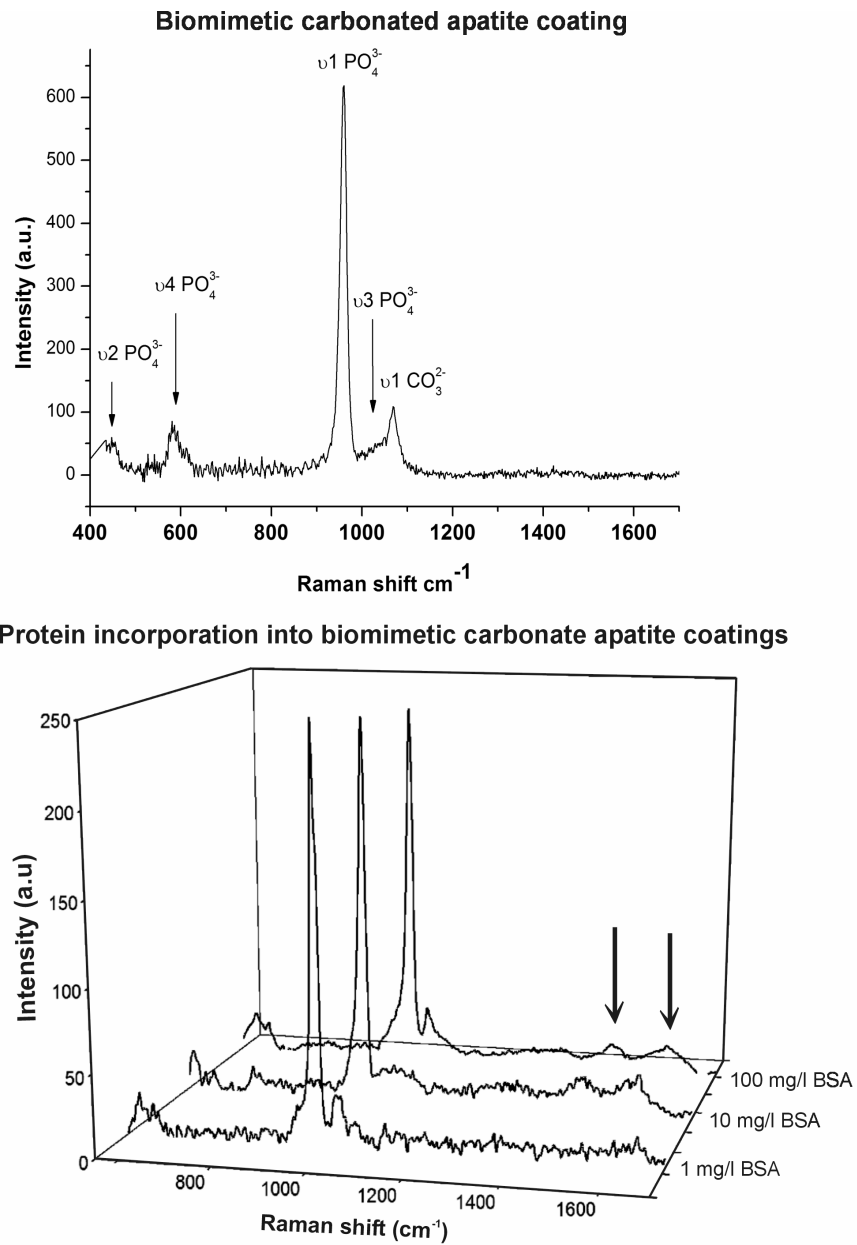


Figure 2: Typical Raman spectrum of carbonated apatite coating showing the different band assignments (top). Raman spectra of BSA containing coatings, the arrows indicate the protein specific bands at 1450 cm⁻¹, 1660 cm⁻¹.

TF-XRD analysis

X-ray diffraction spectra (see figure 3) of coatings were collected directly from the surface of the samples without any other treatment in order to maintain the surface structure. In order to calculate crystallite dimensions the band at 25 degrees (2θ) was Gaussian curve fitted and from these fits the FWHM was determined. The obtained values were compared to 100% crystalline hydroxyapatite and their respective relative values were calculated (table 2 and 3). The results presented in table 2 show that with increase in crystallinity the FWHM ($\theta_{1/2}$) of the peak occurring around 25 degrees is decreasing and therefore the crystallite dimension in the 002 direction is increasing. The presence of BSA lead to a slight decrease in crystallinity from 27.9, for 1 mg/l BSA, to 25.2, for 100 mg/l BSA, while crystallite dimensions decreased from 404 Å towards 296 Å .

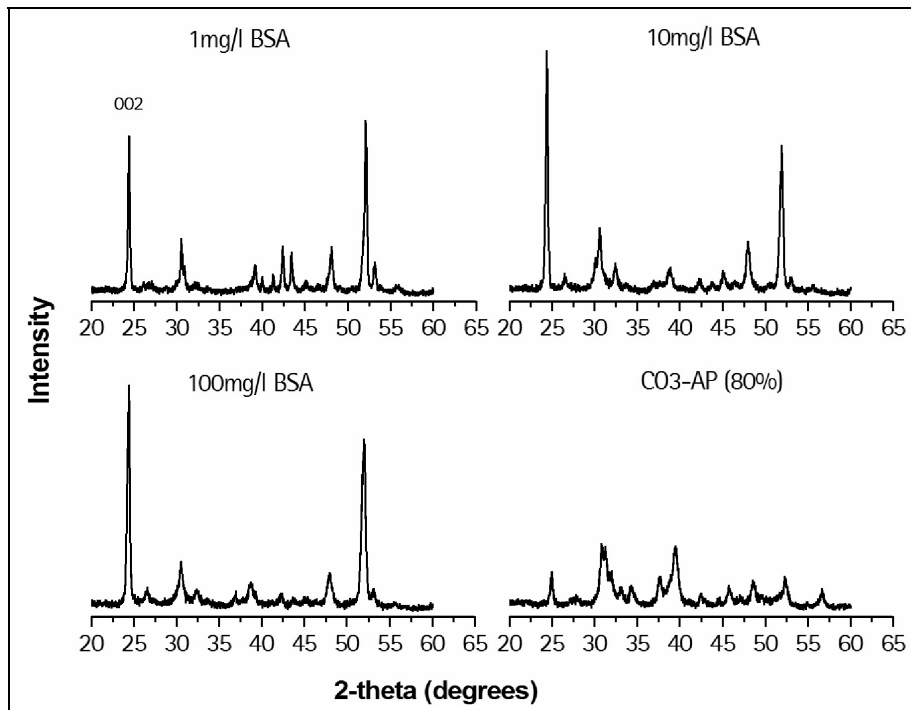


Figure 3: TF-XRD spectra of protein containing coatings compared to the coating containing no protein with high crystallinity the 002 peak was used to determine the D value along the c-axis.

Scanning Electron Microscopy

All the coatings prepared without protein showed a similar morphology of which a representative electron micrograph is shown in figure 4A.

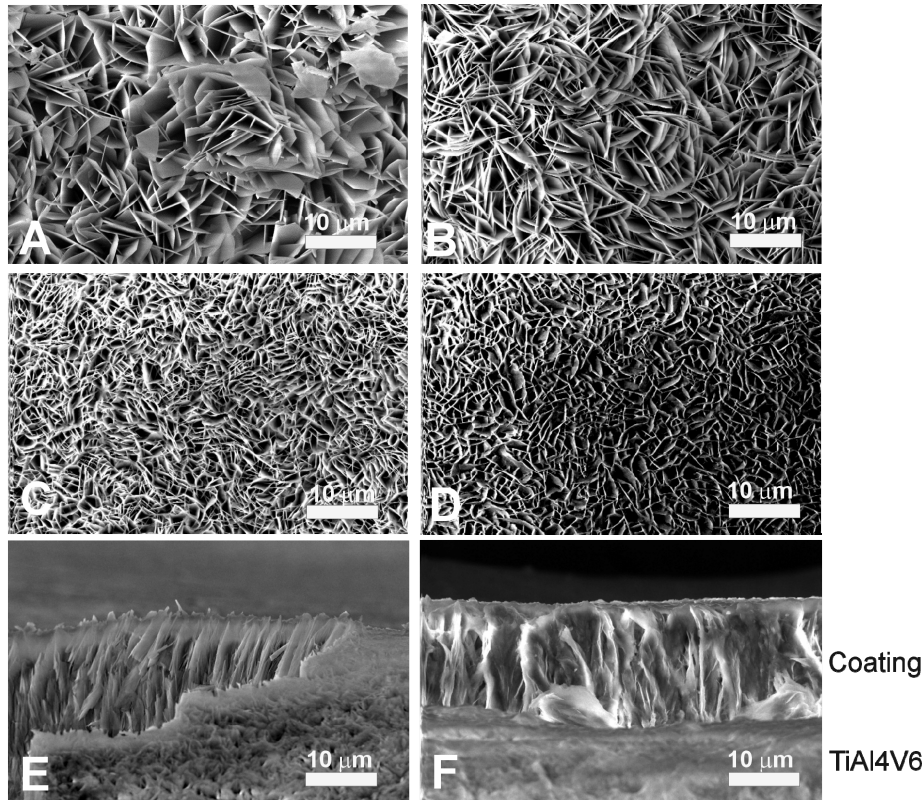


Figure 4: Scanning electron micrographs of different CO₃-AP coatings. A) no protein containing coating (CO₃-AP3). B-D) Coatings prepared with a solution containing 1, 10 and 100 mg/l BSA, note the decreasing crystal size with increasing protein concentration. E and F) Cross-section view of coatings prepared with a solution containing no protein (E) and 100 mg/l BSA (F) showing the morphological changes, sharp crystals versus rounded crystals) when protein is present in the precipitation solution.

In these samples a fairly homogenous distribution of sharp rectangular crystals of similar size can be seen. In this case adding different concentrations of Mg²⁺ does not seem to affect crystal dimensions to the extent protein does. Even though, XRD measurements showed that the crystallite dimensions, the individual units of which the crystals are composed, decrease when more Mg²⁺ or BSA is present in the precipitation solution as was determined by XRD (table 1 and 2). As can be observed on the electron micrographs the surface texture of the coatings changes

with incorporation of BSA (figure 4B-D). Crystal shape and size clearly changes when higher concentrations of BSA in the precipitation solution are used during preparation of the coatings. The electron micrographs show that the crystals become smaller and their shape appears to be more bended at higher concentrations of BSA. Moreover, the size of the crystals in protein containing coatings is clearly smaller than in coatings without protein. When comparing samples prepared with the different concentrations of BSA we found that the crystal size decreases with each increase in BSA concentration. A closer observation of the cross-sections revealed that the crystals, which are standing up from the substrate surface, appear to be more disorganized when protein is present (figures 4E and F).

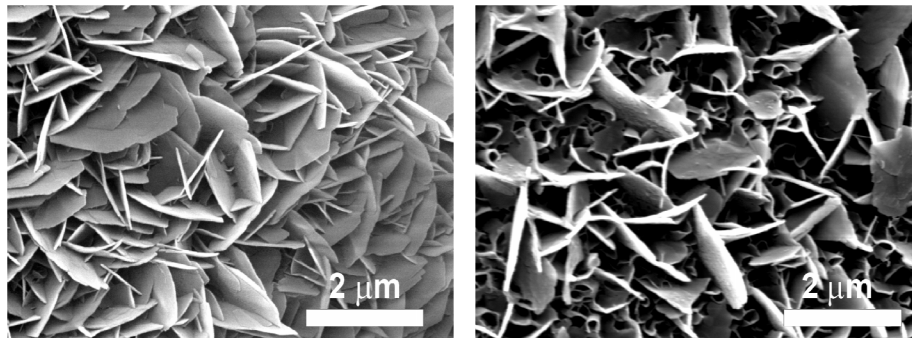


Figure 5: High magnification scanning electron micrographs showing the difference between no protein containing coatings (left) and protein containing coating (right). The protein containing coating is composed of a mixture of large crystal interlaced with smaller rounded and bend crystals, while the no protein containing coating is composed of regular shaped crystal of fairly the same size.

Interestingly, at a higher magnification (see figure 5) the presence of small crystals packed in between large crystals can be seen in the protein containing coatings, which were not found in the coatings without protein, suggesting that the addition of BSA leads to a more heterogenous surface structure.

Discussion

Currently, there are several techniques available to coat an implant e.g. Plasma spraying¹⁶, Electric spray deposition¹⁷ and biomimetic precipitation¹⁸. Until now only the latter has been proven to be suitable for protein incorporation, as this process takes place under conditions where temperature and pH are similar to *in*

vivo conditions. Incorporating growth factors or antibiotics provide the possibility to increase the bioactivity of these coatings. However, incorporation of these factors can not only influence the crystal and surface structure but the crystallinity of these coatings as well. In this study we have used BSA as a model protein for coprecipitation into a biomimetic carbonated apatite coating using 3 different concentrations (1, 10 and 100 mg/l). Scanning Electron Microscopy revealed that with increase of protein concentration the surface structure of these coatings alters. The crystal plates observed in coatings without protein are rectangular and flat, while protein containing coatings seem to be composed of smaller thin crystals curved in shape; this observation is comparable to what others have found in similar studies¹⁹⁻²¹. Although crystallite dimensions are larger in protein containing coatings, increasing the concentration of BSA in the precipitation solution causes the formation of a coating composed of smaller CO_3^{2-} containing apatite crystals than when no protein is present. This finding implies that there is an inhibitory effect of the protein on crystal formation. The crystals decrease with increasing protein concentration ultimately leading to a surface structure composed of small crystals packed in between larger crystals as could be observed by SEM. Based on these observations the change in shape is likely to be caused by the interference of the protein during crystal growth. Determination of the c-axis by XRD showed that with increasing protein concentrations, the D_c value along the c-axis decreases from 404 towards 296 Å. Interestingly; a similar observation can be made as the crystallinity of coatings without protein is decreased by increasing the Mg^{2+} concentration. In these coatings a decrease in crystallinity of approximately 10%, leads to a decrease from a crystal size of 279 to 146 Å. However, the morphology of these coatings was not affected by the change in crystallinity. It has been described that in hydroxyapatite, organic ligands are aligned parallel and/or absorbed to the crystallographic c-axis and mainly influence nucleation from the 100 side planes^{22, 23}. This could explain the fact that the c-axis decreases with increase in protein

concentration. In addition, the intensity of the 002 peak clearly increases, as can be seen from the XRD spectra, when more protein is added to the precipitation solution, which is indicative of the increase in apatite nature of the coating. Raman spectra showed that at higher concentrations of BSA the bands specific for protein (1450 cm^{-1} COO, CH_2 and CH_3 , 1660 cm^{-1} amide I), as can be seen in figure 2, increase in intensity, meaning that more and more protein is likely to have incorporated into the coating when the concentration of BSA is increased. In several studies regarding protein incorporation into calcium phosphate coatings fluorescent labels, protein-staining techniques and ELISA have been used to determine if protein was present^{21, 24}. This study shows that not only the presence of protein can be detected in a non destructive manner by using confocal Raman spectroscopy, but also information about the relative amount of protein present in the coating can be obtained as well. Determination of the relative crystallinity by Raman spectroscopy, which was done by measurement of the FWHM of the 960 cm^{-1} band ($\nu_1\text{ PO}_4^{3-}$ asymmetric stretch mode), proved to be a relatively easy technique to use. Raman spectroscopy is based on the detection of wavelength shifts caused by molecular vibrations and measures the freedom of movement of these vibrations. The more crystalline a ceramic becomes, the more confined the movements of chemical bonds become, leading ultimately to more narrow Raman bands. However, one has to keep in mind that the presence of carbonate in the hydroxyapatite lattice can induce a minor line broadening²⁵, which could lead to a slight underestimation of crystallinity when using pure hydroxyapatite as 100% crystalline standard. In this study all samples were prepared under similar conditions therefore the effect of carbonate is likely to be the same in all of the samples observed. The presence of BSA does not seem to influence the crystallinity towards a great extend as a decrease from an average of 27.9 to 25.2 % could be observed when the concentration in the precipitation solution is decreased. However, the standard deviations of these measurements increase when more

protein is present, indicating that the coating structure probably becomes more heterogeneous in its nature. Electron microscopy on the cross-sections of the coatings, as shown in the electron micrographs of figure 4, seems to confirm this observation. The coating prepared with 1 mg/l BSA shows regular sharp crystals standing up from the titanium alloy substrate, while the coating prepared with 100 mg/ml shows a more disorganized structure containing small irregular crystals with rounded edges packed in between larger crystals. Whereas, the structure of these coatings seems to be build up of a mixture of small crystals packed in between large crystals, only large crystals packed together in a relatively homogenous manner can be observed in the coatings containing no protein (see figure 4 and 5). Combes and Rey²⁶ suggested that there might be two complex processes taking place during precipitation of calcium phosphate coatings in the presence of protein. First, quick absorption of BSA to the metal surface can cause a decrease of surface tension between substrate and liquid, leading to the inhibition of nuclei multiplication (the smaller nuclei however are also more stable by the presence of protein, than without protein). Second, the presence of protein can lead to inhibition of crystal growth rate. In addition, at low protein concentration the multiplication of nuclei is most important while the growth inhibition effect might be weak, which is the opposite when a high concentration of protein is present. Since the formation of these coatings is a dynamic process, the protein concentration in the solution is decreasing in time; the amount of protein able to interact with the already formed crystals is decreasing in time, which in turn leads to less inhibition of crystal growth. At low concentrations of protein there might be a lot of nuclei initially, which can grow relatively uninhibited to a certain size. In contrast at high concentrations of protein the crystal growth, from an initial lower number of nuclei, is hampered leading to smaller size crystals being formed. While at a later stage, when less protein is present, bigger crystals are allowed to form and also more nuclei can appear. This might explain the fact that at a low concentration,

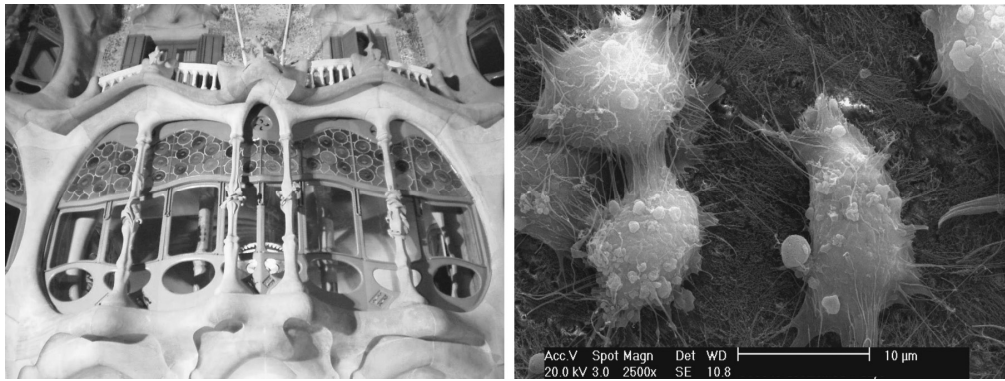
low inhibition of crystal growth, a more homogenous coating seems to be formed while at higher concentrations, initially a high inhibition of crystal growth which decreases in time, the coating becomes more heterogenous in respect to crystal size and shape. The initial larger Dc value for protein containing coatings as compared to coatings without protein can probably be explained by the stabilizing effect of protein on the initial nuclei which can lead to larger crystallite formation. As all coatings were produced in the same time frame this seems to be a plausible explanation. In order to gain more insight into the performance of these coatings an *in vivo* study would be of interest. It is evident that the smaller crystals in these coatings lead to a larger surface area, which in turn may lead to a faster dissolution of Ca^{2+} from these coatings after implantation. The faster dissolution of Ca^{2+} could enhance new bone formation so coatings having a higher surface area due to protein incorporation might initially perform better after implantation. In conclusion, the combination of SEM and confocal Raman spectroscopy seems to be a valuable tool to investigate not only the morphology of these coatings but their physiochemical composition as well.

References

1. Takagi, K.; Urist, M. R., The reaction of the dura to bone morphogenetic protein (BMP) in repair of skull defects. *Ann Surg* **1982**, 196, (1), 100-9.
2. Takagi, K.; Urist, M. R., The role of bone marrow in bone morphogenetic protein-induced repair of femoral massive diaphyseal defects. *Clin Orthop* **1982**, (171), 224-31.
3. Lind, M., Growth factor stimulation of bone healing. Effects on osteoblasts, osteomies, and implants fixation. *Acta Orthop Scand Suppl* **1998**, 283, 2-37.
4. Barrere, F.; Layrolle, P.; van, B. C.; de, G. K., Biomimetic calcium phosphate coatings on Ti6Al4V: a crystal growth study of octacalcium phosphate and inhibition by Mg^{2+} and HCO_3^- . *Bone* **1999**, 25, (2 Suppl), 107S-111S.
5. Barrere, F., Layrolle, P., van Blitterswijk, C.A., de Groot, K., Biomimetic coatings on titanium: a crystal growth study of octacalcium phosphate. *Journal of materials research: Materials in medicine* **2001**, 12, 529-534.
6. Wen, H. B.; de Wijn, J. R.; van Blitterswijk, C. A.; de Groot, K., Incorporation of bovine serum albumin in calcium phosphate coating on titanium. *J Biomed Mater Res* **1999**, 46, (2), 245-52.
7. Liu, Y.; Layrolle, P.; de Bruijn, J.; van Blitterswijk, C.; de Groot, K., Biomimetic coprecipitation of calcium phosphate and bovine serum albumin on titanium alloy. *J Biomed Mater Res* **2001**, 57, (3), 327-35.

8. Fazan, F.; Marquis, P. M., Dissolution behavior of plasma-sprayed hydroxyapatite coatings. *Journal of Materials Science: Materials in Medicine* 2000, 11, (12), 787.
9. Zhang, Q.; Chen, J.; Feng, J.; Cao, Y.; Deng, C.; Zhang, X., Dissolution and mineralization behaviors of HA coatings. *Biomaterials* 2003, 24, (26), 4741-8.
10. Chang, Y. L.; Stanford, C. M.; Keller, J. C., Calcium and phosphate supplementation promotes bone cell mineralization: implications for hydroxyapatite (HA)-enhanced bone formation. *J Biomed Mater Res* 2000, 52, (2), 270-8.
11. Coathup, M. J.; Bates, P.; Cool, P.; Walker, P. S.; Blumenthal, N.; Cobb, J. P.; Blunn, G. W., Osseo-mechanical induction of extra-cortical plates with reference to their surface properties and geometric designs. 1999, 20, (8), 793.
12. A. A. van Apeldoorn, Y. A., M. Stigter, I. Hofland, J. D. de Bruijn, H. K. Koerten, C. Otto, J. Greve, C. A. van Blitterswijk, Parallel high-resolution confocal Raman SEM analysis of inorganic and organic bone matrix constituents. *J. R. Soc. Interface* 2005, 2, (2), 39-45.
13. Barrere, F.; van, B. C.; de, G. K.; Layrolle, P., Nucleation of biomimetic Ca-P coatings on ti6Al4V from a SBF x 5 solution: influence of magnesium. *Biomaterials* 2002, 23, (10), 2211-20.
14. Aksenov, Y. Raman microscopy in an electron microscope: combining chemical and morphological analyses. Doctoral thesis, University of Twente, Enschede, The Netherlands, 2003.
15. de Grauw, C. J., Otto, C., Greve, J., de Bruijn, J.D, Investigation of Bone and Calcium Phosphate Coatings, and crystallinity Determination using Raman Microspectroscopy. *Cells and materials* 1996, 6, (1-3), 57-62.
16. de Groot, K.; Geesink, R.; Klein, C. P.; Serekian, P., Plasma sprayed coatings of hydroxylapatite. *J Biomed Mater Res* 1987, 21, (12), 1375-81.
17. Ducheyne, P.; Radin, S.; Heughebaert, M.; Heughebaert, J. C., Calcium phosphate ceramic coatings on porous titanium: effect of structure and composition on electrophoretic deposition, vacuum sintering and in vitro dissolution. 1990, 11, (4), 244.
18. Kokubo, T.; Kushitani, H.; Abe, Y.; Yamamuro, T., Apatite coating on various substrates in simulated body fluids. *Bioceramics* 1989, 2, 235-242.
19. Wen, H. B.; de Wijn, J. R.; van Blitterswijk, C. A.; de Groot, K., Incorporation of bovine serum albumin in calcium phosphate coating on titanium. *J Biomed Mater Res* 1999, 46, (2), 245-52.
20. Liu, Y.; Hunziker, E. B.; Randall, N. X.; de Groot, K.; Layrolle, P., Proteins incorporated into biomimetically prepared calcium phosphate coatings modulate their mechanical strength and dissolution rate. *Biomaterials* 2003, 24, (1), 65-70.
21. Liu, Y.; Layrolle, P.; de Bruijn, J.; van Blitterswijk, C.; de Groot, K., Biomimetic coprecipitation of calcium phosphate and bovine serum albumin on titanium alloy. *J Biomed Mater Res* 2001, 57, (3), 327-35.
22. Wierzbicki, A.; Cheung, H. S., Molecular modeling of inhibition of hydroxyapatite by phosphocitrate. 2000, 529, (1-3), 73.
23. Fujisawa, R.; Kuboki, Y., Preferential adsorption of dentin and bone acidic proteins on the (100) face of hydroxyapatite crystals. *Biochim Biophys Acta* 1991, 1075, (1), 56-60.
24. Liu, Y.; Hunziker, E. B.; Layrolle, P.; De Bruijn, J. D.; De Groot, K., Bone morphogenetic protein 2 incorporated into biomimetic coatings retains its biological activity. *Tissue Eng* 2004, 10, (1-2), 101-8.
25. de Mul, F. F.; Hottenhuis, M. H.; Bouter, P.; Greve, J.; Arends, J.; ten Bosch, J. J., Micro-Raman line broadening in synthetic carbonated hydroxyapatite. *J Dent Res* 1986, 65, (3), 437-40.
26. Combes, C.; Rey, C., Adsorption of proteins and calcium phosphate materials bioactivity. *Biomaterials* 2002, 23, (13), 2817-23.

Parallel high resolution confocal Raman SEM analysis of inorganic and organic bone matrix constituents



Although humans can build incredibly complex structures, cells are able to build structures engineers can only dream of and they do this seemingly without any effort. Compare the façade of the famous Casa Batlló by Antoni Gaudí with a culture of rat osteoblasts depositing bone extra cellular matrix after 2 weeks and one can see that millions of years of evolution will not easily be surpassed by 2 decades of tissue engineering.

Abstract

In many multidisciplinary fields of science, such as tissue engineering where material and biological sciences are combined, there is a need for a tool which combines ultra structural and chemical data analysis in a non destructive manner at high resolution. We show that combining confocal Raman spectroscopy (CRS) with Scanning electron microscopy (SEM) can be used for such analysis. Studies of atomic composition can be done by x-ray microanalysis (XRMA) in SEM, but this is only possible for atom numbers >5 and does not reveal molecular identity. Raman spectroscopy however, can provide information on molecular composition and identity by detection of wavelength shifts caused by molecular vibrations. In this study, CRS-SEM revealed that early *in vitro* formed bone ECM produced by rat osteoprogenitor cells resembles mature bone chemically. We gained insight in the structure and chemical composition of the ECM, which was composed of mainly mineralized collagen type I fibers and areas of dense carbonated calcium phosphate related to the collagen fiber density, as revealed by Raman imaging of SEM samples. We found that CRS-SEM allows study of specimens in a non-destructive manner and provides high resolution structural and chemical information about inorganic and organic constituents by parallel measurements on the same sample.

Parallel high resolution Confocal Raman SEM analysis of inorganic and organic bone matrix constituents

A.A. van Apeldoorn¹, Y. Aksenov², M. Stigter³, I. Hofland³, J.D. de Bruijn³, H.K. Koerten⁴, C. Otto², J. Greve², C.A. van Blitterswijk¹

¹University of Twente, Faculty of Science and Technology, Dept. of Polymer Chemistry and Biomaterials, PO box 98, 3720 AB Bilthoven, The Netherlands,

²University of Twente, Faculty of Science and Technology, Dept of Biophysical Techniques, PO Box 217, 7500AE Enschede, The Netherlands, ³Isotis NV, PO box 98, 3720 AB Bilthoven, The Netherlands, ⁴Leiden University Medical Center, Dept. of Molecular Cell Biology, PO box 9503, 2300 RA Leiden, The Netherlands

Introduction

Raman spectroscopy provides information on molecular vibrations. Raman spectroscopy is a method based on an inelastic scattering effect. In short, a monochromatic light source (laser) irradiation can excite molecules to a higher vibration state, which then relax to a different vibration level as their original state. As a result a photon is emitted with less energy, therefore a longer wavelength than the initial photons from the laser. This event is called Stokes Raman scattering. The energy difference between the incident and scattered radiations appears as a frequency shift from the incident light. These frequency shifts are specific for a given chemical bond and allow therefore molecular analysis. Scanning electron microscopy (SEM) can not only be used for structural analysis but can also provide chemical information as well, by using x-ray microanalysis (XRMA). XRMA is however limited because no molecular information can be obtained from these data and moreover, detection of elements is limited to the higher atomic numbers (>5). In contrast, Raman spectroscopy can give information on molecular identity, composition, orientation and crystal form by detection of wavelength shifts caused by molecular vibrations. Therefore, combining SEM with confocal Raman

spectroscopy (CRS) allows not only structural and elemental analysis of a sample but, can also provide information about the presence of inorganic and organic molecules in a noninvasive manner. In general, highly sensitive systems, containing high power lasers and liquid cooled CCD-camera's are needed to obtain high signal to noise ratio data when studying biological samples with Raman spectroscopy. A clear example of such a system was shown in a study done on polytene chromosomes showing different DNA-protein ratios in their interbands¹. The abovementioned systems are however in general too large to fit in a vacuum chamber of a SEM. We have built a compact confocal Raman microscope which was incorporated into the vacuum chamber of an environmental SEM, thus allowing us to do non-invasive chemical and ultra structure research on typical biological samples. In tissue engineering (bio) materials are commonly combined with biological components, like adding specific cells or proteins for drug release etc. In most cases inorganic and organic components are present and preferably need to be evaluated in the most non invasive way possible, in order to maintain the structure of the sample. Several different authors investigated the mineralization of a collagen matrix made by osteoprogenitor cells in vitro on different substrata by electron microscopy. In these cases a network of collagen fibers was observed which had undergone calcification ²⁻⁴. Separate FTIR and XRD analysis showed that the observed mineralization consisted of carbonated apatite like calcium phosphate (CO3-AP) comparable to bone ^{2, 5}. In previous studies on bone by using Raman spectroscopy in all cases the samples used were bulk-like and sometimes treated specifically with hydrazine ^{6, 7} or H₂O₂^{8, 9} to decrease fluorescence of the samples. Although giving compositional data, these approaches does not allow for both chemical and ultra structural analysis at the same time. Recently, a combination of transmission light microscopy and Raman spectroscopy has been used to study micro damage in bovine bone and to image damage at low magnifications¹⁰, showing that different types of carbonated apatite were present around micro

cracks. This proved that high resolution Raman analysis on a micrometer scale can reveal crucial information about sample composition, which can then be related to two-dimensional histology. In three dimensional cell cultures it was found, by confocal Raman spectroscopy, that human osteoblasts produced bone cell spheroids under the influence of TGF- β 1, containing microspicules composed of carbonated apatite (CO3-AP) similar to mature bone¹¹. These examples illustrate that there is an increasing demand for combining ultra structural with chemical analysis, at high resolution, to gain better understanding in active cellular processes as the formation of extra cellular matrix (ECM). In this study we investigated in vitro formed bone ECM, produced by osteoprogenitor cells obtained from rats, on titanium alloy plates.

Methods

Biomimetic CO3-AP coatings were provided by IsoTis SA (The Netherlands). The coatings were prepared according to a precipitation method by Barrere et al. (1999; 2001) on sandblasted Ti6Al4V (Smitford Staal BV, The Netherlands) square plates with a surface area of 100 mm² and 1 mm thickness. The plates were ultrasonically cleaned for 15 min. in acetone, 70% ethanol and demi water in sequence. The coatings were analyzed by XRMA, scanning electron microscopy (FEI, model XL-30 ESEM-FEG) and combined confocal Raman scanning electron microscopy described in this article.

Cell culture

Rat bone marrow cells (RBMCs) were isolated from the femora of young (150 g) male wistar rats¹² and cultured in T75 flasks. Cell culture medium used during culture and seeding was composed of α -MEM medium (Life technologies, The Netherlands) containing 0.2×10^{-3} M L-ascorbic-acid-2 phosphate (ASAP, Life technologies, The Netherlands), 0.01 M β -glycerophosphate (β GP, Sigma, The Netherlands), 1×10^{-8} M dexamethasone (DEX, Sigma, The Netherlands), 15% fetal

bovine serum (FBS, Life technologies, The Netherlands), and 1% penicillin-streptomycin. At the third passage the cells were seeded onto Ti6Al4V plates at a density of 1×10^4 cells/cm² and then cultured for 2 weeks to allow sufficient extra cellular matrix (ECM) formation. As a control, the cells were also seeded on tissue culture polystyrene (TCPS) to monitor the growth and morphology of the cells. After 14 days of culture the cells were fixated with 1.5% glutaraldehyde in 0.14 M cacodylate buffer (pH 7.4). After fixation the cells were dehydrated by immersion in an increasing ethanol series (70-100%) and then critical point dried (Balzers CPD 030). In order to reveal the ECM structure underneath the cultured cells, the top cell layer was removed by gently applying either pressurized air to blow of the cell-layer or scotch tape to reveal the underlying ECM and cells. The samples were analyzed by confocal Raman scanning electron microscopy and XRMA. Pure Collagen type I (Sigma, The Netherlands) from bovine tendon was used as a positive control for collagen present in the ECM measured by Raman spectroscopy.

Combined confocal Raman scanning electron microscope

A collimated and circularly symmetrical beam from a diode laser with a frequency of 685nm is reflected by a dichroic beam splitter (BS) into the vacuum chamber of the SEM through a coupling window (Fig. 1). The beam is then focused by a 60X objective (n.a. 0.65) on a sample of interest. The excited Raman scattering is collected by the same objective and the Stokes components of Raman frequencies pass through the BS, a notch filter and a pinhole (\varnothing 25 μ m), which allows for confocality of the system. The scattering is collected by spectrograph-monochromator, in which the incoming light is decomposed by a concave holographic diffraction grating and focused on a thermo-electrically cooled CCD (1056x256 pixels, Princeton Instruments Spec10). The theoretical spatial resolution of the system is ~ 700 nm with an effective laser power of 6mW on the sample. The CCD is connected with a computer for data collection and analysis using WinSpec

(Roper Scientific Inc., USA) and Microcal Origin (Microcal software inc., USA) data analysis software.

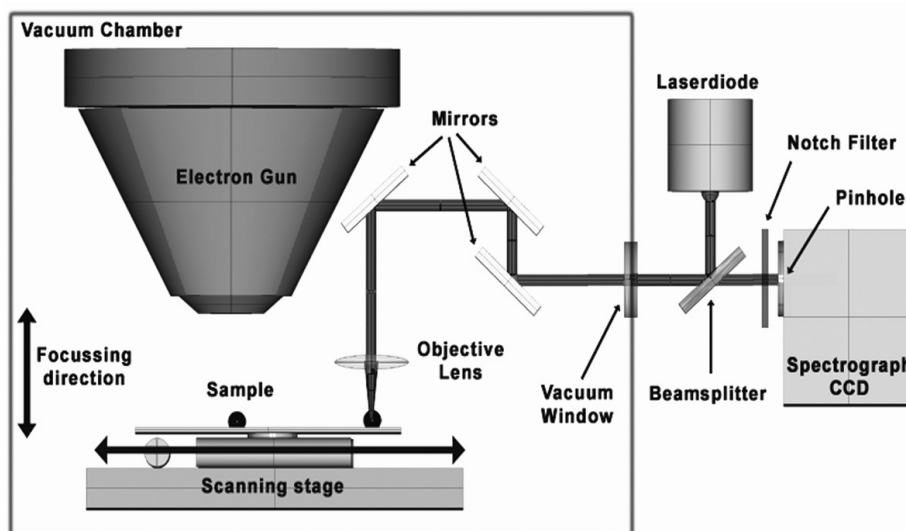


Figure 1: Schematic drawing of the CRSEM. Samples are analyzed by selecting a location by EM and then shifting the sample into the confocal laser spot at exact coordinates. The lasersource consists of a laserdiode with a wavelength of 685nm and is diverted through a side port into the vacuum chamber by a beamsplitter. The laser is then emitted onto the sample by a set of gold coated mirrors through a 60 x objective. The induced Raman scatter is then collected by the same objective and diverted in the opposite direction, passing the beamsplitter and a notch filter, through a pinhole allowing for confocality of the system. Inside the spectrograph, the Raman scattering is subsequently focused on a holographic diffraction grating and the decomposed wavelengths are then detected by a thermo-electrically cooled CCD. The scanning stage (nanometer movement) is equipped with a small light source to use transmission light microscopic observation for easy calibration of stage movement.

The setup was calibrated by using 2, 5 and 10 μm \varnothing polystyrene beads to establish the coordinates needed for lateral movement from the electron gun to the laser spot. Raman measurements were taken of the ECM observed by SEM, in such a way that the focal plane always just touched the titanium alloy substrate surface, in this way all measurement were done in the same way. After collection of whole Raman spectra, images were collected on chosen frequencies by using a nanometer scanning stage (Kleindiek, Germany). The stage was controlled by LabView software (National instruments, USA) and images were then generated from WinSpec data files, by programming in LabView.

Results

Confocal Raman scanning electron microscopy (CRSEM)

We used polystyrene beads of sizes (10-2 μm) to calibrate sample stage positioning. In this manner we established, the exact movement of our samples from our electron micrograph to the laser spot of the confocal Raman microscope. We were able to obtain clear polystyrene spectra (Fig.2A) from these samples, and furthermore were able to select a specific band (1004 cm^{-1}) for vibration of the aromatic ring group of polystyrene for chemically imaging. We decided to image (Fig.2D) the samples with a step size of 1 μm , by using a nanometer scanning stage build onto the SEM sample stage, to show the efficacy of the system. We found that sample movement was very accurate and analysis of very small samples was possible.

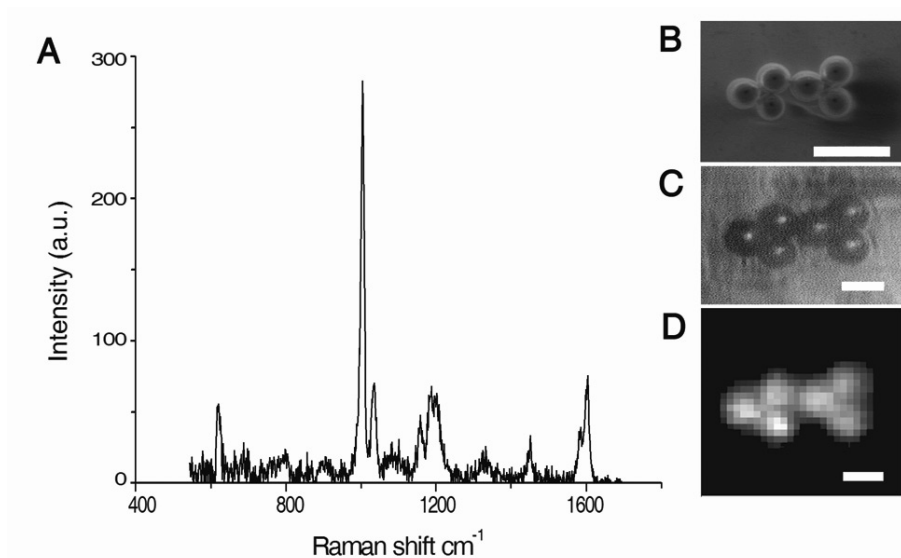


Figure 2: Raman spectrum (A) of the first bead from the left, showed in electron micrograph B. Inset C: 5 μm diameter polystyrene beads, transmission light micrograph observed through the objective lens. Inset D: Corresponding Raman image (1 pixel = 1 μm) using the 1004 cm^{-1} band of polystyrene. Scalebar in B represents 10 μm , C and D 5 μm .

CRSEM and biomimetic carbonated apatite like coatings (CO3-AP)

After establishing the feasibility of our measurement system, we measured several cross-sections of thin CO3-AP coatings on titanium alloy plates, to check if we could reproducibly measure a more complex sample. Cross-sections of coatings were all measured in the center to ensure that all measurements were performed in the same manner (Fig. 3). The obtained spectra (Fig. 4A) show Raman bands belonging to the phosphate group vibration modes: 960 cm^{-1} ν_1 , $430\text{-}450\text{ cm}^{-1}$ ν_2 , $1030\text{-}1040\text{ cm}^{-1}$ ν_3 , $580\text{-}590\text{ cm}^{-1}$ ν_4 and also a band around 1070 cm^{-1} , which is due to the presence of CO_3^{2-} stretch vibration of the carbonate group¹³.

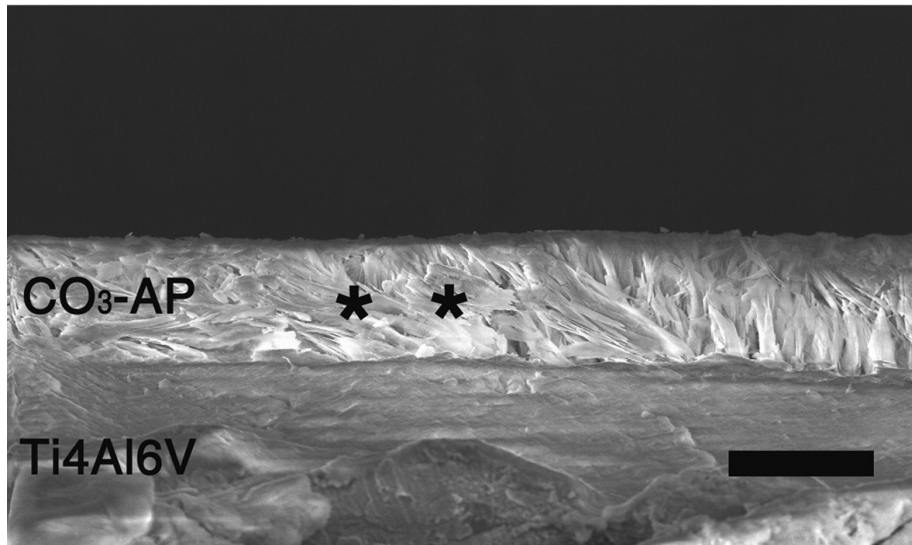


Figure 3: Electron micrograph showing a cross-section of CO3-AP coating, Raman spectra were collected at the center of the cross-section (asterisks). Scalebar represents $20\text{ }\mu\text{m}$.

CRSEM and bone ECM by rat osteoprogenitor cells

After 14 days of culture in osteogenic medium rat osteoprogenitor cells had produced a vast amount of well-organized ECM on the surface of the Ti alloy discs. In all cases the samples were covered with smooth layer of cells. In order to reveal the underlying ECM structure and study the matrix without interference of possible contribution of cells to our Raman spectra we had to gently remove this top-layer. After removing the top layer of cells according to method described in the material

and methods, a network of fibers could be observed, which upon closer examination had a roughened surface (figures. 4C and 4D).

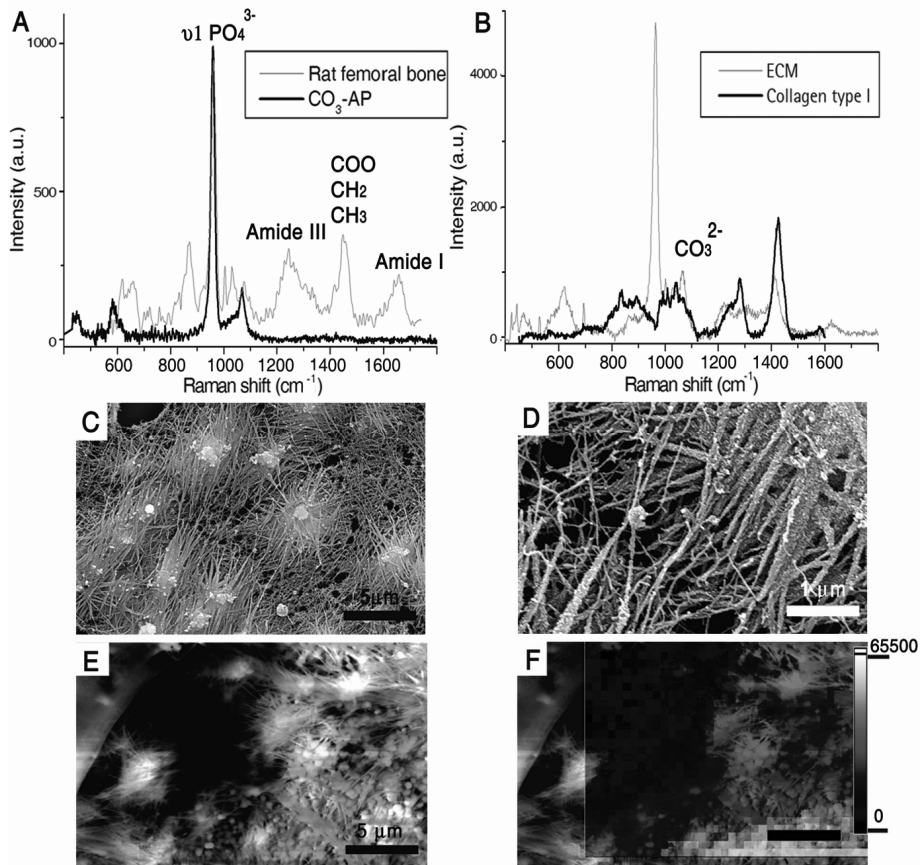


Figure 4: A: Raman spectra of femoral rat bone, CO₃-AP, B: ECM and collagen type I. C, D, E: Electron micrographs of ECM produced by rat osteoprogenitor cells, showing mineralized collagen fiber bundles (width 0.1-0.5 μm). F: Raman image from an area of E, which was subsequently imaged using the 960 cm⁻¹ PO₄²⁻ band (1 pixel = 0.5 μm). Scale bar C, E represent 5 μm and D 1 μm.

We selected locations free of cells and with abundant ECM for our Raman measurements. As a reference, although not exactly similar to native rat bone collagen type I, we measured biochemically purified bovine collagen type I obtained from tendons (commercially available from Sigma, the Netherlands). The Raman spectra of ECM (figure. 4A) show both, bands belonging to carbonated apatite, as well as bands belonging to protein, mainly collagen type I. The spectra obtained from ECM were comparable to spectra from mature bone. Raman

imaging revealed that mineralization of the matrix was found to be heterogeneous (figure. 4F), whereas in mature bone this is found to be homogenous (figure. 5A). XRMA of the same areas revealed the presence of calcium, phosphorus, carbon and oxygen, which confirms the data obtained by Raman spectroscopy (figures. 5 and 6).

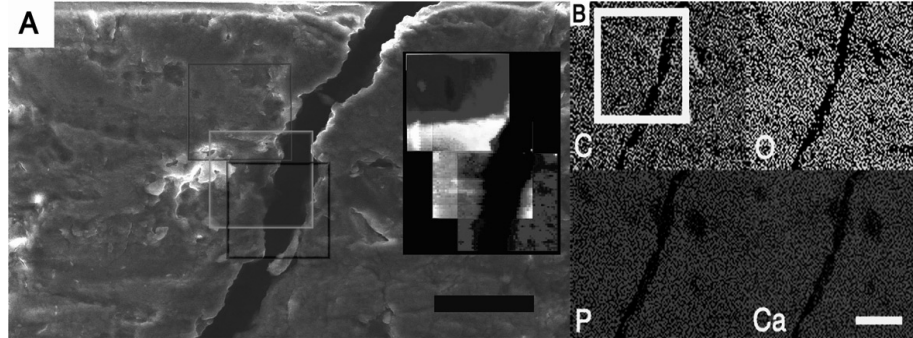


Figure 5A: Electron micrograph of the surface of bone, showing a 15-20 μm microcrack and subsequent corresponding Raman images 50x50 μm (1 pixel=1 μm) of protein (1400-1440 cm^{-1} , red square), CO_3^{2-} (1070 cm^{-1} , green square) and PO_4^{3-} (960 cm^{-1} , blue square). Fig 5B: XRMA maps for C, O, P, and Ca, the white squared area corresponds with electron-micrograph in A. Scale bar in A 50 μm and B 25 μm .

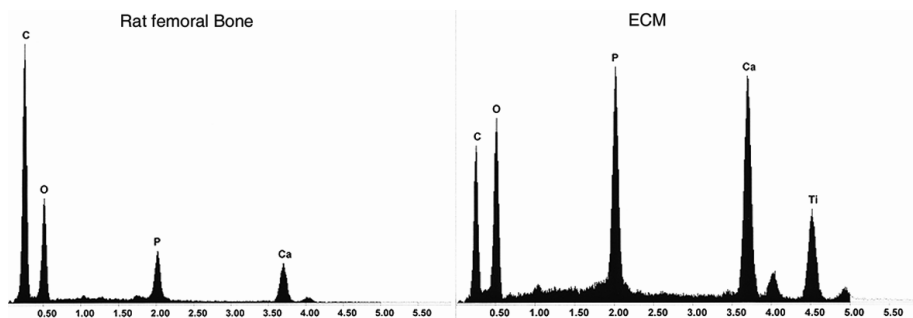


Figure 6: XRMA spectra of bone and ECM, all measurement parameters were kept the same (15 KeV, spotsize 4, collection-time 260 sec. working-distance 10 mm)

Discussion

In this study we investigated the feasibility of combining CRS with SEM and report on the performance of this system on tissue engineered samples. Measurements of 10 to 2 μm diameter polystyrene beads showed that clear Raman spectra, with low signal to noise ratio can be obtained, which in turn can be used for chemical imaging. Investigation of thin layers of carbonated apatite, a major component of

bone, on titanium alloy plates revealed the presence of Raman bands belonging to both PO_4^{3-} and CO_3^{2-} ¹³. SEM investigation of rat osteoprogenitor cells on titanium alloy plates after 14 days showed that ECM had formed, that was composed of a network of fibers which have a mineralized appearance. Measurements taken from different spots of this matrix revealed that Raman bands belonging to PO_4^{3-} , CO_3^{2-} and protein, could be found, which could not be deduced initially from x-ray microanalysis data from the same sites. It is clear that when comparing the ECM spectra to the spectra of CO_3 -AP coatings, pure collagen type I, and the histological observations made by SEM, the extra bands in these spectra are mainly contributed by the presence of collagen type I in the ECM. This was also concluded in studies done on dentin^{14, 15}, bone^{16, 17} and osteoblast cultures¹⁸ in which confocal Raman spectroscopy showed similar bands for collagen as in our study. The spectra of pure collagen type I show differences in intensity of peaks when compared to the spectra of ECM. This can be explained by the fact that we measured biochemically purified protein as a standard, whereas the ECM contains also other proteins and inorganic components each contributing to the total ECM spectrum. The amide III protein band position observed in both ECM (1270-1300 cm^{-1}) and pure collagen type I (1242-1282 cm^{-1}) spectra, indicate that Collagen type I in the ECM is likely to be in the form of a α -helical structure, while the purified collagen type I is probably more disordered and in an irregular form¹⁹⁻²² probably caused by the biochemical purification process of this material. Collagen type I is the major contributing protein to bone extra cellular matrix, but certainly not the only one present in the matrix. It is well established that bone ECM contains also proteins like, osteopontin, bone sialoprotein, bone morphogenic proteins, osteocalcin and many more, however in much lower amounts. The abovementioned added to the fact that the amount and purified form are different, might explain the slight shape differences in the collagen type I specific peaks observed in figure 4. Interestingly, the ratio of the protein to phosphate group Raman band intensities seems to be higher in

mature bone, than in ECM. It is known that during the development of bone ECM deposition of carbonated apatite takes place before a collagen network can accumulate^{23, 24}, this probably explains the difference in ratio found in our study. High resolution Raman imaging revealed that ECM contains areas which are more mineralized than others, caused by the distribution of collagen fibers and the presence of small spherical structures composed of carbonated apatite. Raman images and XRMA maps of mature bone on amide III, CO_3^{2-} and PO_4^{3-} revealed that the composition of bone is much more homogenous than ECM, possibly because in bone the ECM is compacted to a dense structure. Raman imaging of these surfaces showed that with the increase of surface topography complexity, the interpretation of the generated Raman image becomes increasingly more difficult. The difficulty in analysis can be explained by the fact that the confocality of the system allows for so-called "optical sectioning", meaning that scanning of the surface of a sample is done in one focal plane. The focal spot in turn, has a certain measuring volume and therefore the appearance of electron micrograph, which is a 3D observation, and Raman micrograph, which is a 2D observation, can be slightly different. An example of this effect is shown in figure 2, where the edges of the polystyrene beads show clearly a lower intensity than in the center and also to some extent in the Raman micrographs of bone shown in figure 5. The information in the Raman image does not only reveal chemical, but topographical data as well, more than could be found by XRMA (see figure 5), which adds to structural information obtained by SEM. Future research on in vivo bone formation using the abovementioned combined technique can possibly reveal more detailed information on bone growth in defect areas, the data found in this study suggests that bone forming cells start producing ECM resembling mature bone from an early time point. The use of CRS in a SEM can enlarge the field of applications of sample analysis by electron microscopy to a great extent. Although in this paper we investigated bone extra cellular matrix, this application can also be used for other

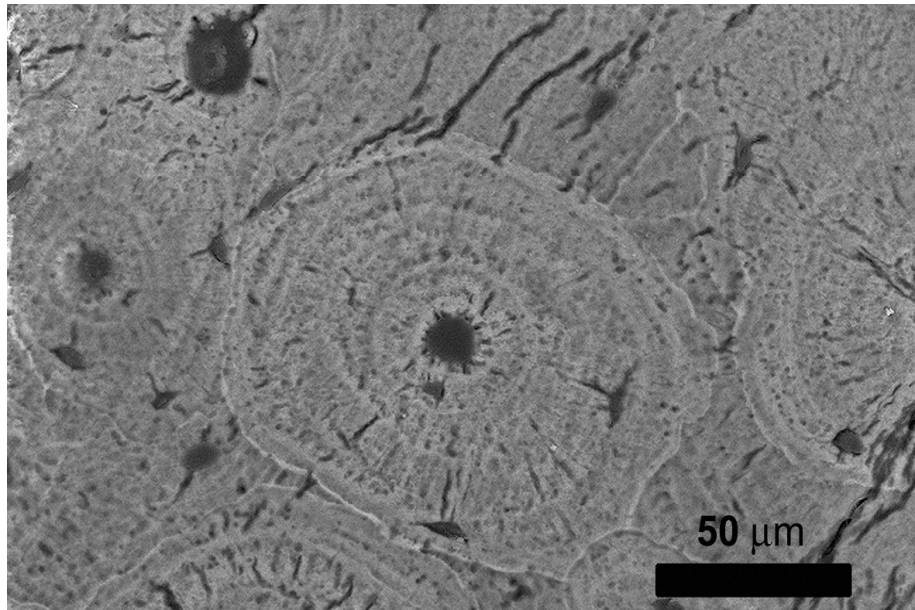
sample types where information about molecular composition is necessary. Newly, non resonant Raman imaging of single cells has been used to map DNA and protein distributions in human cells^{25, 26}. This revealed that protein distribution varies with cell type and that the presence of RNA inside the nucleus of HeLa cells could be detected for the first time. However, light microscopy used in these studies in order to study these distributions, is extremely limited in that the physical properties of light limit the ultimate resolution for observation. Combining confocal Raman spectroscopy with SEM like described in this manuscript could be interesting for studying intra-cellular processes, like phagocytosis, cellular differentiation and apoptosis, while in the same time being able to study cell morphology with very high resolution at very high magnifications. Moreover, this technique allows one to pinpoint structures with submicron dimensions by SEM, and then subsequently analyze them by confocal Raman spectroscopy. In addition, Raman imaging in combination with environmental SEM, would allow one to image directly, without prior labeling of molecules of interest, while in the meantime maintaining the normal functioning of the cells.

References

1. Puppels, G. J.; de Mul, F. F.; Otto, C.; Greve, J.; Robert-Nicoud, M.; Arndt-Jovin, D. J.; Jovin, T. M., Studying single living cells and chromosomes by confocal Raman microspectroscopy. *Nature* **1990**, *347*, (6290), 301-3.
2. Oghushi, H.; Dohi, Y.; Katuda, T.; Tamai, S.; Tabata, S.; Suwa, Y., In vitro bone formation by rat marrow cell culture. *Journal of biomedical materials research* **1992**, *32*, 333-340.
3. Yoshikawa, T.; Ohgushi, H.; Dohi, Y.; Davies, J., Viable bone formation in porous hydroxyapatite: marrow cell-derived in vitro bone on the surface of ceramics. *Biomed Mater Eng* **1997**, *7*, (1), 49-58.
4. Yamamoto, N.; Furuya, K.; Hanada, K., Progressive development of the osteoblast phenotype during differentiation of osteoprogenitor cells derived from fetal rat calvaria: model for in vitro bone formation. *Biol Pharm Bull* **2002**, *25*, (4), 509-15.
5. Ou-Yang, H.; Paschalis, E.; Mayo, W.; Boskey, A.; Mendelsohn, R., Infrared microscopic imaging of bone: spatial distribution of CO₃(2-). *J Bone Miner Res* **2001**, *16*, (5), 893-900.
6. Walters, M.; Leung, Y.; Blumenthal, N.; Le, G. R.; Konsker, K., A Raman and infrared spectroscopic investigation of biological hydroxyapatite. *J Inorg Biochem* **1990**, *39*, (3), 193-200.
7. Rehman, I.; Smith, R.; Hench, L. L.; Bonfield, W., Structural evaluation of human and sheep bone and comparison with synthetic hydroxyapatite by FT-Raman spectroscopy. *J Biomed Mater Res* **1995**, *29*, (10), 1287-94.

8. Penel, G., Leroy, G., Bres, E., New preparation method of bone samples for raman microspectroscopy. *Applied spectroscopy* **1998**, 52, (2), 312-313.
9. Freeman, J. J., Silva, M.J., Separation of the raman spectral signatures of bioapatite and collagen in compact mouse bone bleached with hydrogen peroxide. *Applied Spectroscopy* **2002**, 56, (6), 770-775.
10. Timlin, J. A.; Carden, A.; Morris, M. D.; Rajachar, R. M.; Kohn, D. H., Raman spectroscopic imaging markers for fatigue-related microdamage in bovine bone. *Anal Chem* **2000**, 72, (10), 2229-36.
11. Kale, S.; Biermann, S.; Edwards, C.; Tarnowski, C.; Morris, M.; Long, M. W., Three-dimensional cellular development is essential for ex vivo formation of human bone. *Nat Biotechnol* **2000**, 18, (9), 954-8.
12. Maniopoulos, C.; Sodek, J.; Melcher, A., Bone formation in vitro by stromal cells obtained from bone marrow of young adult rats. *Cell Tissue Res* **1988**, 254, (2), 317-30.
13. Penel, G.; Leroy, G.; Rey, C.; Bres, E., MicroRaman spectral study of the PO₄ and CO₃ vibrational modes in synthetic and biological apatites. *Calcif Tissue Int* **1998**, 63, (6), 475-81.
14. Kirchner, M. T., Edwards, H.G.M., Ancient and modern specimens of human teeth: a fourier transform raman spectroscopic study. *Journal of raman spectroscopy* **1997**, 28, 171-178.
15. Wang, Y.; Spencer, P., Analysis of acid-treated dentin smear debris and smear layers using confocal Raman microspectroscopy. *J Biomed Mater Res* **2002**, 60, (2), 300-8.
16. Tarnowski, C. P.; Ignelzi, M. A., Jr.; Morris, M. D., Mineralization of developing mouse calvaria as revealed by Raman microspectroscopy. *J Bone Miner Res* **2002**, 17, (6), 1118-26.
17. Dopner, S.; Muller, F.; Hildebrandt, P.; Muller, R. T., Integration of metallic endoprotheses in dog femur studied by near-infrared Fourier-transform Raman microscopy. *Biomaterials* **2002**, 23, (5), 1337-45.
18. Stewart, S., Shea, D.A., Tarnowski, C.P., Morris, M.D., Wang, D., Francheschi, R., Lin, D.L., Keller, E., Trends in early mineralization of murine calvarial osteoblastic cultures: a raman microscopic study. *Journal of raman spectroscopy* **2002**, 33, 536-543.
19. Guan, Y., Lewis, E.N., Levin, I.W., Biomedical application of raman spectroscopy: Tissue differentiation and potential clinical usage. In *Raman spectroscopy*, ed.; Pelletier, M. J., 'Ed.' ^ 'Eds.' Blackwell Science Ltd.: London, 1991; 'Vol.' p ^ pp.
20. Renuopalakrishnan, V.; Carreira, L.; Collette, T.; Dobbs, J.; Chandraksasan, G.; Lord, R., Non-uniform triple helical structure in chick skin type I collagen on thermal denaturation: Raman spectroscopic study. *Z Naturforsch [C]* **1998**, 53, (5-6), 383-8.
21. Barron, L., Hecht, L., Blanch, E.W., Bell, A.F., Solution structure and dynamics of biomolecules from raman optical activity. *Progress in Biophysics and molecular biology* **2000**, 73, 1-49.
22. Carden, A.; Rajachar, R.; Morris, M.; Kohn, D., Ultrastructural changes accompanying the mechanical deformation of bone tissue: a Raman imaging study. *Calcif Tissue Int* **2003**, 72, (2), 166-75.
23. Davies, J. E., In vitro modeling of the bone/implant interface. *Anat Rec* **1996**, 245, (2), 426-45.
24. Davies, J., Mechanisms of endosseous integration. *Int J Prosthodont* **1998**, 11, (5), 391-401.
25. Uzunbajakava, N.; Lenferink, A.; Kraan, Y.; Willekens, B.; Vrensen, G.; Greve, J.; Otto, C., Nonresonant Raman imaging of protein distribution in single human cells. *Biopolymers* **2003**, 72, (1), 1-9.
26. Uzunbajakava, N.; Lenferink, A.; Kraan, Y.; Volokhina, E.; Vrensen, G.; Greve, J.; Otto, C., Nonresonant confocal Raman imaging of DNA and protein distribution in apoptotic cells. *Biophys J* **2003**, 84, (6), 3968-81.

The physicochemical composition of osteoporotic bone in the TTD premature aging mouse determined by confocal Raman microscopy



Definitions of bone found on the internet

cram: study intensively, as before an exam; "I had to bone up on my Latin verbs before the final exam"
wordnet.princeton.edu/perl/webwn

Bone is a popular independent comic book series by Jeff Smith. Smith's drawings are inspired by animated cartoons and comic strips, a notable influence being Walt Kelly's Pogo. However, although the series contains a great deal of both visual and character-based comedy, the main storyline is dark and serious, drawing its inspiration from J. R. R. Tolkien and others. [en.wikipedia.org/wiki/Bone_\(comic\)](http://en.wikipedia.org/wiki/Bone_(comic))

In corsetry, a bone is one of the rigid parts of a corset that forms its frame, gives it rigidity, and helps to shape the wearer's body. [en.wikipedia.org/wiki/Bone_\(corsetry\)](http://en.wikipedia.org/wiki/Bone_(corsetry))

Bone refers either to a hardened connective tissue or to one of the individual structures, or organs, into which it is formed, found in many animals. Bones support body structures, protect internal organs, and (in conjunction with muscles) facilitate movement; are also involved with cell formation, calcium metabolism, and mineral storage. The bones of an animal are, collectively, known as the skeleton.
en.wikipedia.org/wiki/Bone

hard type of connective tissue, primarily made up of osteoblasts, osteocytes, and collagen, that supports and protects the body. www.urologychannel.com/common/glossary/index_a_d.shtml

living tissue that makes up the body's skeleton. www.health.uab.edu/show.asp

Dense tissue that forms the skeleton. Bone can be donated and transplanted.
www.organdonor.gov/glossary.html

the hard form of connective tissue that constitutes the majority of the skeleton of most vertebrates; it consists of an organic component (the cells and matrix) and an inorganic, or mineral, component; the matrix contains a framework of collagenous fibers and is impregnated with the mineral component, chiefly calcium phosphate (85%) and calcium carbonate [10%], which imparts the quality of rigidity to bone. Called Osseous

tissue. 2. Any distinct piece of the osseous framework, or skeleton, of the body.
www.cranialtherapies.com/glossary.html

a trick where you bone out your leg means you straighten it all the way out. A "boned out grab" is one where your leg or legs are straightened out while grabbing your board. www.kitesurfschool.org/glossary.htm

the hard extremely dense material that forms the skeleton of the body. It is composed of fibres of a material called collagen filled in with minerals - mainly calcium salts - rather like reinforced concrete. The bones of the skeleton have a thick outer shell or 'cortex' inside which there is a meshwork of 'trabecular' bone.
www.arc.org.uk/about_arth/glossary.htm

Bone is the substance that forms the skeleton of the body. It is composed chiefly of calcium phosphate and calcium carbonate. It also serves as a storage area for calcium, playing a large role in calcium balance in the blood. www.bdid.com/termsb.htm

the hard tissue, composed of both organic and inorganic materials, which makes up the skeletons of adult vertebrates. Because of their density, bones may survive in the archaeological record long after the decomposition of the soft tissue.
www.umanitoba.ca/faculties/arts/anthropology/manarchnet/appendices/glossary.html

Bone is living, growing tissue – made mostly of collagen, a protein that provides a soft framework, and calcium phosphate, a mineral that adds strength and hardens the framework. This combination of collagen and calcium makes bone strong yet flexible to withstand stress. More than 99% of the body's calcium is contained in the bones and teeth. www.osteoporosisflorida.org/Definitions.htm

This raw material was used by native Americans for many tools and ornaments. Bone tools included hide fleshers, fishhooks, hide grainers, arrowheads, paintbones, needles, knife handles, quill flatteners, and agricultural tools such as hoes and rakes. www.natureshift.org/history/glossary/g_first.html

A connective tissue that contains a hardened matrix of mineral salts and collagen fibers. Its cells include osteocytes, which are embedded within lacunae, and the free-roaming osteoblasts and osteoclasts.
www.sci.sdsu.edu/histology/gloss_a.htm

a horse's 'bone' is measured just below the knee. www.horsescanada.com/glossary.htm

The hard tissue that provides structural support to the body, It is primarily composed of hydroxyapatite crystals and collagen. Individual bones may be classed as long, short, or flat.
www.spinaldoc.com/Webpages.asp

Any of numerous anatomically distinct structures making up the skeleton of a vertebrate animal. There are more than 200 different bones in the human body.
www.clover.okstate.edu/fourh/aipc/lessons/glossary/bisfor.html

to remove the bones from meat of fish to facilitate either stuffing or rolling. www.great-cooking-made-easy.com/glossary-A-C.html

Abstract

We previously established a mouse model for trichothiodystrophy (TTD), exhibiting many of the typical features of this human syndrome, including a number of features of premature ageing. A key characteristic of TTD mouse strain is osteoporosis with concomitant skeletal kyphosis as well as osteosclerosis of the calvaria. Although we established that TTD mice display decreased bone mineral density (BMD), typical of osteoporosis, the exact changes in physicochemical properties of the mice remained to be elucidated. We used Confocal Raman microscopy together with histology to study the properties of femora of TTD mice. To establish that Raman microscopy can be applied to measure differences in bone composition, we first measured femora of bones isolated from XPA/TTD double mutant mice. Based on histology, we observed a severe form of osteoporosis, with strongly reduced cortical bone thickness. Accordingly, Raman data obtained from the XPA/TTD mice showed remarkable differences in bone mineral composition compared to wildtype animals. Next, we used Raman spectroscopy to analyse bone composition in mice of 10 wildtype and 10 TTD animals. We observed a decreased level of phosphate and carbonate content in cortical bone of the femora isolated from TTD mice compared to wildtype animals. In contrast, the protein fraction of the bone, representing the bone matrix, was not affected, leading to the conclusion that collagen type I content is not changed in these mice. In conclusion, decreased mineralization rather than a change in bone matrix composition underlies osteoporosis in the TTD mouse model.

The physicochemical composition of osteoporotic bone in the TTD premature aging mouse determined by confocal Raman microscopy

A.A. van Apeldoorn¹, J. de Boer¹, H. van Steeg², J.H.J. Hoeijmakers³, C. Otto⁴, C.A. van Blitterswijk¹

¹Department of Polymer Chemistry and Biomaterials, Faculty of Technology and Sciences, University of Twente, PO Box 98, 3720 AB Bilthoven, the Netherlands,

²Department of Carcinogenesis, Mutagenesis and Aging, The national institute for public health and the environment (RIVM), P.O.Box 1, 3720BA Bilthoven, the Netherlands, ³University Medical Center Rotterdam, Department of Genetics, P.O. Box 1738, 3000DR, Rotterdam, the Netherlands, ⁴Department of Biophysical Techniques, Faculty of Technology and Sciences, University of Twente, PO Box 217, 7500AE Enschede, the Netherlands

Introduction

Trichothiodystrophy (TTD) is a rare autosomal recessive disorder; patients are characterized by premature aging showing symptoms as brittle hair, postnatal mental and growth retardation, peculiar face, ichthyosis, and photosensitivity and skeletal disorders¹. Mice harbouring TTD specific point mutation in the Xeroderma pigmentosum group D gene were found to show symptoms similar to those found in the human disease^{2, 3}. One of the key features found in this mouse strain are skeletal abnormalities, as kyphosis, osteosclerosis of the calvaria and osteoporosis in the vertebra and limbs⁴. Osteoporosis is a condition of the bone where a decreased bone mineral density (BMD) can be found^{5, 6}. In humans osteoporosis can be found in women and men especially at later age (>55 years), in the Netherlands alone around an estimated number of 430.000 people are thought to be positive

for this bone defect⁷. The usage of premature aging mice models as a TTD mouse seems to be an ideal candidate therefore to investigate whether decreased BMD has an effect on the physicochemical bone composition. Nowadays, Raman spectroscopy is more and more used to study biological samples because there is little hindrance from water and complex sample preparation is unnecessary. Several different authors have used Raman spectroscopy to study early mineralization of osteoblasts⁸, mechanical deformation of cortical bone⁹ and fatigue related microdamage of bovine bone samples¹⁰. In order to eliminate the protein background fluorescence that frustrates the detection of the Raman spectra of bone near-infrared excitation can be used¹¹. Frozen or embedded sample sections with thicknesses ranging from less than 1 μm to samples of intact tissues or cells can be analyzed by using a confocal setup. In hydroxyapatite, a major component of bone, the phosphate ν_1 vibration is found at 960 cm^{-1} . When hydroxyapatite becomes less perfect, for example, the mineral lattice has decreased crystalline-to-amorphous ratio, or vacancies and/or substitutions, the Raman band of phosphate can broaden or shift to lower wavenumbers. The phosphate ν_1 vibration (960 cm^{-1}) and monohydrogen phosphate ν_1 vibration (1003 cm^{-1}) are considered accurate markers of substitution and structure of the mineral at hand^{12, 13}. In addition, the Raman bands positioned around 1200–1300 (amide III), 1600–1700 (amide I) cm^{-1} and, 1400–1470 and 2800–3100 cm^{-1} (bending and stretching modes of CH groups, respectively) are markers for the organic component of bone matrix (mainly collagen type I). We have used Confocal Raman microscopy together with histology to study the femora of TTD mice.

Material and methods

Animals

In this study two mouse strains were examined by confocal Raman spectroscopy and histology. The first cohort consisted of mice in a C57BL/6 background, which

were either wildtype (WT mice) or homozygous for the mutation XPD^{R722w} (TTD mice). A group of 8 TTD female mice were observed at 18 months postnatal, at which time points the mice were euthanized and the femora removed to be used for Confocal Raman microscopy.

The second cohort consisted of mice with a mixed C57Bl/6:129 background all with a homozygous mutation in the XPA gene¹⁴. In addition, mice were either wildtype (XPA mice) or homozygous for the mutation in XPD^{R722w} (XPA-TTD mice). A group of 4 female XPA-TTD mice used as a positive control for decreased mineral content was the same as the one previously described earlier.⁴. Since XPA-TTD mice show a very low neonatal survival, and fail to thrive at 3 weeks of age at which point most animals die, the number of animals observed in this group was low (n=4), because of their limited survival. Therefore the data obtained from the XPA-TTD mice can only be used to describe the phenotype in a qualitative manner. The femora from these mice were explanted for confocal Raman microscopy and histology in the same manner as the TTD mice.

Femora

After removal, the femora were fixated in a 4 % paraformaldehyde solution for at least 24 hours, after which excessive tissue, mainly connective tissue and muscle, was removed. The samples were then dehydrated in an increasing ethanol series from 70% until 100% after which they were critical point dried using a BAL-TEC CPD 030 Critical Point Dryer machine. In case of femora obtained from XPA-TTD mice, the left leg was used for histological evaluation while the right leg was used for critical point drying and Raman spectroscopy.

Confocal Raman microscopy

We used an in house build confocal Raman microscope, extensively described elsewhere¹⁵⁻¹⁸, to measure the isolated femora at the bone surface. In short, the

excitation wavelength used was the 647.1 nm line from a Kr ion laser. The field of view is approximately 58 μm in diameter when a $63\times$ NA = 1.2 water immersion objective (Zeiss Plan Neofluar) is used. A blazed holographic grating with 600 grates/mm (Jobin-Yvon, Paris) was used for dispersion. The lateral resolution is limited by the diffraction and is 550 nm for this system. The definition of the resolution is based on the diameter of the laser beam waist at which the beam intensity has fallen to $1/e^2$ of its peak value. In all cases the specimens were measured with 30 mW for 45 seconds in order not to damage the specimens by overexposure and to ensure a good signal to noise ratio. The CCD is connected with a computer for data collection and analysis using WinSpec (Roper Scientific Inc., USA) and Microcal Origin (Microcal software inc., USA) data analysis software. All measurements ($n=10$) per femora ($n=8$) were performed in a randomized manner at the cortex surface. Femora of the wild type mouse strain were measured in the same way for comparison. After data correction for background fluorescence the intensity of specific bone mineral and bone matrix Raman bands was determined. Based on data published by de Boer et al.⁴ of these mice, we expect the TTD bone mineral content to be lower than in the wild type. The average intensities of both wild type and TTD mouse strain bone mineral bands (phosphate and carbonate) were compared using a one-tailed Student T-test with homoscedastic sampling. The intensities of bone matrix specific bands, mostly related to collagen type I, were compared using a two-tailed distribution, while no data on the bone matrix content of these bones was known beforehand.

Histology

In order to study its histology, the complete left hind leg of XPA-TTD mice and control animals were fixated in 4 % paraformaldehyde for at least 24 hours. After fixation the samples were dehydrated in an increasing ethanol series (70-100%) after which they were immersed in a methyl methacrylate (MMA) solution. Vacuum

was applied for 2 hours to ensure air bubbles were removed before placing the samples in a waterbath at 37 °C for 2 days in order to polymerize the MMA. After embedding serial sections were made on a Leica SP 1600 innerlock diamond saw (Leica microsystems, Germany). The obtained sections were stained using methylene blue (Sigma, The Netherlands) and basic fuchsin (Sigma, The Netherlands) for light microscopic examination.

Results

The Raman spectra obtained from one of the four XPA-TTD mice observed in this study showed remarkable differences in respect to the control group. Although the number of animals did not allow for a sound statistical analysis and the differences in the other animals observed were not as extreme, the differences in these spectra are quite noteworthy. In figure 1 an example of a spectrum in which the differences were most extreme from a XPA-TTD mouse is shown in comparison to spectra obtained from a control group animal.

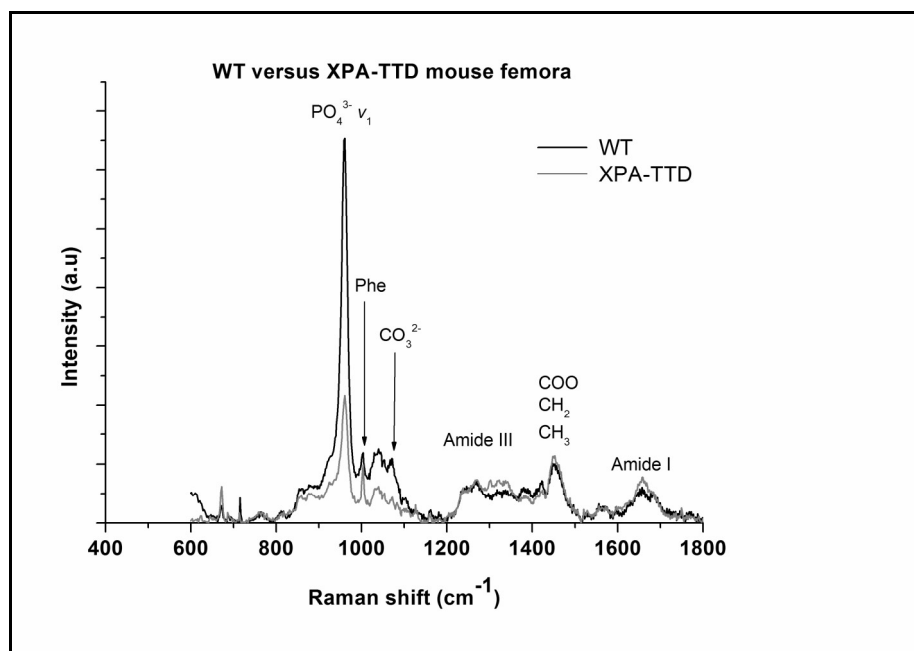


Figure 1: Raman spectrum showing the differences between a wild type and a XPA-TTD mouse in which the lowest amount of bone mineral was observed.

The Raman spectrum of this mouse showed severe decreased intensity of bone mineral specific bands when compared to the control group. The intensities of bone matrix specific bands on the other hand were similar to those found in the control group. Interestingly, during isolation of these femora we noticed that the XPA-TTD mice seemed to have more thinner femora than the wild-type animals, which might be related to the above mentioned spectral data indicating a low mineral content. Based upon these results it was decided to study these samples in more detail by histology to check for altered bone morphology. Several serial cross sections from the femora of XPA-TTD mice were observed using light microscopy. In figure 2 a typical light micrograph from a cross-section of the femur of XPA-TTD mouse shown in figure 1 compared to a control can be seen.

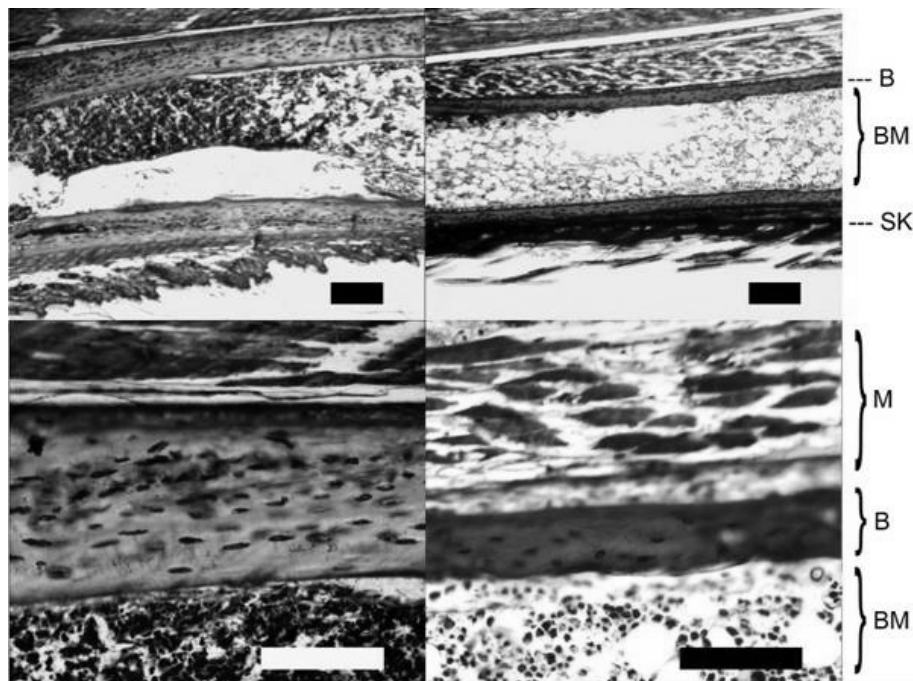


Figure 2: Light micrograph showing the morphology of WT (left panel) and XPA-TTD (right panel) mice. Scale bars are 400 μ m (top) and 200 μ m (bottom). B = bone, BM = bone marrow, SK = skin region, M = muscle region.

In both XPA-TTD and XPA mice a similar appearance of bone marrow and osteocytes can be found. However, in case of the XPA-TTD mouse shown here, the thickness of the cortical bone was at least two fold less than what was observed in the controls. These results relate to what was observed initially during explantation of the femora, at which we found XPA-TTD mouse femora to be more delicate than compared to wild type and TTD femora.

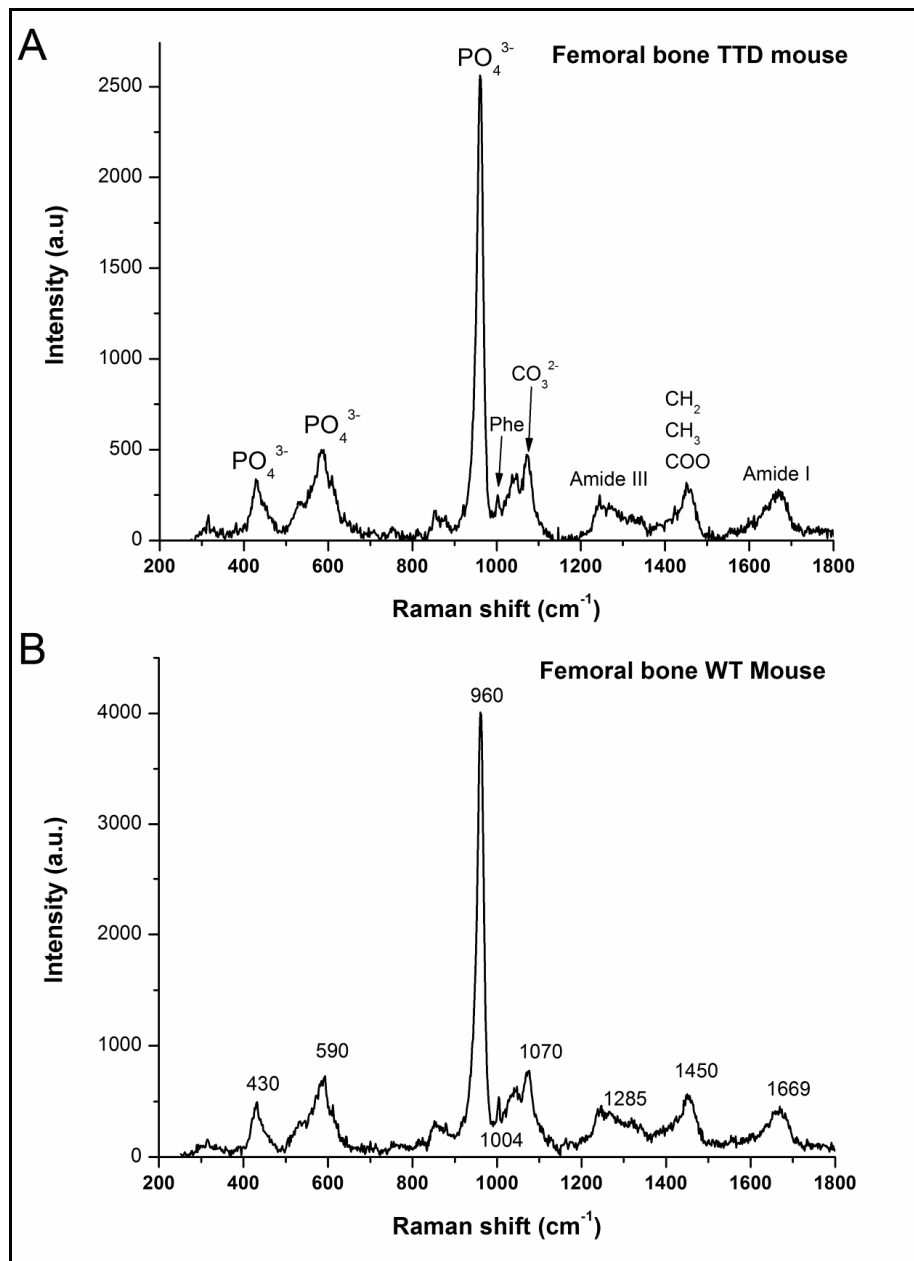


Figure 3: Raman spectra from femora of TTD (A) and WT (B) mice showing both the molecular assignment and band position of bone mineral and matrix specific Raman bands.

In case of TTD mice average Raman spectra were used for determination of peak intensities. Raman spectra of both the controls and TTD mice showed specific bone

mineral and bone matrix Raman bands (see figure 3A and B). The bone mineral bands observed were the phosphate (PO_4^{3-}) ν_1 symmetric stretch at 960 cm^{-1} and the B-type carbonate (CO_3^{2-}) ν_1 symmetric stretch at 1070 cm^{-1} . The bone matrix bands markers for the collagen backbone, amide I at 1655 cm^{-1} , amide III at 1250 cm^{-1} , methylene (CH_2)-wag at 1450 cm^{-1} and phenylalanine at 1004 cm^{-1} could all clearly be observed in both groups. The average spectra of the total number of spectra of TTD mice showed a slightly lower intensity of the main phosphate band in respect to the control mice (see figure 4). In figure 5A and B the average intensities of the individual mice of the most important Raman bands described in table 1 at 960 , 1004 , 1042 , 1070 , 1453 and 1669 cm^{-1} were plotted, showing the variation in mineral content within the group of animals investigated.

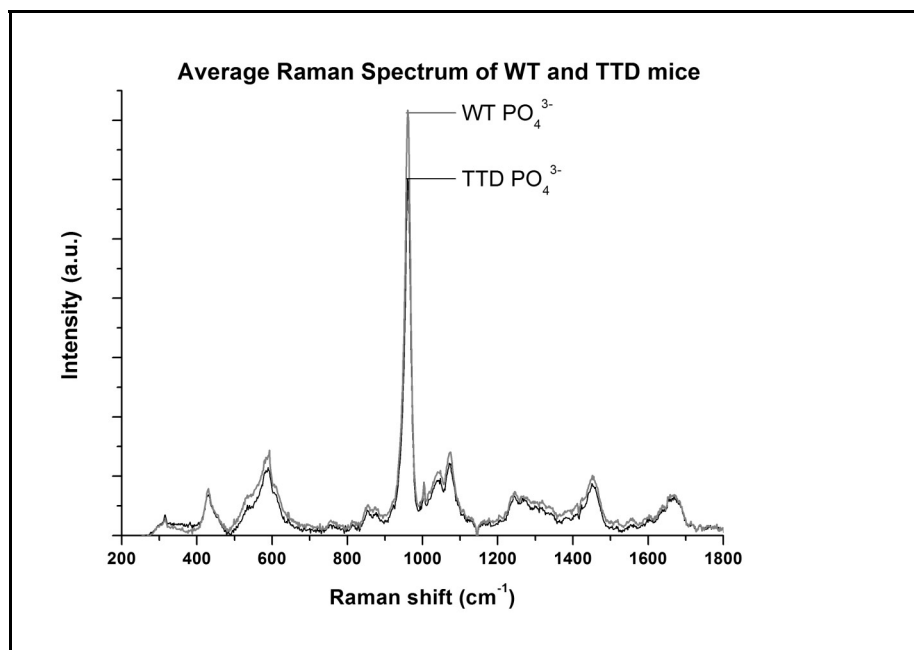


Figure 4: Comparison of average Raman spectra of TTD and wild type mice, showing the difference in intensity of the ν_1 asymmetric stretch mode belonging to PO_4^{3-} , indicating a lower mineral content in TTD mice.

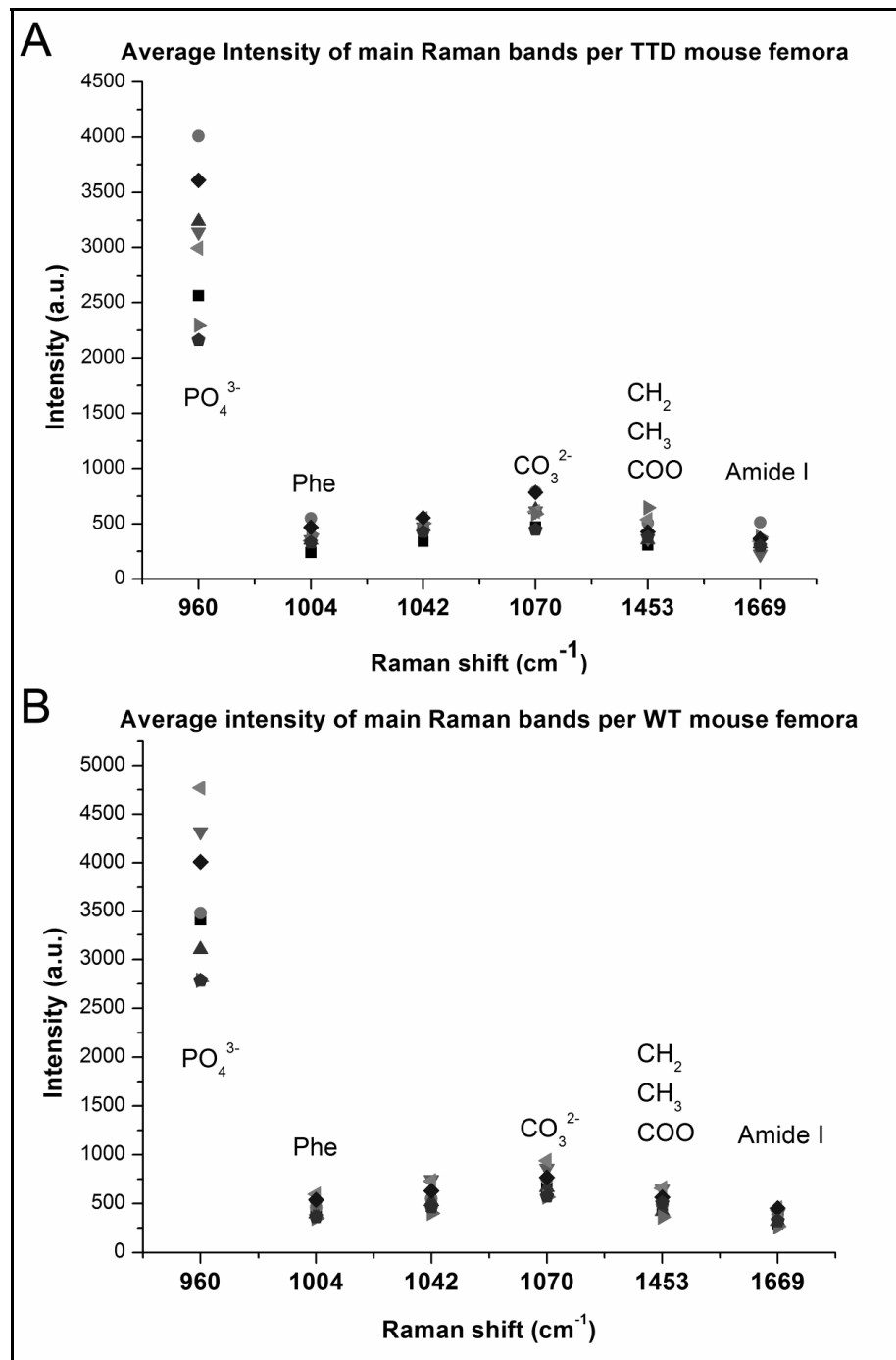


Figure 5: Comparison of the variation of the intensities of the main Raman bands observed in the TTD mouse and the wild type cohort.

A summary of the average intensities of these different Raman bands can be found in table 1.

Strain	Wild type (BL/6)			TTD			
Raman shift (cm ⁻¹)	Average Intensity (a.u.)	sd	Ratio (I _{xcm-1} /I _{960cm-1})	Average Intensity (a.u.)	sd	Ratio (I _{xcm-1} /I _{960cm-1})	Assignment
960	3583.50	724.38	1	3002.13	638.34	1	PO ₄ ³⁻
1004	451.38	87.92	7.939	381.38	93.44	7.872	Phenylalanine
1042	565.63	126.47	6.336	473.13	68.89	6.345	CO ₃ ²⁻
1070	723.50	132.48	4.953	617.13	124.39	4.865	CO ₃ ²⁻
1453	515.00	104.44	6.958	440.75	114.06	6.811	CH ₂ CH ₃ COO
1669	363.00	71.65	9.872	339.50	85.93	8.843	Amide I

Table 1: Bone mineral and bone matrix protein Raman bands obtained from wildtype and TTD mice (n=8).

The data seem to suggest that mineral content in non TTD mice is slightly above that of TTD mice. Results after statistical analysis showed that the average mineral content in TTD mice was lower than could be found in the wildtype group. The band for the ν_1 PO₄³⁻ symmetrical stretch (960 cm⁻¹) and CO₃²⁻ (1070 cm⁻¹) were both lower in the TTD mice than the wild type mice (p=0.029 and p=0.033 respectively), indicating a change in physicochemical content. The bone matrix specific bands, which can be found around 1250, 1450 and 1650 cm⁻¹ do not seem to be affected in the TTD mice as the intensities of these bands did not show any differences in respect to the control group.

Discussion

TTD mice show many symptoms of early aging, including a decreased mineral density in vertebrae and limbs leading to osteoporosis. TTD-XPA mutant mice exhibit an even faster rate of aging resulting in amongst others a severely shortened lifespan (3 weeks) and spinal kyphosis, which is indicative for osteoporosis, compared to TTD mice⁴. The primary indication for osteoporosis is loss of bone, which can be measured by decreased BMD. Raman spectroscopy and/or imaging

have been used in several studies to evaluate bone mineral and bone matrix composition of bone samples^{10, 19-23}. In this study we have used Confocal Raman microscopy to investigate the physicochemical composition of femoral bone from TTD and XPA-TTD mice. Raman measurements of one the XPA-TTD mice used in this study showed remarkable differences in bone mineral composition compared to wildtype animals. Although the data presented here did not allow for a statistical analysis, because of the number of animals observed, the amount of bone mineral seems to be reduced in the femora from these animals. The XPA-TTD mouse showing the lowest amount of bone mineral observed in this study appeared not only to have less bone mineral, but less bone mass as well. The fact that femora isolated from these animals seemed to be more fragile than TTD or WT femora at first glance concurs with these observations. In addition, histology revealed that the thickness of cortical bone for these mice was around two fold less than what could be found in the control mice. The histo- and morphological observations made on XPA-TTD mice were confirmed by the outcome of confocal Raman microscopic observations; this allowed us to use this technique to study TTD mouse femora in more detail. Raman spectroscopy showed a decreased level of phosphate and carbonate content present in cortical bone of femora isolated from TTD mice compared to WT animals. In contrast, the bone matrix content was not affected, leading to the conclusion that collagen type I content is not changed in these mice. The variation in bone mineral content per femora between TTD mice was similar to what was observed for TTD mice where X-ray radiographs were used to determine bone density⁴. Although the differences in bone mineral content in TTD and WT mice found in this study are not large, it might explain the decreased bone density found in the abovementioned study. A study in Sprague-Dawley rats has shown that bone stiffness increased with increase of degree of mineralization, carbonate content and crystallinity of bone mineral²⁴. Although no crystallinity and mechanical measurements were done during our study the differences found in

bone composition of TTD and XPA-TTD mice compared to the control animals could mean that bone stiffness in these animals is lower than that of the wildtype animals. Bone formation is highly dependent on the presence of sufficient osteoblasts, which actively deposit bone extra cellular matrix. However, the amount of cells with osteogenic potential which are present depends of the individual's age and physiological state. Research, done on the effect of donor age and the capacity of mesenchymal stem cells isolated from patients, showed a significant decrease in osteogenic potential of these cell populations at age 50 years and higher. The decrease in osteogenicity was related to proliferative capacity of the mesenchymal stem cells (MSCs) in culture, especially at older age²⁵. The ability to form so called colony forming units, or CFU's, from human bone marrow was also found to be negatively influenced at later age²⁶. Furthermore, studies performed in animals ²⁷ and humans ^{28, 29} showed that the capacity to express alkaline phosphatase, an osteoblast specific marker, also decreases during aging in these cells. For future experiments it would be interesting to isolate MSCs from TTD and XPA-TTD mice to gain insight in their proliferative and differentiation capacity. Since these mice show fast premature aging, MSCs isolated from these animals could very well be hampered in their ability to form bone, like was shown for MSCs from human origin. In this study we concentrated on the usage of confocal Raman microscopy for the analysis of bone physicochemical composition derived from a well known premature aging mouse model in called trichothiodystrophy. The data found by Raman spectroscopy presented in this paper adds to results published by us on these mouse models, bone mineral content in TTD mice was found to be lower, while bone matrix protein content was similar to the WT animals observed in this study.

Acknowledgements

This research was funded by the Dutch technology foundation (STW).

References

1. Bergmann, E.; Egly, J.-M., Trichothiodystrophy, a transcription syndrome. *2001*, 17, (5), 279.
2. de Boer, J.; de Wit, J.; van Steeg, H.; Berg, R. J.; Morreau, H.; Visser, P.; Lehmann, A. R.; Duran, M.; Hoeijmakers, J. H.; Weeda, G., A mouse model for the basal transcription/DNA repair syndrome trichothiodystrophy. *Mol Cell* **1998**, 1, (7), 981-90.
3. de Boer, J.; Donker, I.; de Wit, J.; Hoeijmakers, J. H.; Weeda, G., Disruption of the mouse xeroderma pigmentosum group D DNA repair/basal transcription gene results in preimplantation lethality. *Cancer Res* **1998**, 58, (1), 89-94.
4. de Boer, J.; Andressoo, J. O.; de Wit, J.; Huijman, J.; Beems, R. B.; van Steeg, H.; Weeda, G.; van der Horst, G. T.; van Leeuwen, W.; Themmen, A. P.; Meradji, M.; Hoeijmakers, J. H., Premature aging in mice deficient in DNA repair and transcription. *Science* **2002**, 296, (5571), 1276-9.
5. Kanis, J. A., Osteoporosis and osteopenia. *J Bone Miner Res* **1990**, 5, (3), 209-11.
6. Kanis, J. A., Assessment of fracture risk and its application to screening for postmenopausal osteoporosis: synopsis of a WHO report. WHO Study Group. *Osteoporos Int* **1994**, 4, (6), 368-81.
7. van der Klift, M.; Burger, H.; de Laet, C. E. D. H.; Pols, H. A. P.; Gijsen, R.; Poos, M. J. J. C., Hoe vaak komt osteoporose voor en hoeveel mensen sterven eraan? In *Volksgezondheid Toekomst Verkenning, Nationaal Kompas Volksgezondheid*, ed.; RIVM: 2003.
8. Stewart, S.; Shea, D.A.; Tarnowski, C.P.; Morris, M.D.; Wang, D.; Francheschi, R.; Lin, D.L.; Keller, E., Trends in early mineralization of murine calvarial osteoblastic cultures: a raman microscopic study. *Journal of raman spectroscopy* **2002**, 33, 536-543.
9. Carden, A.; Rajachar, R.; Morris, M.; Kohn, D., Ultrastructural changes accompanying the mechanical deformation of bone tissue: a Raman imaging study. *Calcif Tissue Int* **2003**, 72, (2), 166-75.
10. Timlin, J.; Carden, A.; Morris, M.; Rajachar, R.; Kohn, D., Raman spectroscopic imaging markers for fatigue-related microdamage in bovine bone. *Anal Chem* **2000**, 72, (10), 2229-36.
11. Pezzuti, J. A.; Morris, M. D.; Bonadio, J. F.; Goldstein, S. A., Hyperspectral Raman imaging of bone growth and regrowth chemistry. *Proc. SPIE* **1998**, 3261, (Three-Dimensional and Multidimensional Microscopy: Image Acquisition and Processing V), 270-276.
12. Timlin, J.; Carden, A.; Morris, M., Chemical microstructure of cortical bone probed by Raman transects. *Applied Spectroscopy* **1999**, 53, (11), 1429-1435.
13. Penel, G.; Leroy, G.; Rey, C.; Bres, E., MicroRaman spectral study of the PO₄ and CO₃ vibrational modes in synthetic and biological apatites. *Calcif Tissue Int* **1998**, 63, (6), 475-81.
14. Vries, A. d.; van Oostrom, C. T. M.; Hofhuis, F. M. A.; Dortant, P. M.; Berg, R. J. W.; Gruijl, F. R. d.; Wester, P. W.; van Kreijl, C. F.; Capel, P. J. A.; Steeg, H. v.; Verbeek, S. J., Increased susceptibility to ultraviolet-B and carcinogens of mice lacking the DNA excision repair gene XPA. **1995**, 377, (6545), 169.
15. Uzunbajakava, N.; Lenferink, A.; Kraan, Y.; Volokhina, E.; Vrensen, G.; Greve, J.; Otto, C., Nonresonant confocal Raman imaging of DNA and protein distribution in apoptotic cells. *Biophys J* **2003**, 84, (6), 3968-81.
16. Uzunbajakava, N.; Lenferink, A.; Kraan, Y.; Willekens, B.; Vrensen, G.; Greve, J.; Otto, C., Nonresonant Raman imaging of protein distribution in single human cells. *Biopolymers* **2003**, 72, (1), 1-9.
17. Uzunbajakava, N.; Otto, C., Combined Raman and continuous-wave-excited two-photon fluorescence cell imaging. *Opt Lett* **2003**, 28, (21), 2073-5.
18. van Manen, H. J.; Uzunbajakava, N.; van Bruggen, R.; Roos, D.; Otto, C., Resonance Raman imaging of the NADPH oxidase subunit cytochrome b558 in single neutrophilic granulocytes. *J Am Chem Soc* **2003**, 125, (40), 12112-3.
19. Bohic, S.; Rey, C.; Legrand, A.; Sfihi, H.; Rohanizadeh, R.; Martel, C.; Barbier, A.; Daculsi, G., Characterization of the trabecular rat bone mineral: effect of ovariectomy and bisphosphonate treatment. *Bone* **2000**, 26, (4), 341-8.
20. Carden, A.; Rajachar, R. M.; Morris, M. D.; Kohn, D. H., Ultrastructural Changes Accompanying the Mechanical Deformation of Bone Tissue: A Raman Imaging Study. *Calcif Tissue Int* **2002**.
21. Freeman, J.; Wopenka, B.; Silva, M.; Pasteris, J., Raman spectroscopic detection of changes in bioapatite in mouse femora as a function of age and in vitro fluoride treatment. *Calcif Tissue Int* **2001**, 68, (3), 156-62.
22. Penel, G.; Leroy, G.; Leroy, N.; Behin, P.; Langlois, J.; Libersa, J.; Dupas, P., Raman spectrometry applied to calcified tissue and calcium-phosphorus biomaterials. *Bull Group Int Rech Sci Stomatol Odontol* **2000**, 42, (2-3), 55-63.
23. Tarnowski, C. P.; Ignelzi, M. A., Jr.; Morris, M. D., Mineralization of developing mouse calvaria as revealed by Raman microspectroscopy. *J Bone Miner Res* **2002**, 17, (6), 1118-26.
24. Akkus, O.; Adar, F.; Schaffler, M. B., Age-related changes in physicochemical properties of mineral crystals are related to impaired mechanical function of cortical bone. *Bone* **2004**, 34, (3), 443-53.
25. Mendes, S. C.; Tibbe, J. M.; Veenhof, M.; Bakker, K.; Both, S.; Platenburg, P. P.; Oner, F. C.; de Bruijn, J. D.; van Blitterswijk, C. A., Bone tissue-engineered implants using human bone marrow stromal cells: effect of culture conditions and donor age. *Tissue Eng* **2002**, 8, (6), 911-20.
26. Bab, I.; Passi-Even, L.; Gazit, D.; Sekeles, E.; Ashton, B. A.; Peylan-Ramu, N.; Ziv, I.; Ulmansky, M., Osteogenesis in in vivo diffusion chamber cultures of human marrow cells. *Bone Miner* **1988**, 4, (4), 373-86.
27. Knight, S. M.; Gowen, M., The effect of age and sex on bone cell function. *Calcified Tissue International* **1992**, 50, A12.
28. D'Ippolito, G.; Schiller, P. C.; Ricordi, C.; Roos, B. A.; Howard, G. A., Age-related osteogenic potential of mesenchymal stromal stem cells from human vertebral bone marrow. *J Bone Miner Res* **1999**, 14, (7), 1115-22.

29. Glowacki, J., Influence of age on human marrow. *Calcif Tissue Int* 1995, 56 Suppl 1, S50-1.

Summary

This dissertation describes the use of confocal Raman microscopy and spectroscopy in the field of tissue engineering. Moreover, it describes the combination of two already existing technologies, namely scanning electron microscopy and confocal Raman spectroscopy in one apparatus for the enhancement of the chemical analytical capabilities of the electron microscope. The combined technology is described in two chapters; one focussing on the analysis of typical tissue engineered specimens where cells are combined with materials, and the other one focussing on the alteration of the physicochemical properties of biomimetic calcium phosphate coating materials by introduction of a model protein. Furthermore, in this dissertation the use of Raman spectroscopy for the analysis of the degradation of a polymer used for tissue engineering applications is described in two chapters. These two chapters led to the idea of designing a simple cell culture model which could be used to observe biomaterial degradation inside single cells by using a technique called Raman imaging. Last but not least a study on the quality of bone obtained from two premature aging mice strains showing altered bone composition in comparison to normal mice is described.

In tissue engineering the analysis of degradation of biomaterials has always been an important issue. An optimal biomaterial should remain intact long enough to support healing of damaged or diseased tissue in order to restore its function. Although this sounds relatively simple, one has to take numerous factors into account. For example, the location where an implant is to be placed could demand certain biomechanical properties, such as elasticity and/or stability. In addition, the rate of degradation, slow or fast, the ability to take up water or inorganic molecules, as well as issues like toxicity and biocompatibility are of great importance. This means that biomaterials should be easy to tailor, for this allows a scientist in tissue

engineering to alter the mechanical, chemical and physical properties to the implant site's specific needs.

In chapter one a brief history of microscopy and the role Raman microscopy plays during the development of microscopy is described. In chapters two and three the use of confocal Raman spectroscopy for the analysis of poly ethylene glycol terephthalate poly butylene terephthalate elastomers is investigated. These thermoplastic elastomers are composed of a soft hydrophilic segment called poly ethylene glycol terephthalate (PEOT) and a hard hydrophobic segment called poly butylene terephthalate (PBT). The material properties, i.e. stiffness, thermal behaviour and degradability, can be customized by either varying the molecular weight of PEG, used for the production of these polymers and/or the PEOT to PBT mass ratio in the polymer. PEOT PBT copolymers are currently being used as degradable materials for the use in medical applications and are sold under the brand name Polyactive™. A number of studies have revealed the good biocompatibility of PEOT PBT made materials *in vitro* as well as *in vivo* in several different animals species varying from rats to goats. Since the unique composition of these materials allows for the manufacturing of devices with a broad range of physical and biological properties, these materials are intensively being studied for tissue engineering applications. Several destructive chemical analysis techniques, i.e. nucleio magnetic resonance spectroscopy, gel permeation chromatography and differential scanning calorimetry, have been used in the past to study the degradation of these polymers. However, when valuable morphological information is needed to examine the effect of degradation on tissue engineering, a non destructive analysis technique is preferred. Raman spectroscopy is a non destructive molecular analysis technique which uses a monochromatic light source for the detection of wavelength shifts caused by chemical bond vibrations. Until now, no studies have been done on PEOT PBT polymers by using Raman

spectroscopy. Therefore it is necessary to characterize Raman spectra obtained from these polymers, not only to gain knowledge about their spectral properties, but also to check the feasibility of using this analysis technique for studying the degradation of these materials in *in vitro* and *in vivo* models. In chapter two an assessment was done of the Raman bands present in the spectra belonging to these types of materials. We were able to assign several Raman bands to corresponding molecular groups present in PEOT PBT polymers. Moreover, we could show in a relatively simple laboratory degradation model, that Raman spectroscopy could qualitatively be used to show signs of degradation by evaluating the decrease and shape changes of certain specific Raman bands. In chapter three a more elaborate investigation of degradation was done on certain specific polymer compositions often used for tissue engineering applications in an animal model. We were not only able to show similar signs of degradation *in vivo* as could be found in the laboratory model, but we found that certain types of compositions, especially those with a high polyethylene glycol content, were able to take up calcium phosphate, leading to a so-called calcification of the polymeric material. Furthermore, it was shown that the more soft and flexible materials with relatively high ratio of PEOT versus PBT degraded faster than when a lower ratio of these blocks was present and that macrophage like cells probably play a crucial role in the extended degradation of these materials. In chapter four a simple intra cellular degradation model was studied in combination with Raman imaging in order to investigate how small polymeric fragments composed of poly lactic co glycolic acid (PLGA), would be degraded inside single macrophages. The idea was that PLGA microspheres would either degrade in a homogenous manner from the outside in, or by a autocatalytic degradation process, where a build up of acidic endgroups in the center of the material cause a faster degradation from the inside out. The latter process can be observed in large implants composed of this particular material. The rationale behind this study was the observation of polymeric fragments inside

macrophage like cells, during our *in vivo* degradation study with PEOT PBT materials, and the fact that in literature a controversy exists on the issue of degradation behaviour of small PLGA devices. The use of Raman imaging showed that PLGA microspheres, are degrading through both autocatalytic and homogenous degradation and that this degradation takes place mainly through a scissoring of the ester bond belonging to the glycolic acid groups. In chapter five the use of a combination of scanning electron microscopy with confocal Raman spectroscopy for the analysis of a ceramic coating containing biological factors is described. Orthopedic implants are generally composed of titanium and its alloys mainly because of its excellent mechanical properties. In order to enhance bone-bonding capacities of these implants they can be coated with calcium phosphate coatings. The benefit of using a biomimetic calcium phosphate coating is that these are produced at 37 °C and a controlled pH and as a result permit for the incorporation of antibiotics and proteins. Previous studies on protein incorporation in biomimetic calcium phosphate coatings showed an effect of protein on crystal shape. In these studies bovine serum albumin (BSA) was used at different concentrations in the precipitation solution in order to study its incorporation into the coating. The result of these studies was that not only BSA had coprecipitated with a carbonate apatite like coating, but the crystal structure had been altered as well. Scanning electron microscopy revealed that the use of increasing concentrations of BSA lead to a decrease in crystal size and changes in shape. Nonetheless, the precise effect of the changes in crystal size and shape on crystallinity of these coatings remained unclear. In this chapter the consequence of different concentrations of BSA incorporated into biomimetic carbonated apatite coatings in relation to the effect on crystal size, crystallinity and physical appearance is described. The biomimetic carbonated apatite coatings were examined by thin film X-ray diffraction (TF-XRD), and a combination of confocal Raman spectroscopy and SEM. Results obtained during this study showed that not

only the presence of protein could be detected in a non destructive manner, but information about the relative amount of protein present in the coating could be obtained as well by using confocal Raman microscopy. Although the increase of the BSA concentration did not seem to influence the crystallinity towards a great extend, the increase in standard deviation of the calculated values together with scanning electron microscopic observations suggest that the coating structure had become more heterogeneous in its nature. The combination of SEM and confocal Raman spectroscopy proved to be feasible analysis technique to investigate both the morphology of these coatings and their physiochemical composition.

In chapter six another application of combined confocal Raman microscopy and Scanning electron microscopy is shown for the analysis of typical bone tissue engineered samples. In this chapter it is shown that a combination of confocal Raman spectroscopy and scanning electron microscopy can be used for a non destructive analysis with high resolution of cellular matrix deposited by specific cells on a biomaterial surface. By using confocal Raman scanning electron microscopy we could reveal that early *in vitro* formed bone extra cellular matrix produced by rat osteoprogenitor cells chemically resembles mature bone. However, ratio differences were observed with regard to phosphate versus protein specific Raman bands, indicating that the *in vitro* cultured bone matrix is likely to be in a very early state of bone formation. In addition we gained insight in the structure and chemical composition of the ECM, which was composed of mainly mineralized collagen type I fibers and areas of dense carbonated calcium phosphate related to the collagen fiber density, as revealed by Raman imaging of SEM samples. We also established that CRS-SEM allows the study of scanning electron microscopy specimens in a non-destructive manner and provides high resolution structural and chemical information about inorganic and organic constituents by parallel measurements on the same sample.

In the last chapter confocal Raman spectroscopy was used for the analysis of physicochemical composition of bone obtained from mice showing symptoms of accelerated aging. In previous studies mice mutated in the human trichothiodystrophy (TTD) allele were found to show symptoms similar to those found in the human disease. TTD is a rare autosomal recessive disorder with patients showing clear signs of premature aging. Some of the key characteristics of this mouse strain are skeletal abnormalities, such as kyphosis, osteosclerosis of the calvaria and osteoporosis in the vertebrae and limbs. Osteoporosis is a condition of the bone where a decreased bone mineral density (BMD) can be found. We used Confocal Raman microscopy together with histology to investigate the femora of two mice models for premature aging. The first model, a so called XPA-TTD mouse known for its severe premature aging was shown to have decreased BMD in its vertebrae. The second model we studied was a so called TTD mouse model. The XPA-TTD model consisted of mice with a mixed C57Bl/6:129 background all with a homozygous mutation in the xeroderma pigmentosum A (XPA) gene and homozygous for the mutation in XPD^{R722w} (TTD). The TTD mouse model was comprised of mice from a C57Bl/6 background, which were only homozygous for the mutation in XPD^{R722w}. Raman data obtained from the XPA-TTD mice showed remarkable differences in bone mineral composition compared to wildtype animals. Additionally, histology revealed that the thickness of cortical bone for this mouse was about two fold less than the thickness of cortical bone of control mice of the same age. Raman spectroscopy showed a decreased level of phosphate and carbonate content in cortical bone of the femora isolated from TTD mice compared to wildtype animals. In contrast, the bone matrix composition was not affected, leading to the conclusion that collagen type I content is not changed in these mice. The data found by Raman spectroscopy presented in this manuscript add to results published by others on these mouse models; bone mineral content in

TTD mice was found to be lower, whilst bone matrix protein content was comparable to the wildtype animals observed in this study.

Samenvatting

Dit proefschrift beschrijft de toepassing van confocale Raman microscopie en spectroscopie op het gebied van de weefsel vervangings techniek ("tissue engineering"). Verder beschrijft dit proefschrift het gebruik van een confocale Raman microscoop in combinatie met een scanning elektronen microscoop om de chemische analytische mogelijkheden van de elektronenmicroscoop te vergroten. Het gebruik van de gecombineerde technologie wordt beschreven in twee hoofdstukken; één waarin de analyse van objecten waarin cellen worden gecombineerd met materialen wordt beschreven, en het andere waarin de invloed van een model eiwit op de fysico-chemisch eigenschappen van biomimetische coatings, bestaande uit calciumfosfaat, afgezet op een titanium legering wordt beschreven. Verder wordt in dit proefschrift het gebruik van Raman spectroscopie voor de analyse van de afbraak van een polymeer biomateriaal dat voor tissue engineering wordt gebruikt geëvalueerd in twee hoofdstukken. Deze twee hoofdstukken leidden tot het ontwerp van een eenvoudig celkweek model dat kan worden gebruikt om materiaal afbraak binnen individuele cellen te bestuderen door een techniek te gebruiken die "Raman imaging" wordt genoemd. In het laatste hoofdstuk wordt confocale Raman spectroscopie toegepast in een studie van de kwaliteit van femoraal bot afkomstig van twee muizen stammen die specifieke symptomen van versnelde veroudering vertonen.

In "tissue engineering" is de analyse van afbraak zgn. "biomaterialen" altijd een belangrijke kwestie geweest. Een optimaal "biomateriaal" zou lang genoeg intact moeten blijven om de reparatie van beschadigd of ziek weefsel te kunnen ondersteunen of bevorderen om de functie te kunnen herstellen. Hoewel dit vrij

simpel klinkt moet men met talrijke factoren rekenschap houden; bijvoorbeeld de locatie in het lichaam waar een implant wordt toegepast kan bepaalde biomechanische eigenschappen, zoals elasticiteit en/of stabiliteit, of een langzame of snelle afbraak, of de mogelijkheid om water of anorganische molecules op te nemen vereisen, ook zaken als cytotoxiciteit en biocompatibiliteit kunnen van groot belang zijn. Dit houdt in dat biomaterialen relatief eenvoudig aan te passen zouden moeten zijn, om een wetenschapper die zich bezig houdt met “tissue engineering” makkelijk verandering kan maken aan mechanische, chemische en fysieke eigenschappen van een implantaat naargelang de specifieke eigenschappen die een toepassingslocatie vereist.

Afgezien van de introductie in hoofdstuk 1 waarin een overzicht van de ontwikkeling en geschiedenis van microscopie en de rol die Raman microscopie hierin speelt wordt gegeven, wordt in hoofdstuk 2 en 3 het gebruik van confocale Raman spectroscopie voor de analyse van een veelgebruikt biomateriaal in tissue engineering, bestaande uit een elastomeer samengesteld uit polyethyleenglycol terephthalaat en polybutyleen terephthalaat, beschreven. Deze zgn. thermoplastische elastomeren zijn samengesteld uit een zacht waterminnend segment polyethyleen glycol terephthalaat (PEOT) en een hard waterafstotend segment polybutyleen terephthalaat (PBT) genoemd. De materiaal eigenschappen, i.e. de stijfheid, het thermische gedrag en afbreekbaarheid, kunnen worden aangepast door of het molecuul gewicht van polyethyleenglycol, dat voor de productie van deze polymeren wordt gebruikt, en/of de massaverhouding van PEOT en PBT in het polymeer te variëren. Deze zogenaamde blok co-polymeren worden momenteel gebruikt als afbreekbare materialen voor het gebruik in medische applicaties en worden verkocht onder de merknaam Polyactive™. Een aantal studies hebben de uitstekende biocompatibiliteit aangetoond van PEOT PBT materialen *in vitro* (in het laboratorium), in celkweek modellen en *in vivo* (in het lichaam), door middel van

studies in verschillende diersoorten variërend van ratten tot geiten. Aangezien de unieke samenstelling van deze materialen de productie van implantaten toestaat met een scala van verschillende fysieke en biologische eigenschappen worden deze materialen intensief bestudeerd voor toepassingen in tissue engineering. Tot nog toe zijn er verscheidene destructieve chemische analysetechnieken, zoals; nucleomagnetische resonantie spectroscopie, gel permeatie chromatografie en differentieel scanning calorimetrie gebruikt om de afbraak van deze polymeren te bestuderen. Nochtans, wanneer waardevolle morfologische informatie nodig is om te onderzoeken wat het effect van afbraak is op door tissue engineering geproduceerde implantaten zal een niet destructieve analyse techniek de voorkeur hebben. Een belangrijk voordeel van Raman spectroscopie is dat het een niet destructieve moleculaire analyse techniek betreft die een monochromatische lichtbron (laser) voor de detectie van golflengte verschuivingen, die door chemische binding vibraties worden veroorzaakt, gebruikt. Tot nu toe, zijn er geen studies gedaan van polymeren bestaande uit PEOT PBT door middel van Raman spectroscopie van enige importantie. Daarom was het noodzakelijk om de Raman spectra te karakteriseren die van deze polymeren kunnen worden verkregen. Dit is nodig om niet alleen kennis over de spectrale eigenschappen te verkrijgen, maar ook om de haalbaarheid van het gebruik van Raman spectroscopie als analysetechniek voor de studie van afbraak van deze materialen binnen *in vitro* en *in vivo* modellen te kunnen toetsen. In hoofdstuk 2 is een analyse gemaakt van de banden die aanwezig zijn in de Raman spectra verkregen van bovengenoemde materialen. Verscheidene Raman banden konden worden toegewezen aan hun overeenkomstige moleculaire groepen die aanwezig zijn in PEOT PBT polymeren. Verder was het mogelijk om met behulp van confocale Raman spectroscopie in een vrij eenvoudig laboratoriummodel de afbraak van deze materialen aan te tonen. Het is gebleken dat Raman spectroscopie voornamelijk kwalitatief kan worden gebruikt om afbraak van deze polymeren aan te kunnen tonen door een

evaluatie van de afname en vormveranderingen van bepaalde specifieke Raman banden. In hoofdstuk 3 werd een meer uitgebreid onderzoek van de afbraak in een diermodel gedaan van bepaalde specifieke polymeersamenstellingen die vaak voor de toepassingen in tissue engineering worden gebruikt. Het bleek niet alleen mogelijk vergelijkbare resultaten van degradatie aan te tonen *in vivo* zoals die in het *in vitro* laboratoriummodel waren gevonden, maar ook bleek dat bepaalde soorten samenstellingen, vooral die met een hoog polyethyleenglycol gehalte, calciumfosfaat konden opnemen wat leidt tot een zogenaamde verkalking van het polymeer materiaal. Verder hebben we aangetoond dat meer zachte en flexibele materialen met een relatieve hoge verhouding van PEOT ten opzichte van PBT sneller afgebroken worden dan wanneer een lagere verhouding van deze blokken aanwezig is, en dat macrophaag achtige cellen waarschijnlijk een essentiële rol spelen in de verdere afbraak van deze materialen. In hoofdstuk 4 is een eenvoudig intra cellulair afbraakmodel bestudeerd met behulp van Raman imaging. Hierbij is onderzocht of kleine micrometer grote polymeer fragmenten die uit een combinatie van poly melkzuur en glycol zuur (PLGA) bestonden, afbreken vanaf de buitenkant naar binnen, op relatief homogene wijze, of door een autokatalytisch afbraak proces, waarbij een opeenhoping van zuurrijke eindgroepen in het centrum van deze materialen een snellere afbraak veroorzaken waardoor een uitholling plaatsvindt. Dit laatste proces is vergelijkbaar met wat wordt gevonden in grote implantaten die uit dit materiaal zijn samengesteld. De reden voor deze studie was de observatie van kleine polymeer fragmenten in macrofaag-achtige cellen tijdens onze studie van afbraak van PEOT PBT materialen in een diermodel, en het feit dat in literatuur een controverse bestaat over de kwestie van afbraak van kleine uit PLGA samengestelde implantaten. Door gebruik te maken van Raman imaging kon worden aangetoond dat in microbolletjes van PLGA zowel een autokatalytisch als een homogeen afbraak proces plaatsvindt, en dat deze afbraak hoofdzakelijk veroorzaakt wordt door het uiteenvallen van een esterverbinding die

tot de glycol zuur groepen behoort. In hoofdstuk 5 wordt het gebruik van een combinatie van de elektronenmicroscopie met confocale Raman spectroscopie beschreven voor de analyse van een keramische coating die biologische factoren bevat. Orthopedische implantaten zijn over het algemeen samengesteld uit titanium of een titanium legering voornamelijk vanwege de uitstekende mechanische eigenschappen van dit materiaal. Om de bot hechtende eigenschappen van deze implantaten te verbeteren worden deze met een laagje calciumfosfaat bedekt. Het voordeel van biomimetisch geproduceerde calciumfosfaat coatings is dat deze bij een lichaamstemperatuur kunnen worden geproduceerd en een gecontroleerde pH en diensgevolge de integratie van antibiotica en proteïnen tijdens het coating proces mogelijk maken. Deze factoren kunnen de biologische eigenschappen van deze coatings verder verhogen. Voorgaande studies over eiwitintegratie in biomimetische calciumfosfaat coatings toonden een effect van de aanwezigheid van eiwit op de kristalvorm aan. Tijdens dit onderzoek werd albumine verkregen uit runderserum (BSA) gebruikt in verschillende concentraties in de precipitatie oplossing bij het coating proces om integratie hiervan in de coating te bestuderen. Het resultaat van deze studies was dat niet alleen BSA aanwezig was in de geprecipiteerde carbonaat apatiet coating, maar dat tevens de kristalstructuur was beïnvloed. Het gebruik van stijgende concentraties van BSA leidde dan ook tot wijzigingen in de kristal grootte en vorm welke konden waargenomen door middel van scanning elektronen microscopie. Niettemin bleef het daadwerkelijke effect van de wijziging in kristalgrootte en de vorm op de kristalliniteit van deze coatings onduidelijk. In dit hoofdstuk wordt dan ook het effect van verschillende concentraties BSA die in biomimetische carbonaat apatiet coatings kan worden opgenomen met betrekking tot het effect op kristalgrootte, kristalliniteit en structuur beschreven. De biomimetische carbonaat apatiet coatings werden onderzocht door middel van dunne film röntgen diffractie (TF-XRD), en een combinatie van confocale Raman spectroscopie en scanning

electronen microscopie. De resultaten die tijdens deze studie werden verkregen toonden aan dat niet alleen de aanwezigheid van eiwit in deze coatings op een niet destructieve manier kan worden aangetoond, maar dat ook informatie over de relatieve hoeveelheid eiwit aanwezig in de coating kan worden verkregen door gebruik te maken van confocale Raman spectroscopie in een electronen microscoop. Hoewel, de verhoging van de concentratie BSA in de precipitatie oplossing niet de kristalliniteit leek te beïnvloeden, bleek uit het hoger worden van standaardafwijking, berekend uit de waarden verkregen d.m.v. confocale Raman spectroscopie, samen met de electronen microscopische observaties dat structuur van de coatings meer heterogeen van aard werd. De combinatie van scanning electronen microscopie en confocale Raman spectroscopie bleek een analyse techniek te zijn die niet alleen onderzoek en observatie van de structuur en de fysiochemische samenstelling van deze materialen mogelijk maakte.

In hoofdstuk 6 wordt wederom een toepassing van gecombineerde confocale Raman microscopie en elektronenmicroscopie beschreven. Dit maal voor de analyse van uit bot-cellen geweekte en biomateriaal bestaande preparaten veel voorkomend in tissue engineering onderzoek. In dit hoofdstuk wordt aangetoond dat de combinatie van confocale Raman spectroscopie en scanning electronen microscopie voor een niet destructieve hoge resolutie analyse van bot cel matrix, die door botvormende cellen op een materiaal oppervlakte is afgezet, gebruikt kan worden. Door confocale Raman scanning electronen microscopie te gebruiken kon worden aangetoond dat *in vitro* gevormd bot afgezet door rat osteoprogenitor cellen grote chemische overeenkomsten vertoont met volwassen bot. Nochtans, konden er verschillen in de verhouding van fosfaat en eiwit specifieke Raman banden worden waargenomen die erop wijzen dat de *in vitro* gevormde botmatrix een zeer vroeg stadium van botvorming representeert. Daarnaast is er meer inzicht verkregen in de structuur en de chemische samenstelling van bot extra cellulaire

matrix, welke hoofdzakelijk uit gemineraliseerde collageentype I vezels bestaat. Verder is vastgesteld dat confocale Raman scanning electrone microscopie de studie van de elektronenmicroscopie preparaten op een niet destructieve manier mogelijk maakt en dat structurele en chemische informatie, over de anorganische en organische samenstelling van deze preparaten door parallelle metingen met hoge resolutie verkregen kan worden.

In het laatste hoofdstuk wordt het gebruik van confocale Raman spectroscopie beschreven voor de analyse van fysico-chemische samenstelling van bot verkregen uit muizen welke symptomen van een versneld verouderings-syndroom vertonen. Uit voorgaande studies aan muizen die een mutatie hebben in het zogenaamde trichothiodystrophy (TTD) allel is gebleken dat deze symptomen vertonen gelijkend aan het menselijke syndroom. TTD is een zeldzame autosomale recessieve afwijking waarbij de patiënten duidelijke tekenen van vroegtijdige veroudering vertonen. Enkele zeer belangrijke kenmerken van deze muizen stam is de aanwezigheid van skelet abnormaliteiten, zoals kyfose, osteosclerose van de schedel en osteoporose in wervels en de ledematen. Osteoporose wordt gekenmerkt doordat in bot een verminderde bot mineraal dichtheid (BMD) wordt gevonden. Wij hebben confocale Raman spectroscopie gebruikt in combinatie met histologisch onderzoek om femora verkregen van twee verschillende muizen stammen specifiek voor versnelde veroudering te onderzoeken. Het eerste model, een zogenaamde XPA-TTD muis gekenmerkt door extreem versnelde veroudering werd eerder aangetoond een verminderde BMD te bezitten in de ruggewervels. Het tweede model dat wij hebben bestudeerd was een zogenaamd TTD muismodel. Het XPA-TTD model bestond uit muizen met van gemengde C57Bl/6:129 achtergrond allen met een homozygote mutatie in het xerodermapigmentosum A (XPA) gen en homozygoot voor een mutatie in $XPDR^{722w}$ (TTD). Het TTD muismodel bestond uit muizen van een C57Bl/6 achtergrond, die slechts homozygoot waren voor een mutatie in $XPDR^{722w}$. De

Raman gegevens die van een van de XPA-TTD muizen konden worden verkregen toonden opmerkelijke verschillen aan in de bot minerale samenstelling in vergelijking met normale dieren. Bovendien, liet de histologie zien dat de dikte van het corticale bot in deze muis ongeveer twee maal zo dun was als in normale muizen van de zelfde leeftijd. Verder werd door middel van Raman spectroscopie gevonden dat er een verminderde hoeveelheid van fosfaat en carbonaat in corticaal bot van femora geïsoleerd uit TTD muizen in vergelijking met normale dieren aanwezig is. Daarentegen was de organische botmatrix samenstelling niet beïnvloed, leidend tot de conclusie dat de collageen type I inhoud niet veranderd was in deze muizen. De gegevens die door middel van Raman spectroscopie werden gevonden zoals beschreven in dit hoofdstuk voegen nieuwe informatie toe aan resultaten toe aan de kennis en data die door anderen werden gepubliceerd over deze muismodellen.

Acknowledgement

Dear family, friends and colleagues,

It looks like I've made it after all. I would like to thank all you who have supported me throughout these harsh years of research. Clemens and Cees thanks for your trust in me and allowing me to do this project. Although not always ideal, working in a company and a University at the same time provided me with unique experiences and opportunities I would probably not have had otherwise. I am grateful for having worked together with an amazing group of colleagues. A melting pot of different nationalities and scientific backgrounds makes doing science with you a lot of fun. Thanks for all your help, discussions, arguments, suggestions, drinks, special international lunches, BBQ's and parties during my PhD project, you all know who you are. A special thank you goes out to my climbing buddies for not having dropped me down yet; I hope we can continue to have more high altitude adventures in the future. To all my other friends and family thanks for all the good times we have had in all those years we know each other. A very special thank you goes out to my direct family, Maggie and Bert (mom and dad), Frédérique and Paul, Bertel and Raven, for supporting me and enduring my good and bad times throughout my live, you guys have never let me down, love you always.



Aart

"....to me, everything I see is incredible, something absolutely incredible. We take it all for granted. But I think the essence of the scientific spirit is to look beyond and to realize what a wonderful world it is we live inThe moment you ask 'Why is the sky blue?' you go deeper and deeper into the problems of physics...."

Chandrasekhara Venkata Raman -- born 1888; died 1970 (winner of the Nobel Prize in Physics 1930 "for his work on the scattering of light and for the discovery of the effect named after him)

Curriculum Vitae

Aart A. van Apeldoorn was born on February 27th 1968 in Utrecht, the Netherlands. In 1987 he started to study Zoology at the higher laboratory school for laboratory technicians in Utrecht (Hogeschool Utrecht). After successfully finishing his studies by doing a research project at the Complutense University of Madrid, Spain. He started a parttime study of Biology at the University of Utrecht. During this period (1997) he started working at Isotis BV, the Netherlands which was then a start-up company dedicated to several aspects of Tissue Engineering as a research technician in the bone tissue engineering group. After 3 years of research experience in the bone tissue engineering group he started to work as a pHd student on a STW funded research project at the University of Twente. This project entitled "the integration of confocal Raman spectroscopy with electron microscopy" was a close cooperation between the department of polymer chemistry and biomaterials (Prof. Dr. C.A. van Blitterswijk) and the department of biophysical techniques (Dr. C.Otto and Y. Aksenov) at the University and IsoTis BV (Prof. Dr. J.D. de Bruijn). The research involved with this project, was the basis for the articles used in the current dissertation and a number of presentations at (inter)national conferences. Based on the outcome of this work he obtained a first stage Biopartner grant from the ministry of economic affairs for research into the commercialization of the combination of confocal Raman spectroscopy and scanning electron microscopy

Publications and conferences related to this dissertation

S.C. Mendes, J.D. de Bruijn, K. Bakker, A.A. van Apeldoorn, P.P. Platenburg, G.J.M. Tibbe and C.A. van Blitterswijk, "Human bone marrow stromal cells for bone tissue engineering: In vitro and in vivo characterisation", In: Bone Engineering, JE Davies (Ed), EM Square Inc., Toronto, pp. 505-515 (2000).

A. A. Deschamps, A. A. van Apeldoorn, H. Hayen, J. D. de Bruijn, U. Karst, D. W. Grijpma and J. Feijen. In vivo and in vitro degradation of poly(ether ester) block copolymers based on poly(ethylene glycol) and poly(butylene terephthalate), *Biomaterials*. 2004 Jan;25(2):247-58.

A. A. Deschamps, A. A. van Apeldoorn, J. D. de Bruijn, D. W. Grijpma and J. Feijen, Poly(ether ester amide)s for tissue engineering, *Biomaterials*. 2003 Jul;24(15):2643-52.

A.A. van Apeldoorn, Structuur en chemie volgen in weefsel, *Chemisch weekblad*, 2004, 100 (4), 16-17

A.A. van Apeldoorn, H.J. van Manen, J.M. Bezemer, J.D. de Bruijn, C.A. van Blitterswijk, C Otto, Raman imaging of PLGA microsphere degradation inside macrophages, *J Am Chem Soc*. 2004 Oct 20;126(41):13226-7.

A.A. van Apeldoorn, Y.Aksenov, M.Stigter, I.Hofland, J.D.deBruijn, H.K.Koerten, C.Otto, J.Greve and C.A. van Blitterswijk, Parallel high resolution confocal Raman SEM analysis of inorganic and organic bone matrix constituents, *Journal of the Royal Soc. Interface*, 2005, 2 (2), 39-45.

R.Siddappa, C.Gaspar, A.A. van Apeldoorn, R. Fodde, C.A. van Blitterswijk J. de Boer, Wnt signalling inhibits osteogenic differentiation of human mesenchymal stem cells, *Bone*, 34(2004), 818–826

A.A. van Apeldoorn, Confocal Raman Scanning Electron Microscopy: Parallel high resolution Confocal Raman SEM analysis of inorganic and organic bone matrix constituents IRDG (Infrarood & Raman Discussie Groep) najaarsbijeenkomst 2004.

A.A. van Apeldoorn, H.J. van Manen, J.M. Bezemer, J.D. de Bruijn, C.A. van Blitterswijk, C Otto, Raman imaging of PLGA microsphere degradation inside macrophages, In J. Feijen & W.M.G.F. Pontenagel (Eds.), *Proceedings of the 11th Dutch annual conference on biomedical engineering* (pp. 134-135).

A.A. van Apeldoorn, Keynote lecture on the commercialization of confocal Raman spectroscopy for scanning electron microscopes, the 11th Dutch annual conference on biomedical engineering, Papendal, 2004

A.A. van Apeldoorn & Y. Aksenov & M. Stigter & J.D. de Bruijn & C. Otto & C.A. van Blitterswijk Confocal raman scanning electron microscopy a method for parallel non-invasive high resolution analysis of bone samples. NVVM (Nederlandse Vereniging voor Microscopie) bijeenkomst November 2004, Papendal.

A.A. van Apeldoorn & H.-J. van Manen & J.M. Bezemer & J.D. de Bruijn & C.A. van Blitterswijk & C. Otto Raman imaging of PLGA microsphere degradation inside macrophages. NVVM (Nederlandse Vereniging voor Microscopie) bijeenkomst November 2004, Papendal.

A.A. van Apeldoorn, Y. Aksenov, I. Hofland, J.D. de Bruijn, C. Otto, J. Greve & C.A. van Blitterswijk, Combined confocal raman spectroscopy and scanning electron microscopy reveals early in vitro bone formation is comparable to organized mature bone, Genova 2003 ETES Meeting 2nd Annual Meeting of the European Tissue Engineering Society, Genua (Genova), Italy.

Apeldoorn, A.A. van, Aksenov, Y., Hofland, I., Bruijn, J.D. de, Otto, C., Greve, J., & Blitterswijk, C.A. van (2003). Combined confocal raman spectroscopy and scanning electron microscopy reveals early in vitro bone formation comparable to organized mature bone. In J. Feijen & W.M.G.F. Pontenagel (Eds.), Proceedings of the 10th Dutch annual conference on biomedical engineering (pp. 64-65).

Apeldoorn, A.A. van, Aksenov, Y., Stigter, M., Hofland, I., Bruijn, J.D. de, Otto, C., Greve, J., & Blitterswijk, C.A. van (2002, September). Confocal Raman scanning electron microscopy; parallel analysis of tissue engineered bone synthesized by rat osteoprogenitor cells. Barcelona (ESP), ESB 2002.

Apeldoorn, A.A. van, Bruijn, J.D. de, Otto, C., Greve, J., Blitterswijk, C.A. van, Aksenov, Y., Stigter, M., & Hofland, I. (2002, September). Confocal raman scanning electron microscopy: parallel analysis of tissue engineered bone synthesized by rat osteoprogenitor cells. Durban (South-Africa), ICEM 15.

Aksenov, Y., Apeldoorn, A.A. van, Bruijn, J.D. de, Blitterswijk, C.A. van, Greve, J., & Otto, C. (2002). Combined electron and Raman microscopy: SEM/ESEM - CRM.. In W.M.G.F. Pontenagel & J. Feijen (Eds.), Proceedings of The Dutch Annual Conference on BioMedical Engineering (pp. 5-6).

Aksenov, Y., Apeldoorn, A.A. van, Blitterswijk, C.A. van, Greve, J., Otto, C., & Bruijn, J.D. de (2002). Combined Confocal Raman Microscope with Scanning Electron Microscope; Degradation of the Bio-Degradable Polymers.. In J. Mink, G. Jalsovszky & G. Keresztury (Eds.), XVIIIth International Conference on Raman Spectroscopy (pp. 193-194). Budapest, Hungary.

Aksenov, Y., Reinders, E.G.J., Greve, J., Blitterswijk, C.A. van, Apeldoorn, A.A. van, Otto, C., & Bruijn, J.D. de (2001). Integration of a Confocal Raman Microscope with a Scanning Electron Microscope. In V. Kopecky, K. Ruzova & J. Stepanek (Eds.), 9th European Conference on the Spectroscopy of Biological Molecules (pp. 23-23). Prague: Institute of Physics, Charles University.

Aksenov, Y., Reinders, E.G.J., Greve, J., Blitterswijk, C.A. van, Apeldoorn, A.A. van, Otto, C., & Bruijn, J.D. de (2000). Confocal Raman microspectrometer (CRM) for combination with electron microscope.. In (Ed.), Proceedings of the Dutch Annual Conference on BioMedical Engineering (pp. 5-7). Papendal.

A. A. van Apeldoorn, Y. Aksenov, J.D. de Bruijn, C.Otto, C.A. van Blitterswijk, A preliminary study on the application of confocal Micro Raman Spectroscopy for the analysis of in vivo PEOT PBT Degradation, London (UK), ESB 2001

Table of contents

Contents	4
Introduction	6
Introduction	8
A brief history of Microscopy	8
Practical problems of optics	11
Confocal microscopy	13
Electron microscopy	15
Raman spectroscopy	17
The phenomenon called Raman Effect	17
The Raman effect	17
The logical next step: combining Confocal Raman Microscopy with Electron Microscopy	20
Working principle of the combined system	21
Raman imaging in the Scanning Electron Microscope	23
Tissue engineering and materials	24
Bone and Raman spectroscopy	27
Cells, tissues, materials and confocal Raman spectroscopy	29
References	32
Characterization of PEOT PBT block copolymers by confocal Raman spectroscopy	37
Abstract	39
Characterization of PEOT PBT block copolymers by confocal Raman spectroscopy	41
Introduction	41
Materials and methods	42
Degradation	43
Confocal Raman spectroscopy	44
Results	44
Degradation study	48
GPC	50
Discussion	50

Conclusions	55
References	56
<i>In vivo</i> degradation of PEOT PBT block copolymers evaluated by confocal Raman microscopy	59
Abstract	61
In vivo degradation of PEOT PBT block copolymers evaluated by confocal Raman microscopy	62
Introduction	62
Material and methods	64
Polymers	64
Polymer processing	64
<i>In vivo</i> implantation	65
Confocal Raman spectroscopy	65
Histology	67
Results	67
Raman spectroscopy on 300PEOT55PBT45 polymers	67
Raman spectroscopy on 300PEOT70PBT30 polymers	70
Raman spectroscopy of 1000PEOT70PBT30 polymers	72
Histology	75
Discussion	79
Mineralization	82
References	85
Annex	87
A preliminary study on the application of confocal Micro Raman Spectroscopy for the analysis of in vivo PEOT PBT Degradation.	87
Introduction	87
Materials and methods	88
Histology	88
Raman spectroscopy	89
Results	89
Histology	90

Conclusions	91
Raman imaging of PLGA microsphere degradation inside macrophages	92
Abstract	94
Raman Imaging of PLGA Microsphere Degradation inside Macrophages	95
Introduction	95
Materials and methods	96
Results and discussion	97
Conclusions	101
Acknowledgement	101
References	102
Combined confocal Raman spectroscopic and SEM study of protein incorporation into biomimetic coatings	103
Abstract	105
Combined confocal Raman spectroscopic and SEM study of protein incorporation into biomimetic coatings	106
Introduction	106
Materials and methods	108
Preparation of carbonated apatite coatings (CO ₃ -AP)	108
Combined Confocal Raman Scanning Electron Microscope (CRESEM)	109
CRESEM on biomimetic CO ₃ -AP coatings	110
TF-XRD analysis	110
Results	111
CRESEM on biomimetic CO ₃ -AP coatings	111
TF-XRD analysis	114
Scanning Electron Microscopy	115
Discussion	116
References	120
Parallel high resolution confocal Raman SEM analysis of inorganic and organic bone matrix constituents	122
Abstract	124

Parallel high resolution Confocal Raman SEM analysis of inorganic and organic bone matrix constituents	125
Introduction	125
Methods	127
Cell culture	127
Combined confocal Raman scanning electron microscope	128
Results	130
Confocal Raman scanning electron microscopy (CRSEM)	130
CRSEM and biomimetic carbonated apatite like coatings (CO ₃ -AP)	131
CRSEM and bone ECM by rat osteoprogenitor cells	131
Discussion	133
References	136
The physicochemical composition of osteoporotic bone in the TTD premature aging mouse determined by confocal Raman microscopy	138
Definitions of bone found on the internet	139
Abstract	141
The physicochemical composition of osteoporotic bone in the TTD premature aging mouse determined by confocal Raman microscopy	141
Introduction	142
Material and methods	142
Animals	143
Femora	143
Confocal Raman microscopy	144
Histology	145
Results	146
Discussion	152
References	155
Summary	157
Samenvatting	163
Acknowledgement	171
Table of contents	176
	179

Color Figures

Chapter 1



Figure 1: Original Antonie van Leeuwenhoek Microscope property of the Utrecht University museum, the Netherlands. The instrument consists of two brass plates (2.4x4.6 cm) riveted together at 3 locations. The hole contains a lens. On the tip of the sharp pin an object can be placed for observation. By using the screw on the pin one is able to focus the image. Van Leeuwenhoek made about 500 microscopes of which 9 have survived. This Utrecht example has a magnification of 266 X, while the other remaining magnify between 70 until 170 X. The Utrecht microscope allows for the observation of samples with a size of 0,00135 mm. Only after 1840 AD it was possible to build microscopes which could be used to study smaller objects. Antonie van Leeuwenhoek was not the original inventor of the microscope. Around 1600 a spectacles maker from Middelburg in the Netherlands found out that smaller objects could be more easily observed when placing two lenses at certain distance from each other. The microscope shown here was discovered around 1850 in the physics laboratory at the Minrebroederstraat in Utrecht the Netherlands by Prof. P. Harting. It was kept in a leather lined box with the inscriptions BB. Focal point 0,94 mm, Magnification 266x, Lens aperture 0,7 mm, Resolving power 1,35 mm. The painting showing van Leeuwenhoek using his microscope is by Robert A. Thom and appeared in "Great Moments in Medicine" published by Parke Davis & Company, in 1966.

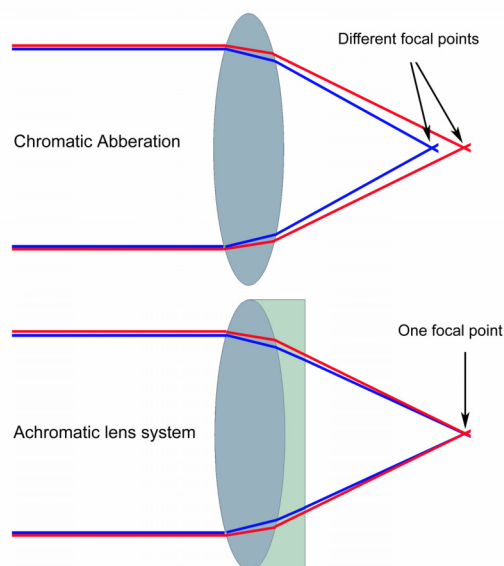


Figure 4: The problem of chromatic aberration could be solved by placing an extra the achromatic lens behind the initial single lens.

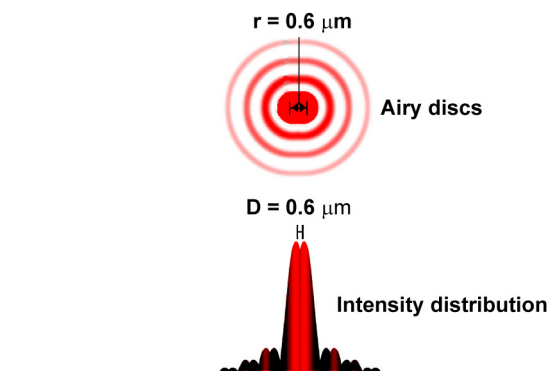


Figure 5: Resolution is the minimal distance at which two point objects still can be recognized from each other. Airy diffraction pattern sizes and their corresponding radial intensity distribution functions are depended on the combination of numerical apertures from the objective and condenser, as well as the wavelength of light used. For a well-corrected objective with a uniform circular aperture, two adjacent points are just resolved when the centres of their airy patterns are separated by a minimum distance which is equal to the radius of the central disk in the airy pattern. In this example $\lambda=685\text{nm}$ and the $\text{NA}=0.6$ and resolution $r = 1.22 \lambda / 2\text{NA}_{\text{obj}}$.

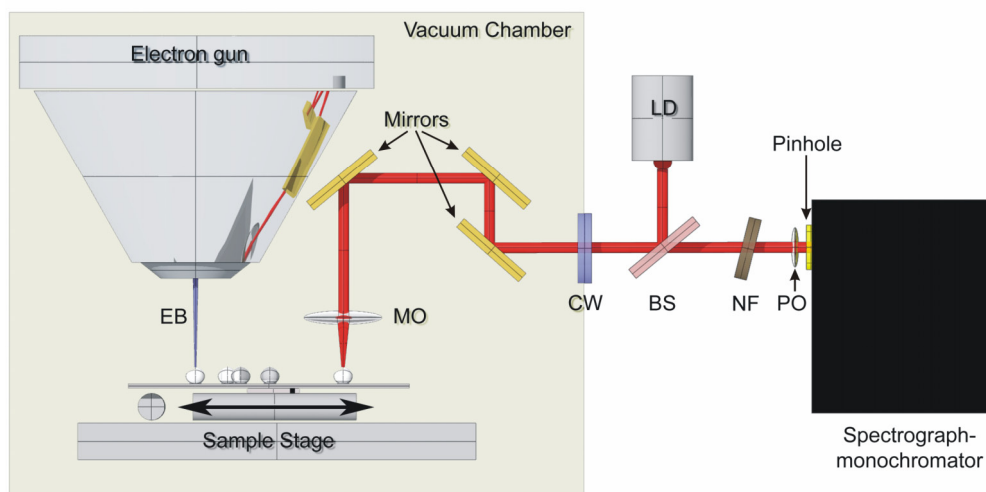


Figure 9: schematic representation of the combined confocal Raman microscope with a scanning electron microscope. Samples are analyzed by selecting a location by EM using the electron beam (EB) subsequently moving the sample into the confocal laser spot at exact coordinates. The laser source consists of a laserdiode (LD) with a wavelength of 685nm and is diverted through a side port into the vacuum chamber by a beamsplitter (BS). The laser is then emitted onto the sample by a set of gold coated mirrors through a 60 x objective (MO). The induced Raman scatter is then collected by the same objective and diverted in the opposite direction, passing a notch filter (NF) to eliminate the laser light obscuring the Raman signal and focussed by a pinhole objective (PO) on a pinhole allowing for confocality of the system. Inside the spectrograph monochromator, the Raman scattering is subsequently focused on a holographic diffraction grating and the decomposed wavelengths are then detected by a thermo-electrically cooled CCD. The sample stage (allowing for nanometer movements) is equipped with a small light source to use transmission light microscopic observation for easy calibration of stage movement.

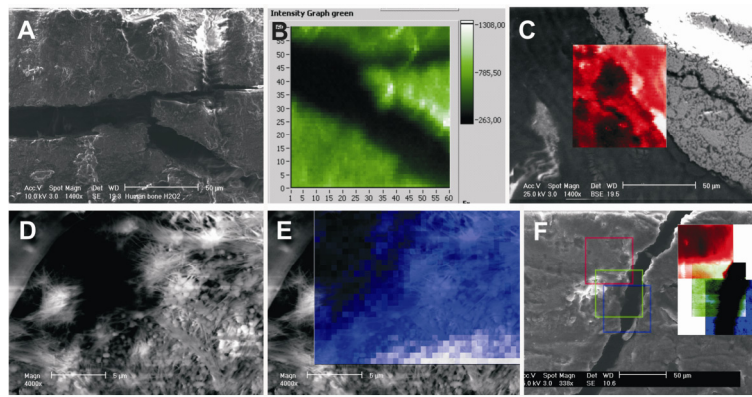
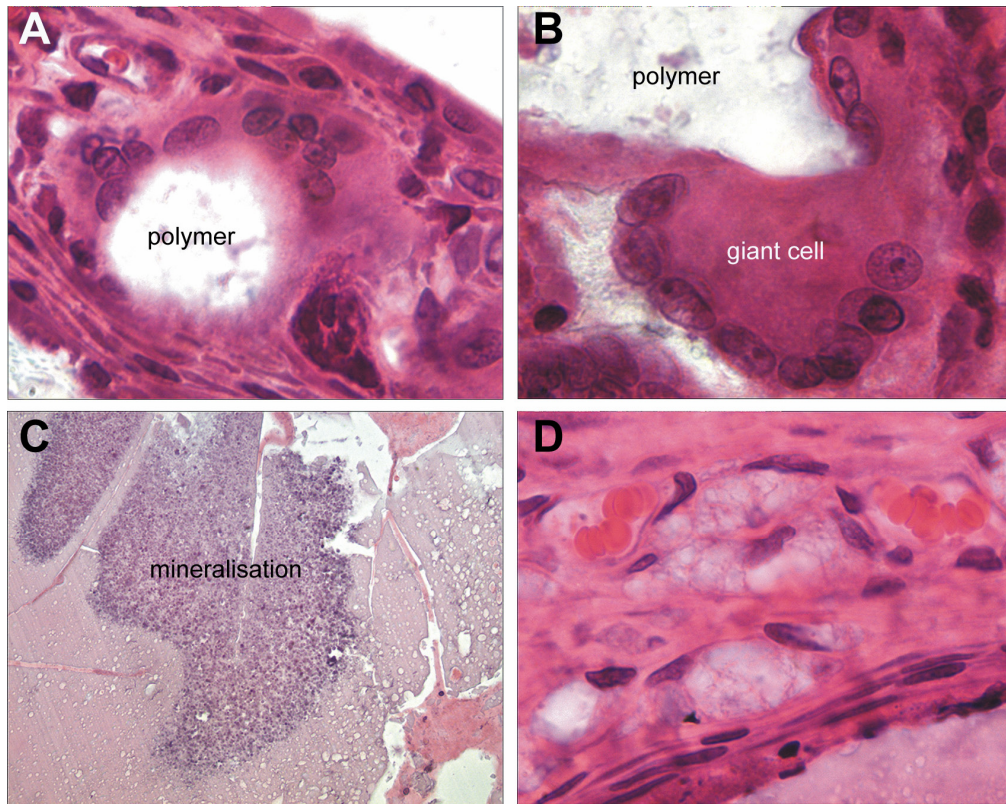


Figure 10: Examples of Raman imaging on different SEM samples. Micrographs A and B; surface of human cancellous bone and corresponding Raman image on phosphate C: typical backscatter sample of bone filler and overlaying PO43- distribution. D: electron micrograph of bone ECM produced by osteoprogenitor cells and (E) corresponding Raman image of mineralized matrix. F: Surface of rat femoral bone and corresponding Raman images on protein (red), carbonate (green) and phosphate (blue).

Chapter 3



After implantation of block copolymers composed of polyethylene oxide terephthalate and polybutylene-terephthalate. Certain compositions show fast degradation, especially the materials where the molecular weight of polyethylene glycol is 1000 g/mole and higher. In many occasions so called giant cells, which are fused macrophages, can be found surrounding polymer fragments (A and B) and macrophages containing small polymer fragments (D). An interesting feature of this material is that it can mineralise *in vivo*, which is thought to enhance the bone bonding capability of this material, which appears as dark purple granulated regions in the polymer (C).

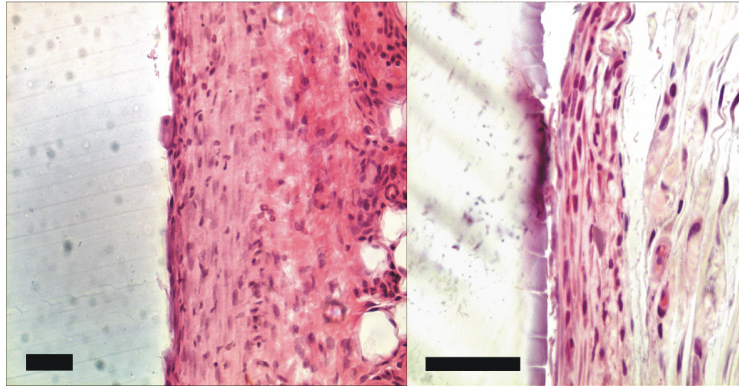


Figure 9: Light micrograph of 300PEOT55PBT45 polymer at 1 week (left) and 12 weeks of implantation (right). Apart from a slight change of surface morphology no effects on polymer morphology can be observed after 12 weeks of implantation. Scalebars are 100 μ m.

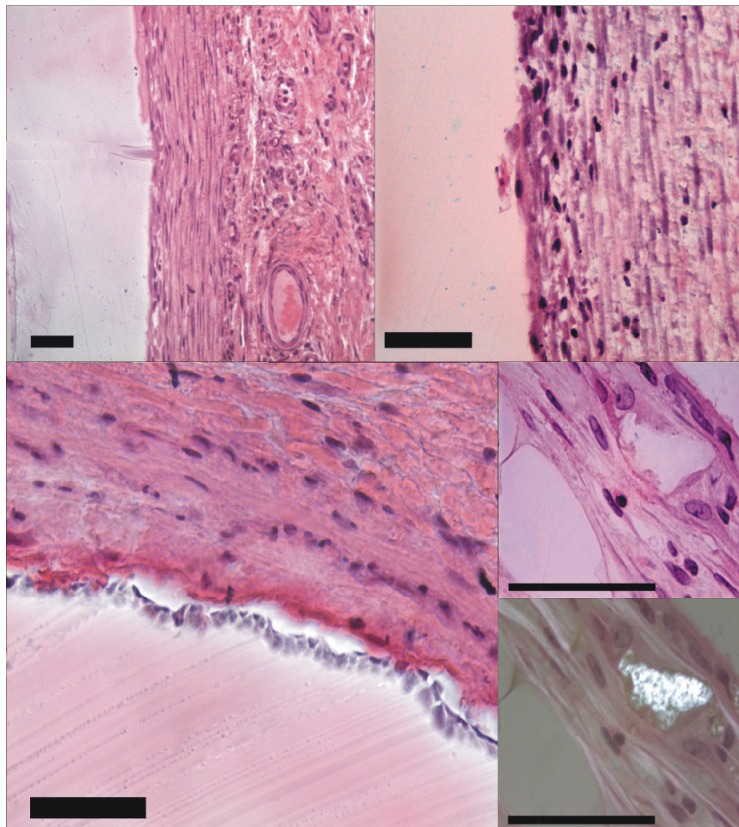


Figure 10: Light micrographs of 300PEOT70PBT30 polymer at 1 (top left) 4 (top right) and 12 (bottom left) weeks of implantation. Bottom right small polymer fragments observed by normal light microscopy (bottom right top) and polarized light microscopy (bottom right bottom) at 12weeks. The dark blue granulation at the polymer surface at 12 weeks, indicates calcification of the polymer. Scalebars are 100 μ m.

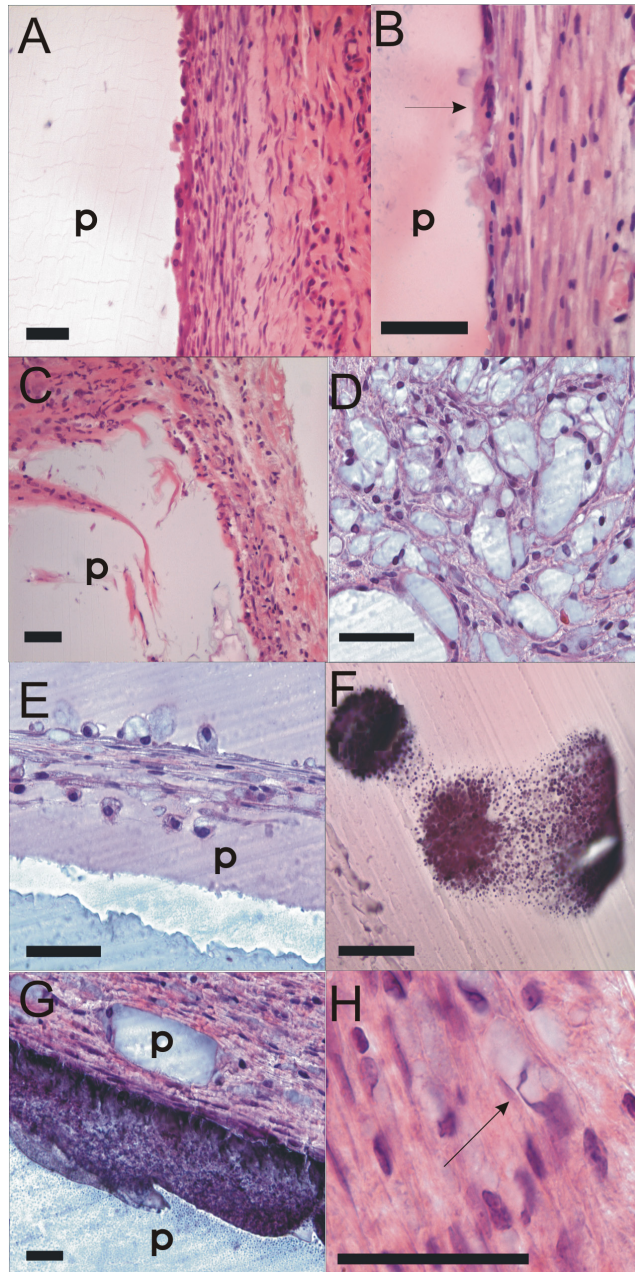


Figure 11: Light micrographs of 1000PEOT70PBT30 polymer at 1 (A), 2 (B), 4 (C) and 12 weeks (E-H) of implantation. A shows the onset of beginning lacunae formation on the polymer (p) surface, which progressed after 2 weeks (B), where macrophage-like cells (arrow) occupying the lacunae can be observed. After 4 weeks of implantation (C) large cracks have formed throughout the polymer filled with connective tissue. After 12 weeks of implantation severe defragmentation of the polymer discs was observed (D and E), and also signs of extensive calcification (dark blue and purple granulation) not only at the surface (G) but also inside the polymer (F). Figure G and H not only show that a large number of small polymer fragments were present in the connective tissue surrounding the implant, but in the cytoplasm of macrophage-like cells as well (arrow). Scalebars are 100 μm .

Annex chapter 3

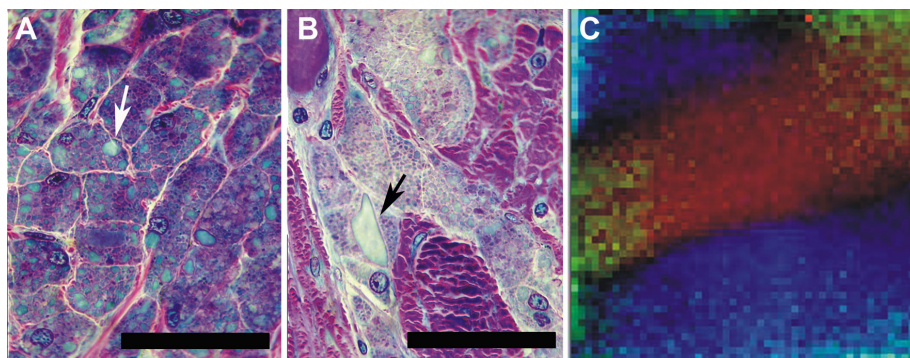
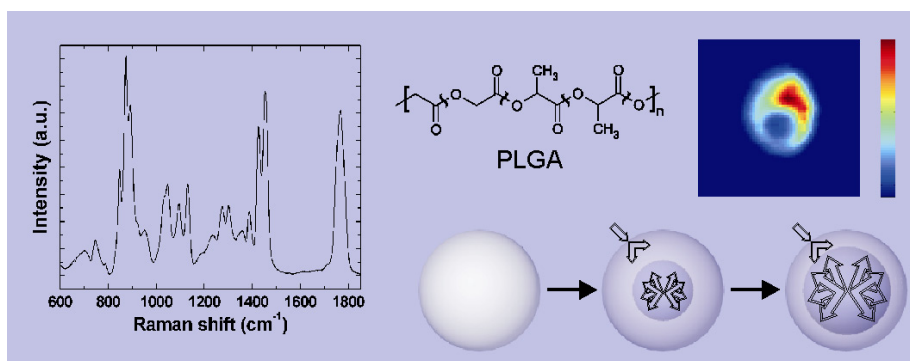


Figure 2. A: Light micrograph (100x) of cells containing polymer fragments (arrow) B: Light micrograph of macrophage like cells containing polymer fragments (arrow) C: Composite Raman image (90x90 μm) of an *in vivo* polymer fragment showing the intensity of the 800 (blue), 1280 (green), 1623 (dark Red) and 1725 cm^{-1} (red) Raman bands.

Chapter 4



In order to study material degradation by single cells we developed an *in vitro* cell culture model. Adding microspheres composed of polylactic-co-glycolic-acid (PLGA), which were first incubated with serum, to a macrophage cell line allowed the study of material degradation in individual cells. In literature there is a debate whether, autocatalytic degradation, a rapid self sustaining degradation process caused by an accumulation of acidic end groups in the interior of implants composed of PLGA, also takes place in small devices. Observing the degradation by confocal Raman imaging, lead to the finding that both fast autocatalytic (inside out) and slow homogenous (outside in) degradation processes were present. Moreover, PLGA degradation seems to occur for the most part through scissioning of the glycolic acid bonds. By using this information we were able to design a schematic model depicting the aforementioned degradation process.

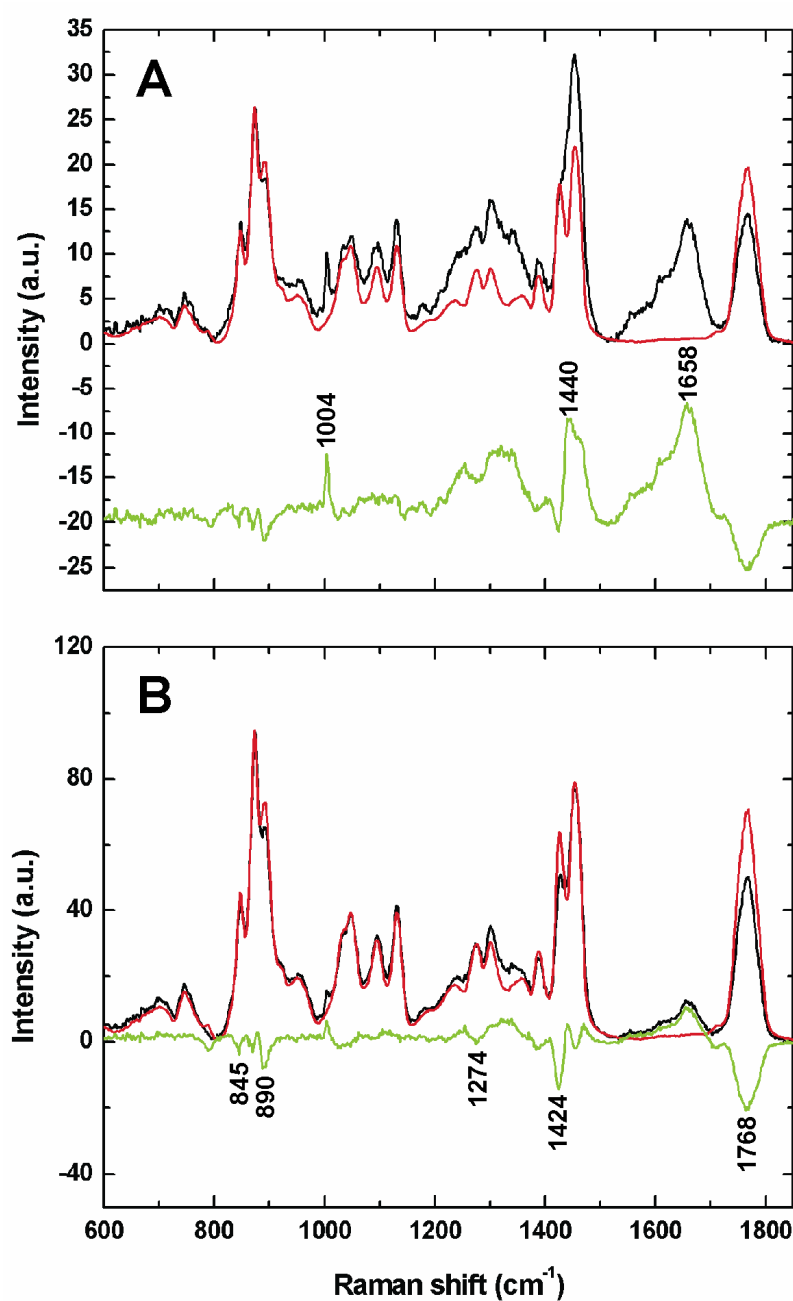


Figure 2. Raman spectra (in black) of the low- (A) and high-intensity (B) regions of the PLGA microsphere in Figure 3D. Pure PLGA is shown in red, and difference spectra (after scaling to the 875 cm⁻¹ band) in green. Note the negative band at 1768 cm⁻¹, indicating a decrease of ester bonds, and the negative bands specific for glycolic acid at 845, 890, 1274, and 1424 cm⁻¹.¹²

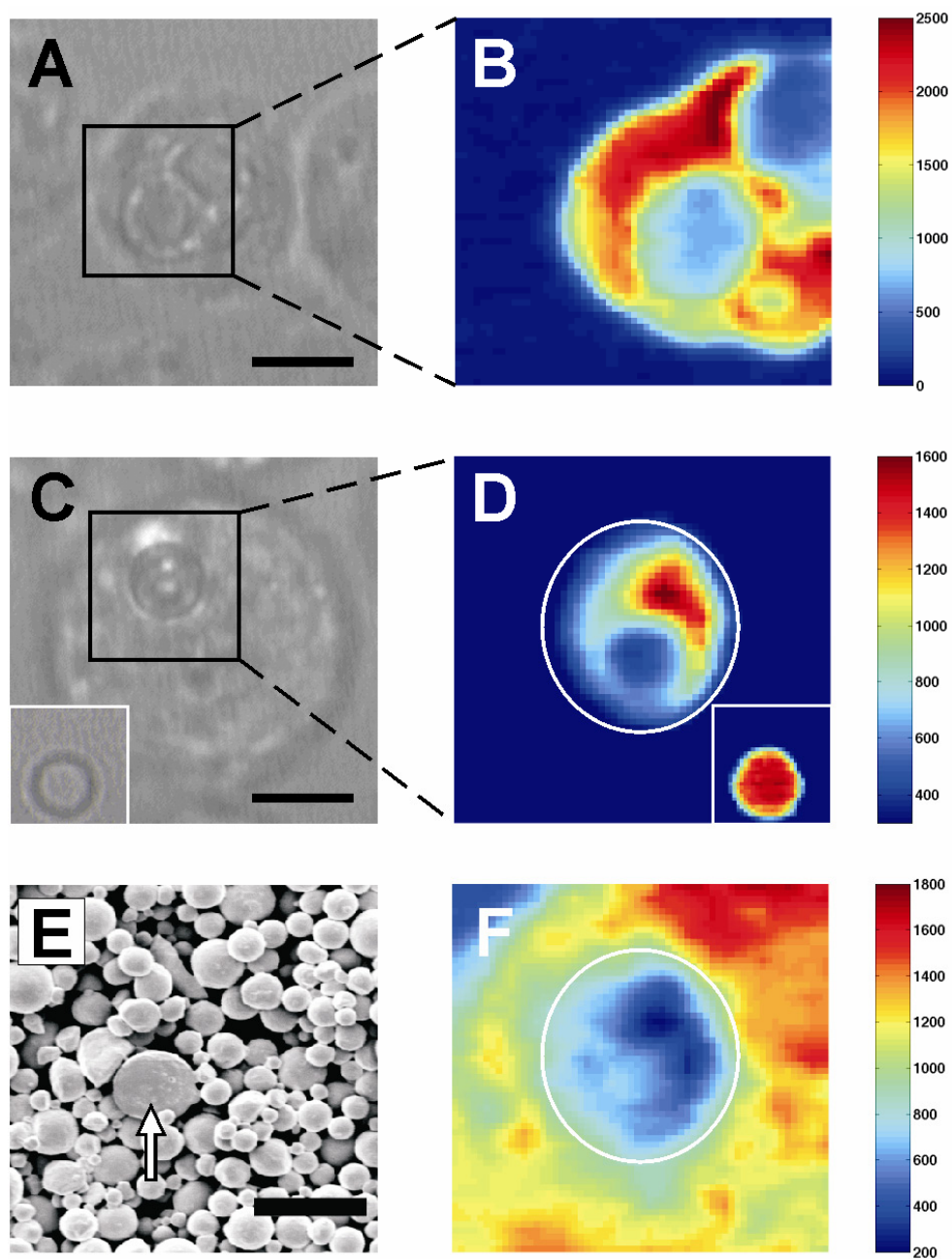


Figure 3. (A and C) Light micrographs of macrophages containing phagocytosed beads cultured for 1 and 2 weeks, respectively (scale bar 5 μm). The Raman images ($7.5 \times 7.5 \mu\text{m}^2$) of these beads are shown in B and D. The scale in B and D shows the relative intensity of the 1768 cm^{-1} band used for imaging (specific for PLGA ester bonds). Insets in C and D show controls (image size $7.5 \times 7.5 \mu\text{m}^2$). The Raman image in 3F depicts the intensity of the 1527-1714 cm^{-1} region, which contains bands from cytoplasmic species. (E) Electron micrograph of PLGA microspheres after freezing and crushing in liquid nitrogen. A cross-section of a broken sphere, showing the solid center, can be seen (arrow) (scale bar 10 μm).

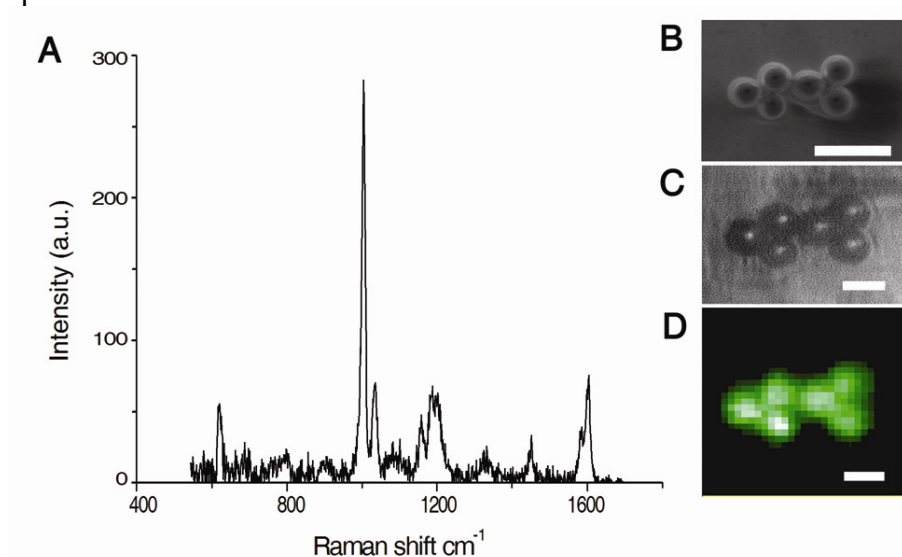


Figure 2: Raman spectrum (A) of the first bead from the left, showed in electron micrograph B. Inset C: 5 μm diameter polystyrene beads, transmission light micrograph observed through the objective lens. Inset D: Corresponding Raman image (1 pixel = 1 μm) using the 1004 cm^{-1} band of polystyrene. Scalebar in B represents 10 μm , C and D 5 μm .

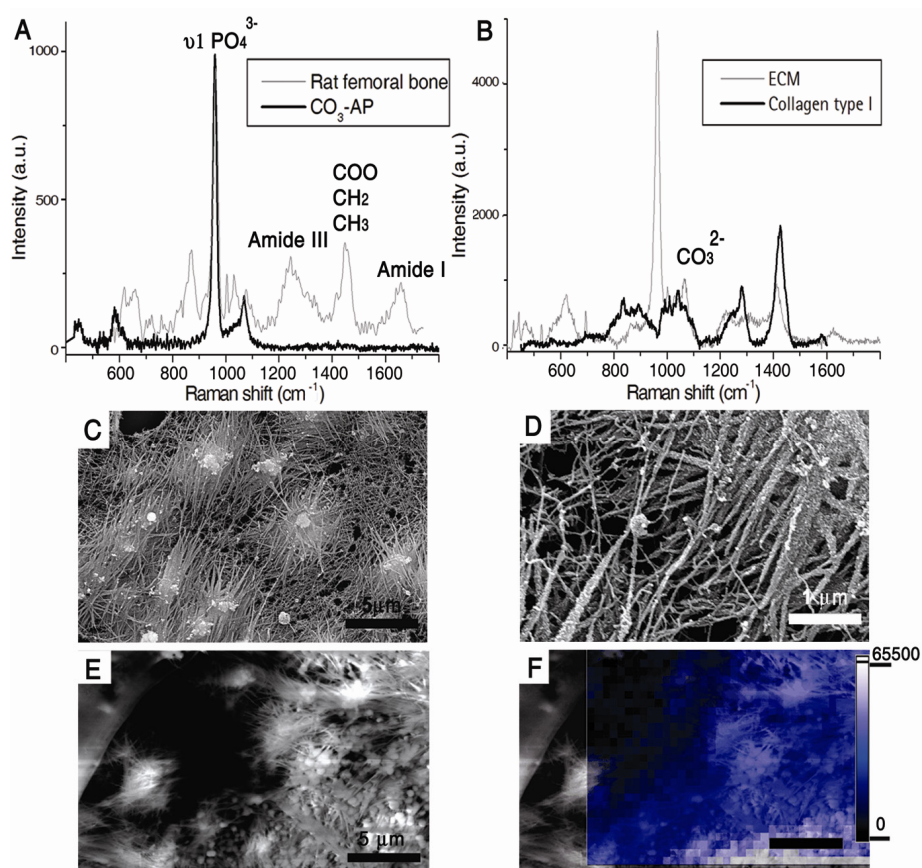


Figure 4: A: Raman spectra of femoral rat bone, CO₃-AP, B: ECM and collagen type I. C, D, E: Electron micrographs of ECM produced by rat osteoprogenitor cells, showing mineralized collagen fiber bundles (width 0.1-0.5 μm). F: Raman image from an area of E, which was subsequently imaged using the 960 cm⁻¹ PO₄²⁻ band (1 pixel=0.5 μm). Scale bar C, E represent 5 μm and D 1 μm.

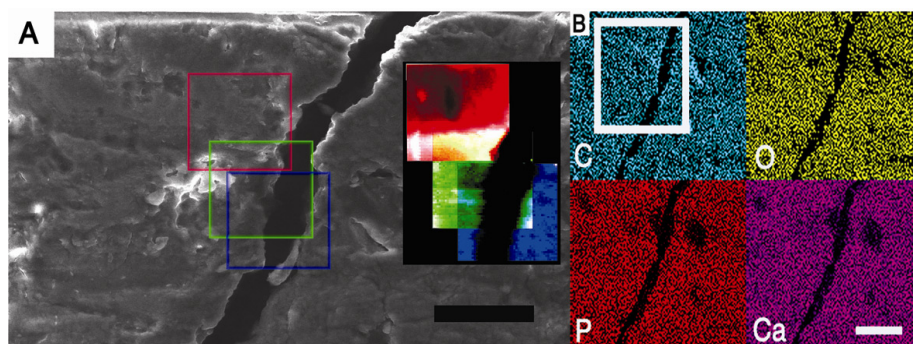


Figure 5A: Electron micrograph of the surface of bone, showing a 15-20 μm microcrack and subsequent corresponding Raman images 50x50 μm (1 pixel=1 μm) of protein (1400-1440 cm⁻¹, red square), CO₃²⁻ (1070 cm⁻¹, green square) and PO₄³⁻ (960 cm⁻¹, blue square). Fig 5B: XRMA maps for C, O, P, and Ca, the white squared area corresponds with electron-micrograph in A. Scale bar in A 50 μm and B 25 μm.

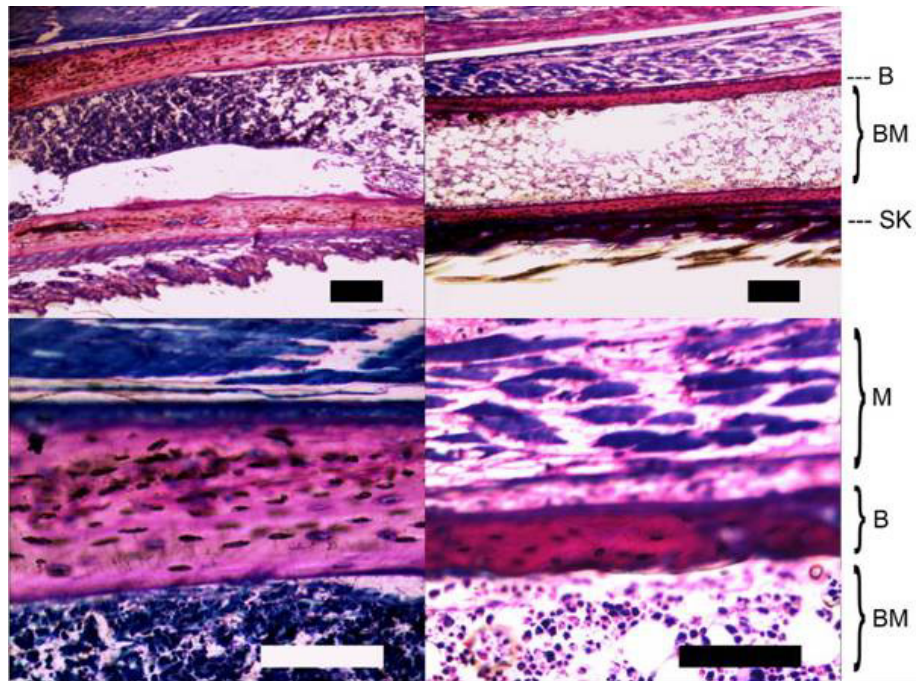


Figure 2: Light micrograph showing the morphology of WT (left panel) and XPA-TTD (right panel) mice. Scale bars are 400 μ m (top) and 200 μ m (bottom). B = bone, BM = bone marrow, SK = skin region, M = muscle region.